

**Implementing Dynamic Foot Shape Models to Improve  
Spacesuit Boot Fit**

by

**Abhishektha Boppana**

B.S., Case Western Reserve University, 2017

M.S., University of Colorado Boulder, 2019

A thesis submitted to the  
Faculty of the Graduate School of the  
University of Colorado in partial fulfillment  
of the requirements for the degree of  
Doctor of Philosophy

Ann and H.J. Smead Department of Aerospace Engineering Sciences

2022

Committee Members:

Allison P. Anderson, Chair

Dr. Torin Clark

Boppana, Abhishektha (Ph.D. Aerospace Engineering Sciences)

Implementing Dynamic Foot Shape Models to Improve Spacesuit Boot Fit

Thesis directed by Dr. Allison P. Anderson

Abstract to be written.

## **Dedication**

To all of the fluffy kitties.

## Acknowledgements

Here's where you acknowledge folks who helped. But keep it short, i.e., no more than one page, as required by the Grad School Specifications.

## Contents

### Chapter

<b>1</b>	<b>Motivation</b>	<b>2</b>
1.1	EMU Spacesuit Injury Incidence . . . . .	3
1.1.1	Spacesuit Contact Injuries . . . . .	4
1.1.2	Spacesuit Musculoskeletal Injuries . . . . .	5
1.2	Hypothesized Spacesuit Injury Mechanisms . . . . .	5
1.3	Spacesuit Injury Countermeasures . . . . .	7
1.4	Summary . . . . .	8
<b>2</b>	<b>Background</b>	<b>9</b>
2.1	Planetary Ambulation . . . . .	9
2.2	Gas Pressurized Spacesuit Characteristics . . . . .	11
2.2.1	An Inherently Stiff Structure . . . . .	11
2.2.2	Mobility Design Features . . . . .	12
2.3	MK III Ambulation Performance . . . . .	13
2.3.1	Cost of Transport Factors . . . . .	14
2.3.2	Ambulation Biomechanics . . . . .	15
2.3.3	Subjective Feedback . . . . .	15
2.4	Spacesuit Fit . . . . .	16
2.4.1	Spacesuit Sizing Process . . . . .	17

2.4.2	Quantifying Fit . . . . .	18
2.4.3	Body Shape Characterization to Improve Fit . . . . .	19
2.5	Summary . . . . .	20
<b>3</b>	<b>Investigative Approach</b>	<b>22</b>
3.1	Expected Outcomes . . . . .	25
<b>4</b>	<b>Specific Aim 1 : Challenges in Quantifying Heel-Lift during Spacesuit Gait</b>	<b>27</b>
4.1	Introduction . . . . .	27
4.2	Methods . . . . .	28
4.2.1	Data Collection . . . . .	28
4.2.2	Data Analysis . . . . .	29
4.3	Results . . . . .	32
4.4	Summary . . . . .	33
<b>5</b>	<b>Specific Aim 2: Predictively model dynamic changes in foot morphology during gait</b>	<b>37</b>
5.1	Introduction . . . . .	37
5.2	DynaMo: Dynamic Body Shape Capture with Intel RealSense Cameras . . . . .	39
5.3	Development of a Predictive Dynamic Foot Shape Model from Statistical Shape Modeling . . . . .	41
5.3.1	Methods . . . . .	41
5.3.2	Results . . . . .	45
5.3.3	Foot Shape Changes . . . . .	49
5.3.4	Study Limitations . . . . .	52
5.3.5	Study Conclusions . . . . .	53
5.4	Analysis of Dynamic Instep and Arch Height Changes . . . . .	53
5.4.1	Methods . . . . .	56
5.4.2	Results . . . . .	58

5.4.3	Translating Instep and Arch Height to Footwear Design . . . . .	59
5.5	Summary . . . . .	62
<b>6</b>	<b>Specific Aim 3: Define a design process integrating dynamic foot morphology data for a novel spacesuit boot</b>	<b>63</b>
6.1	Existing Knowledge on Foot Shape Mobility . . . . .	64
6.1.1	Linear Anthropometry . . . . .	64
6.1.2	Gait Joint Kinematics . . . . .	66
6.2	Biomechanical Boot Design Framework . . . . .	67
6.2.1	Mobility . . . . .	69
6.2.2	Toe box . . . . .	70
6.2.3	Upper . . . . .	70
6.2.4	Sole . . . . .	72
6.3	Novel Planetary Spacesuit Boot Design . . . . .	73
6.3.1	Ankle Convolute . . . . .	74
6.3.2	Upper and Toe Box . . . . .	77
6.3.3	Instep Lacing . . . . .	80
6.3.4	Heel Counter . . . . .	82
6.3.5	Sole . . . . .	82
6.3.6	Summary . . . . .	83
6.4	Novel Planetary Spacesuit Boot Construction . . . . .	85
6.4.1	Ankle Convolute Construction . . . . .	86
6.4.2	Upper and Toe-Box Construction . . . . .	88
6.4.3	Sole Construction . . . . .	89
6.4.4	BOA Lacing Integration . . . . .	91
6.4.5	Heel Counter . . . . .	91
6.4.6	Pressure Sealing . . . . .	91

6.5	Classic Spacesuit Boot Design and Construction . . . . .	91
6.5.1	Pressurization Test Interface . . . . .	92
6.6	Summary . . . . .	96
<b>7</b>	<b>Specific Aim 4: Evaluate novel planetary spacesuit boot design for fit and comfort</b>	<b>98</b>
7.1	Experimental Design . . . . .	98
7.2	Methods . . . . .	99
7.2.1	Subjects . . . . .	99
7.2.2	Procedures . . . . .	100
7.2.3	Quantitative Measures . . . . .	100
7.2.4	Survey Measures . . . . .	103
7.2.5	Quantitative Data Processing . . . . .	104
7.2.6	Statistical Analysis . . . . .	105
7.3	Results . . . . .	107
7.4	Discussion . . . . .	113
7.5	Summary . . . . .	116
<b>8</b>	<b>Summary</b>	<b>118</b>
8.1	Future Work . . . . .	121

## **Appendix**

<b>Bibliography</b>	<b>123</b>
---------------------	------------

## Tables

### Table

4.1 Drift rate estimations (mean +/- std dev) of raw, filtered, and post-ZVU/ZPU positional estimates for IMUs mounted on the spacesuit lower leg assembly and shank .	33
5.1 Enrollment groups based on reported height. 5 subjects were enrolled in each group	41
5.2 Pearson correlation coefficients between maximum instep height change and subjects' anthropometric measurements . . . . .	59
7.1 Summary of subjects' foot measurements . . . . .	99

## Figures

### Figure

1.1	Overview of how deficiencies in spacesuit design and fit can lead to increased injury risk . . . . .	6
2.1	Knee (left) and foot (right) trauma identified in the MK III following 10 km walkback evaluation. From Norcross et al. 2009 . . . . .	16
2.2	Heel-lift occurring during heel-off, as subjectively reported in the MK III. The poor fit and indexing in the boot and lower torso allows the heel to lift inside the boot during heel-off . . . . .	19
4.1	Location of IMUs (red squares, placed both the spacesuit and operator) and padding (gray). The sacrum IMU is placed on the back of the operator and spacesuit, where the upper-most black band is located, and is therefore out of view in this diagram. The table on the right outlines the IMUs corresponding locations between the operator and spacesuit. . . . .	29
4.2	Heel-off lag distributions between all subjects and configurations, with discrete heel-off lag measurements being represented as black dots. Positive lag values are indicative of spacesuit-delayed heel-off, while negative lag values are indicative of operator-delayed heel-off . . . . .	33

4.3 (Top): DWT IMU vertical acceleration data for shank and SLL. Shaded regions represent the detected foot-flat phases of zero-acceleration regions for each step. (Middle) Zoomed-in view of the foot-flat phase for two steps, with annotated spacesuit and operator heel-off points. When the shank IMU registers a vertical acceleration in foot-flat phase prior to the SLL IMU (middle-left), this could suggest heel-lift (bottom-left). When the SLL IMU registers a vertical acceleration in foot-flat phase prior to the shank IMU, this would ordinarily suggest that the SLL experiences heel-off prior to the operator (middle-right). However, there may be pressure forces which allow the SLL to extend, registering a vertical acceleration for the SLL-mounted IMU and falsely suggesting that the spacesuit is experiencing heel-off (bottom-right). . . .	34
5.1 Capture setup of 6 Intel RealSense D415 Depth Cameras (circled in red) placed around a treadmill. The checkerboard shown was used to calibrate the cameras using the DynaMo package. . . . .	40
5.2 Sample frames, shown in 10 frame intervals (bottom), collected by DynaMo showing dynamic shape capture of the foot (top) at 90 frames-per-second, and the capture of reflective markers on the foot shown as white dots . . . . .	40
5.3 Flowchart of processing steps for statistical shape model creation . . . . .	43
5.4 Processed and registered scans of one subject during heel-off, shown 10 frames (0.11 seconds) apart. . . . .	46
5.5 Distribution of mean root-mean-square (RMSE) error and mean Hausdorff distance (HD) across the various prediction models leave-subject-out cross-validation results. Model error values and standard deviation are shown below each distribution . . . .	47
5.6 Each graph represents the predictor's effects on the shape mode by visualizing the model's normalized coefficients. Larger absolute values indicate a larger effect from the predictor on the shape mode. . . . .	48

5.7 Landmarks and vectors used for instep height measurement, shown in top and side views. The principal foot axis is defined from the pternion to the middle metatarsal head landmark (top). A triangle is defined with a base between the middle metatarsal head and the pternion, and an upper vertex at the instep landmark (bottom). The height of this triangle (red) is taken as the instep height. The MLA location is also shown for comparison. . . . .	57
5.8 Correlation between selected subjects instep height and MTP joint angle over stance phase. Subjects with high correlation between their MTP joint angle and instep height are shown on the top row. Subjects with lower correlations between their MTP joint angle and instep height are shown on the bottom row. Locations of where mid-stance and late-stance instep height values are taken for each subject are highlighted as vertical lines. The Pearson correlation coefficient for each subject is shown on their graph. . . . .	59
6.1 Foot-specific measures which directly affect mobility and comfort . . . . .	64
6.2 (Top-right) Inequality in distribution of equivalent shoe size between male and female. (Top-left) Distribution of male and female foot widths. (Left) relationship between foot length and arch length; visualizations developed from the ANSUR II Dataset . . . . .	66
6.3 Overview and classification of measurements to footwear design variables with representative shoe . . . . .	68
6.4 Mobility and flexibility of joints needed in the spacesuit boot . . . . .	70
6.5 Desired sole flexibility (red) needs to be properly indexed to the MTP joint, which can be located by the arch length measurement . . . . .	72

6.6 Actuation of a convolute joint. The upper convolute segment overlaps the lower convolute segment by a fixed amount, held static at the center by the restraint strap. When the joint is bent, the upper convolute segment rotates around the lower convolute segment. One side of the upper segment rolls over the lower segment, increasing its overlap. The opposite side unrolls from the lower segment, reducing its overlap. . . . .	74
6.7 Simplified triangle representing a convolute assembly. The left side of the triangle represents the collapsing side of the convolute assembly, while the right side represents the expanding side of the convolute assembly. . . . .	75
6.8 Angling the convolutes with respect to the plantar surface allows the joint center of the convolutes to sit much closer to the malleolus, which is the joint center of the ankle. . . . .	77
6.9 Modification of the last to have a wider ankle to accommodate the ankle convolute assembly. . . . .	78
6.10 Seam lines on taped last. The lateral (A), medial (B), lateral profile (C), medial profile (D), and top-down (E) views are presented . . . . .	79
6.11 Evolution of lacing convolute design. Originally, the lacing convolute ran the length of the boot (left). The lacing convolute was then iterated to pivot at the MTP joint, and provide greater capture closer to the heel . . . . .	80
6.13 3D view of the sole generated from the last. . . . .	83
6.14 Overview of the novel spacesuit boot. Only the medial side is shown, but the lacing is mirrored on the lateral side. The heel counter's location is shown as a dotted line as it is internal to the pressure bladder. When plantarflexed, the distance the lace has to travel is increased and is shown by the arrow. Therefore, the lacing near the guides further tightens. . . . .	84

6.15 Prototype planetary spacesuit boot constructed with BOA lacing, ankle rolling convolutes, and a heel counter. The heel counter is not visible as it is inside the pressure bladder . . . . .	85
6.16 Two pressure bladder patterns (left, right) are connected by a single strip of material (middle) at the team. This strip is heat-sealed to both patterns, creating an air-tight seam. . . . .	86
6.17 Ankle convolute flat pattern construction. . . . .	88
6.18 Patterns for the upper, toe-box, and sole. These patterns are cut from the last taping process, and flattened onto a piece of paper. New patterns are then traced around the flattened tape patterns, and used to make the respective panels. A 1cm seam is added around each pattern to provide flexibility in manufacturing. Patterns were generated for the forward (A) and rear (B) toe-box, inferior (C) and superior (D) medial upper, inferior (F) and superior (E) lateral upper, and the sole (G). . . . .	89
6.19 Two halves of the mold used to cast the sole. . . . .	90
6.20 Classic spacesuit boot which was constructed with similar techniques as the prototype spacesuit boot, but without lacing, or a heel-counter. . . . .	92
6.21 Patterning of the base neoprene layer (top) which results in a much smaller opening (bottom, yellow highlight) for the wearer's calf to enter through. . . . .	95
6.22 Overview of straps used to create a seal around the wearer's ankle. . . . .	95
7.1 Marker locations for the novel spacesuit boot (A), work boot (B), and a subject's left shoe (C). The novel spacesuit boot and left shoe use black Duck tape for markers on their sole. The work boot uses a silver reflective tape for its markers. The Kinovea software's annotations are shown on each of the image: Marker 1 is tracked to provide heel rise magnitude, and the orange line is used to calibrate the coordinate system. .	101

7.2	Location of the FSR embedded into the sole of the novel spacesuit boot (A) and the work boot (B). The FSR was embedded in the classic spacesuit boot's sole in the same fashion as the novel spacesuit boot . . . . .	102
7.3	Voltage response curves of the FSR to an applied force from a force gauge, for each of the three boots. . . . .	103
7.4	Modified Corlett-Bishop Discomfort Scale mapping used for this evaluation, limited to areas below the knee . . . . .	104
7.5	Mean and maximum of reported Corlett-Bishop discomfort ratings on both the left (control) and right (test) shoe. Results are presented across all subjects. . . . .	108
7.6	Estimate (black) of the heel performance rating across all boot conditions, as compared to the subjects' data. The subjects' data is offset along the x-axis to show all data points. Each boot's posterior distributions' overlap as compared to the novel spaceboot are annotated. . . . .	109
7.7	Estimate (black) of the rating of perceived exertion across all boot conditions, as compared to the subjects' data. The subjects' data is offset along the x-axis to show all data points. Each boot's posterior distributions' overlap as compared to the novel spaceboot are annotated. . . . .	109
7.8	Example FSR and heel-rise data trace from a heel-rise set. Detected peaks and heel-off times are shown with the vertical lines . . . . .	110
7.9	Estimate (black) of the difference in heel-rise magnitude across all boot conditions, as compared to the subjects' data. heel-rise magnitude difference is calculated by subtracting the magnitude of the right foot from the left foot. The subjects' data is offset along the x-axis to show all data points. Each boot's posterior distributions' overlap as compared to the novel spaceboot are annotated. . . . .	111

7.10 Estimate (black) of the difference in heel-off time across all boot conditions, as compared to the subjects' data. The difference in heel-off time is calculated as the left foot's (control) heel-off time minus the right foot's (test) heel-off time. Therefore, negative numbers indicate that the right foot lifted after the left foot. The subjects' data is offset along the x-axis to show all data points. Each boot's posterior distributions' overlap as compared to the novel spaceboot are annotated. . . . .	111
7.11 Estimate (black) of the FSR voltage at maximum heel-rise across all boot conditions, as compared to the subjects' data. The subjects' data is offset along the x-axis to show all data points. Each boot's posterior distributions' overlap as compared to the novel spaceboot are annotated. . . . .	112
7.12 Estimate (black) of the FSR voltage at heel-off across all boot conditions, as compared to the subjects' data. The subjects' data is offset along the x-axis to show all data points. Each boot's posterior distributions' overlap as compared to the novel spaceboot are annotated. . . . .	113
7.13 Video frame of heel-rise by subject FT in the novel spaceboot. As the BOA lace length cannot change, the sole is kept at a constant distance to the instep throughout the heel-rise motion. This ensures that the heel is continuously making contact with the . . . . .	115

---

## **Chapter 1**

### **Motivation**

The Apollo missions represent the last time humans set foot on another planetary surface, the Moon. Future human spaceflight missions are retargeting planetary surface exploration by sending astronauts back to the Moon and onward to Mars. While robotic missions can perform many of the scientific aspects of planetary exploration, human exploration still plays a key role in planetary mission success [44].

Spacesuits are designed to both provide life support and help protect the astronaut during activities conducted outside a space habitat, known as extravehicular activity (EVA). EVA is an important consideration of planetary exploration, allowing astronauts to perform scientific experiments, collect geological samples, perform habitat maintenance, and construct infrastructure. During EVA, astronauts are subject to many physiological and environment factors, including reduced gravity loading, dust, radiation, and extreme environment temperatures. In addition, the lack of atmosphere does not provide life support. Therefore, an EVA spacesuit's primary design objectives are to protect its operator from the environment and allow them to perform EVA tasks.

Humankind's current planetary EVA experience is limited to a total of 78 hours over 6 Apollo surface missions [113]. During the Apollo missions, astronauts performed almost 10 hours of EVA in a 24 hour period without the assistance of a rover during Apollo 14, and 22 hours of EVA in a 36-hour period with the assistance of a rover during Apollo 17 [113]. The longest traverse performed on the lunar surface occurred during Apollo 12, where astronauts Charles Conrad and Alan Bean walked 1.8 km [113]. Apollo 15-17 missions involving a rover assumed astronauts would be able to walk 5 km

in case of rover failure [113], but this requirement is doubled for future missions. Future planetary mission design assumes astronauts can walk up to 10 kilometers to return to their habitat, and that astronauts can perform 8-hour EVAs, with a limit of 12 hours of EVA per 24 hours and 24 hours of EVA per 7 days [44]. In addition, NASA's current planetary exploration plans focus on extended stays and colonization, increasing surface mission time and therefore increasing total EVA time. Future planetary EVA missions will therefore need a spacesuit that comfortably protects astronauts while they perform EVA tasks and traverse across the surface on these long duration missions.

### 1.1 EMU Spacesuit Injury Incidence

Following the Apollo era, space missions have all occurred in low Earth orbit in a microgravity environment. New spacesuits, such as the Extra-Vehicular Mobility Unit (EMU) were designed for microgravity operations. This included greater upper-torso mobility while reducing lower-torso mobility, as astronauts would be floating in space and not be required to ambulate. However, the increase in EVA activities that accompanied the construction of the International Space Station have increased the incidence rates and severity of crew injuries, prompting studies into the human-spacesuit interactions and deficiencies in suit design that lead to these injuries.

Crewmember difficulties with the spacesuit have existed since the first EVA, where Alexi Leonov had difficulties moving the suit to re-enter the spacecraft. Apollo astronauts have commented on the fatiguing reduced mobility of their spacesuits [125]. Gas pressurized spacesuits are known to be inherently stiff and rigid [110, 2, 128, 68], difficult to move [104, 6], and have the potential to cause injuries both during operations and ground-based training [150, 135, 125, 126, 11, 34].

The prevalence of injury has been well studied in the era of on-orbit microgravity EVAs performed with the EMU. Strauss [135] found that 24.6% of training sessions at the Neutral Buoyancy Laboratory (NBL) between 2004 to 2006 study had reported injury symptoms. Viegas [143] found a 67.5% reporting rate of injury symptoms from astronauts training in the NBL between 2002 to 2003. An in-flight injury incidence of 0.24 was reported by Scheuring [127] for EVAs occurring on

Space Shuttle flights 90 to 113. These injuries can be classified as contact injuries, including bruises and abrasions; and musculoskeletal injuries, including muscle tears, strains, and inflammation.

### **1.1.1 Spacesuit Contact Injuries**

Spacesuit contact injuries have been the most reported operational injury mechanism in the US space program [125], and in the EMU [135, 143, 127]. Contact injuries occur through repeated contact between the wearer and the spacesuit. High contact pressure between the wearer and spacesuit can lead to bruises, while shear can lead to abrasions [89, 28].

EVA hand injuries have been reported since the Apollo era, with symptoms including swollen and abraded joints, putting the mission at risk [127]. Hand injuries continue to be most frequently reported injury in the EMU [135, 143, 127]. Hand contact injuries include fingernail delamination, abrasions, contusions, and nerve impingement [135, 143, 127]. These injuries have widely been attributed to the poor fit and unprotected contacts between the hand and the spacesuit glove [135, 143].

Shoulder contact injuries occur from the combination of unprotected contact and high weight loading in the EMU [135, 143, 11]. Shoulder injuries are reported as the second most common EMU injury location and frequently occur during ground-based training in the NBL, when the wearer may be inverted in the suit [135, 143]. While the suit and operator together are made neutrally buoyant, the operator is able to shift relative to the suit due to gravity. Therefore, they “fall” into the suit, and are now making contact with the hard upper torso (HUT). Therefore, the increased contact and high levels of load leads to shoulder contact injuries.

The feet are the next most reported areas of in-flight EMU contact injuries in the spacesuit [127]. Traditionally, not much motion occurs in the lower torso of the EMU spacesuit due to its design targeting microgravity operations. The feet are normally restrained in a fixed foot restraint, while the astronaut performs tasks utilizing their upper body. One astronaut reported a “searing, knife-like pain” on their foot during on-orbit EVA which was unable to be rectified [127]. This resulted in a blister and decreased sensation on the foot’s dorsal surface, and was later attributed

to having excess pressure bladder material in the boot [127]. Strauss [135] also reports contact injuries on the toes and dorsal surface stemming from the boot sizing insert, which does not adequately project the astronaut from contact from the foot restraint or bladder folds.

Other reported locations for EMU contact injuries include the elbow, knee, and trunk [135, 127]. Injuries at wearer's elbows and knees are reported to come from rubbing against the convolute joints [135]. Injuries at the trunk are reported to occur from contact between the wearer's back and the Liquid Cooling and Ventilation Garment (LCVG) in the spacesuit [135].

### **1.1.2 Spacesuit Musculoskeletal Injuries**

Fatigue from high exertion may lead to musculoskeletal injuries EMU Musculoskeletal injuries have been reported in the hands, due to the high exertion needed to actuate fingers on the pressurized glove [143]. Fatigue may occur after many hours of completing EVA tasks [135, 127]. Similarly, the elbow joints in the EMU have also reportedly caused strains [135].

Limitations of the EMU suit design can also lead to musculoskeletal injuries, the most severe which occurred at the shoulder [135]. EMU operators can overuse their rotator cuff during EVA tasks, leading to muscle strains, sprains, tears, and overuse injuries [150, 135, 136, 127]. Some of these injuries have required surgical intervention [136].

## **1.2 Hypothesized Spacesuit Injury Mechanisms**

Limitations in suit joint design and the poor fit between the suit and its operator can both lead to contact or musculoskeletal injuries. While other environmental factors, such as increased humidity, were also found to have a role in EMU fingernail de-lamination [34], this section will focus on the design and fit factors for spacesuits. High exertion needed to actuate joints and poor indexing can lead to excessive musculoskeletal injuries, while poor sizing and poor indexing can lead to contact injuries, increasing the risk of injury fig. 1.1.

Pressurized spacesuit joints require more energy to move than compared to unsuited motions [101, 6]. While design features aim to reduce the effort needed to bend joints [65], these joints are

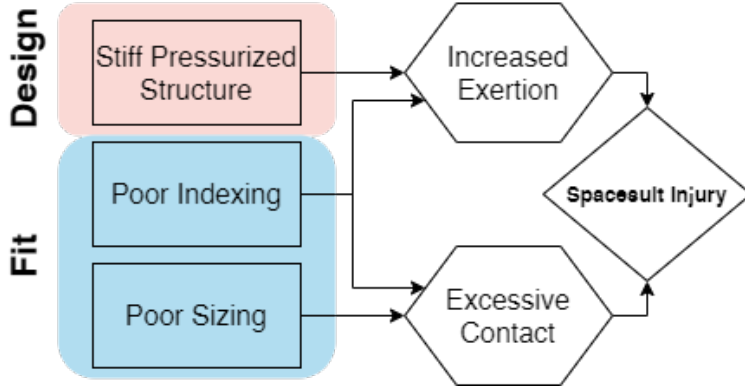


Figure 1.1: Overview of how deficiencies in spacesuit design and fit can lead to increased injury risk

difficult to engineer in areas such as the hand. Therefore, the fatigue and strain injuries reported in the hand could be due to inherent design deficiencies of EMU spacesuit gloves [135, 143].

Spacesuit joints also need to be properly aligned to the wearer to reduce both contact and musculoskeletal injury risk. Indexing is a specific fit measurement regarding the alignment of the operator's joints to the spacesuit's joints. Poor indexing can lead to contact injuries when suit-operator joint centers become misaligned and cause rubbing against the suit during motion, as seen in the elbow and knee of the EMU [135]. Deficiencies in suit design, including the high exertion to actuate joints and range-of-motion limitations, can also cause poor indexing and lead to injury. Viegas reports a specific mechanism in the EMU glove where the high exertion required to actuate the glove results in dorsal displacement of the metacarpophalangeal joints, pushing the tops of fingers against the surface of the glove and causing inflammation [143]. Poor indexing at the the EMU HUT design forces internal rotation of the shoulder due to the scye opening not allowing for full range-of-motion of the shoulders, leading to potential overuse and injury of the rotator cuff muscle [150, 135, 136, 127]. Suit joints should therefore be designed and sized to ensure proper indexing.

Suit components also need to be properly sized to the operator to reduce contact injury risk. Sizing, along with indexing, ensures that the suit is fit to the operator. Spacesuits in the Apollo era were custom tailored to each astronaut. However, as the astronaut corp grew, the EMU presented a modular sizing system, where differently-sized suit components had to be selected

for each astronaut. Gaps between the wearer and the spacesuit could lead to excessive contact when the wearer moves and shifts inside the spacesuit [17]. Suit components which are too small can also cause higher contact pressures, leading to potential contact injuries [10]. Poorly sized bladder inserts were found to be a factor in EMU foot injuries [135]. Opperman et al. [107] found that higher hand circumferences have a larger incidence of fingernail delamination in the spacesuit glove, while Charvat et al. [35] found smaller hand circumferences to be a risk factor in fingernail delamination, showing how sensitive fit is in leading to injury. Suit components should therefore be sized accurately to the suit's operator to ensure proper fit.

### **1.3 Spacesuit Injury Countermeasures**

Attempts to mitigate spacesuit injury have focused on addressing the fit and mobility limitations of the EMU. Newer spacesuit prototypes feature larger scye openings for better indexing and more mobile shoulder bearings compared to the EMU [61]. However, testing of microgravity EVA task performance in the NBL found that while the new design allowed for more shoulder compatibility, larger subjects still reported discomfort in the shoulder area [93]. This shows how sizing and indexing are just as important as spacesuit mobility to ensure a properly compatible spacesuit. It still remains impossible to perfectly fit every person to the EMU spacesuit due to the wide ranges of anthropometry and limited sizing components [17]. Back padding on the EMU was found to potentially assist wearers in controlling the upper torso of the suit, reduce over-rotation of the torso to keep upper extremity joints aligned, and improve indexing at the gloves [34]. For wearers with a smaller anthropometry however, indexing at the hip bearings was unable to be fixed by padding, due to the limitations in torso length. In addition, effects of indexing on performance are inconclusive [50]. Therefore, there is a need to improve spacesuit sizing and indexing to work with any improvements in spacesuit mobility to reduce the risk of contact and musculoskeletal injuries.

## 1.4 Summary

The push towards planetary exploration requires advancements in spacesuit design to create a safe and comfortable environment for astronauts to perform EVAs. Our planetary exploration experience is limited to just 6 Apollo missions to the Moon as missions have shifted towards microgravity research, but future plans call for an extended human presence on the Moon and Mars. Microgravity EVAs and training have resulted in many upper torso injuries due to hard-to-move joints and poorly fitted suits. The transition to planetary EVAs, with a focus on ambulation, may result in a higher incidence rate of injuries in the lower torso without significant changes in the way spacesuits are designed and fitted. Therefore, it is important to understand how operator-spacesuit interactions and spacesuit performance may lead to injury in the context of planetary tasks such as ambulating as planetary surface missions are planned. This will allow for the construction of safer and more comfortable spacesuits to reduce the risk of injuries during EVA.

## **Chapter 2**

### **Background**

Poor suit design and suit fit are two of the main suit variables leading to injury risk and compromised performance during EVA [34]. Pressurized spacesuits will continue to be used for EVAs through the transition from microgravity to planetary exploration, and therefore will require improvements to their joint design and fit to ensure safe and comfortable EVA. As future missions target planetary exploration, ambulating across the surface becomes a critical EVA task, and requires an understanding of reduced-gravity ambulation and suited effects on ambulation. There are also many challenges that are associated with fitting spacesuits which have not yet been solved. This chapter introduces how current suits perform in planetary ambulation and introduces the challenges with fitting spacesuits.

#### **2.1 Planetary Ambulation**

Walking is not always the most energetically preferable gait. Astronauts during the Apollo missions did not walk while traversing the surface; they famously loped across the surface. In fact, loping is the energetically preferred gait on the Lunar surface, while walking, skipping, and running are energetically preferable on Mars [3]. As speeds increase in lunar gravity, a transition occurs from walking to skipping rather than from walking to running as on Earth [95]. However, the energetically preferred speed is not always achievable or possible, and slower walking speeds may be necessary when performing EVA tasks.

Studying the walk-run or walk-skip transition gives further insight into ambulation on a planetary surface. Walking is modeled as an inverted pendulum which conserves some energy between each step; but energy is not conserved at faster walking speeds and needs muscular power input [32, 31]. Griffin et al. [62] found as gravity is reduced, the amount of mechanical energy conserved between each step is reduced, and the maximum energy recovery occurs at slower speeds. Ivanenko et al. [70] found that muscle activation and ground contact forces decreased with lower gravity levels, but kinematic coordination of the lower limbs were not affected by gravity levels. The Froude number is the ratio between the centripetal and gravitational forces in the inverted pendulum model, as shown in eq. 2.1.

$$Fr = \frac{v^2}{gL} \quad (2.1)$$

Where  $Fr$  is the Froude number,  $v$  is the velocity of ambulation,  $g$  is the gravitational force, and  $L$  is the leg-length [4]. At some critical value, walking is theoretically impossible as the gravitational force cannot match the required centripetal force, which is where the walk-run transition occurs ( $Fr^*$ ). Humans typically switch to running at  $Fr = 0.5$ . Kram et al. [82] offloaded subjects by their waist as they walked and ran on a treadmill, and found that  $Fr^*$  increases at lower gravity levels. The increase in  $Fr^*$  was hypothesized to be from the arms and legs not being offloaded and still under the influence of gravity [82]. Donelan and Kram [43] also found that elastic forces were unable to predict the dynamics of reduced-gravity running. This suggests that other factors may be at play with walking in reduced gravity.

Ambulating with the suit involves additional forces both applied by the suit, and applied by the user to control the suit. Newman and Alexander [102] suggested that energy may be expended at low speeds and lower gravity levels for stability and postural control for ambulation. Chappell [33] found that when the offload system was set to lock waist rotation for stability, subject's gait was constrained and showed changes in braking and propulsion force for Lunar gravity. Therefore, stability is an important factor in walking at lower gravity levels.

Carr and McGee [29] developed the Apollo number  $Ap$  to explain the effects of the space-suit's pressure forces on gait (eq. 2.2).

$$Ap = \frac{Fr}{M}, \text{ where } M \text{ is the mass ratio of the spacesuit.} \quad (2.2)$$

$M$  incorporates the self-supported weight of the spacesuit. The self-supported weight of the spacesuit is from the spacesuit's pressurization. Carr and McGee validated the Apollo number against gait events during Apollo missions, but found that the Apollo number did not fully explain the walk-skip transitions. **Therefore, a gas-pressurized spacesuit's mobility restrictions and joint mechanical work, along with its pressure forces, may also be affecting suited ambulation.**

## 2.2 Gas Pressurized Spacesuit Characteristics

### 2.2.1 An Inherently Stiff Structure

Gas pressurized spacesuits have been used for all EVAs throughout the history of human spaceflight. However, gas pressurized suits become stiff and rigid when pressurized, requiring great effort to bend. The first EVA spacesuit, the Gemini suit, did not include any design features to reduce bending effort [137]. If a gas pressurized suit component is represented as a pressurized cylinder, bending the cylinder along its axis causes a reduction in volume at the bend [65]. As a result, pressure at the bend will increase, causing resistance to the bending force. The force required to change the volume at the bend is presented in eq. 2.3 [101, 65],

$$F = \frac{W}{d} = \frac{\frac{p\pi D^3 \phi}{8}}{\frac{L\phi}{2}} = \frac{p\pi D^3}{4L} \quad (2.3)$$

where  $F$  is the force required,  $W$  is the work required,  $d$  is the distance the joint is flexed,  $p$  is the pressure,  $D$  is the cylinder's diameter,  $\phi$  is the joint deformation angle, and  $L$  is the length of the cylinder. It can be seen that the force required to bend a pressurized joint is not dependent on the bending angle, but rather the length and diameter of the pressurized section. Without dedicated

mobility features to maintain a constant volume at joints, the forces required to bend representative spacesuit components can be as high as 200 lbs for the waist joint [101].

### **2.2.2 Mobility Design Features**

Mobility design features allow for bending of a pressurized joint by creating a point at which the joint can buckle, and allowing the joint to maintain constant volume through the bending motion [65]. This greatly reduces bending resistance and allows for joint flexibility [65]. These mobility features typically feature some form of bellows or convolutes to maintain constant volume and axial restraints to prevent elongation of the joint under pressurization [65].

Mobility design features have been studied and iterated since the advent of space travel, but were not implemented in the Apollo mission suits. The Litton company built and tested spacesuits for EVA use in the 1950s, predating both the US and Russian space programs. These suits iterated on the use of convolutes by inventing the rolling convolute, annular convolute, and cardonic hard joint [65]. While these suits never saw operations on spaceflight, they did prove benefits in mobility over the International Latex Corporation (ILC) designed A7L suits, which were eventually used by US astronauts on the moon. The Litton suits were able to match the center of restraint and center of pressure when convolute joints were bent, reducing the bending torque and spring return force of the joint [65]. Therefore, the suit's operator is able to easily bend the joint and not exert much force to keep the joint bent. The A7L suit's convolute joints did not match the center of restraint and center of pressure, requiring operators to exert additional force to both bend the joint and keep it bent [65]. Such drawbacks of the A7L suit required astronauts to come up with clever workarounds. On an Apollo 16 EVA, astronaut John Young found that “by hopping into the air and landing on his feet, the weight of his suit overcame the suit’s internal pressure, so he could get to his knees and pick up rocks without using geological tools” [113]. Integrating convolutes into the A7L suits may have improved mobility on the Moon.

Advancements since the Apollo era have brought us improvements in pressurized joint design to increase mobility, including the toroidal mobility joint, dual-axis joint, hard component joints,

hybrid hard-component/fabric joints, and improvements to flat-patterned joints [65]. The Mark III Advanced Space Suit Technology Demonstrator EVA Suit (MK III) is a spacesuit designed by NASA as a planetary spacesuit design testbed [80]. These advancements have allowed for increased lower-torso mobility as shown in the MK III spacesuit technology demonstrator; operators are easily able to recover from a fall and kneel in the MK III while these tasks were done with much difficulty in the A7L and EMU spacesuits [79].

Lessons from EMU and MK III design were applied to the design of the new Z2 planetary spacesuit prototype. The Z2 prototype was first developed by NASA and ILC Dover in 2016 to demonstrate planetary surface exploration technologies, but parts of the Z2 suit are now being used for the Exploration EMU (xEMU), to supplement or replace the EMU for ISS EVAs [61, 93]. The Z2 also serves as the basis for the design of the Artemis spacesuits, which will be worn by the first crew to step foot on the Moon. The Z2 spacesuit features a larger scye opening and more mobile shoulder bearings compared to the EMU [61]. Tests of the Z2 in the NBL found range-of-motion and reach envelope improvements over the EMU, but many microgravity EVA tasks were reported to be harder and more limited in the Z2 [93]. Subjects also reported similar muscle fatigue and exertion ratings between the EMU and Z2 [93]. Larger subjects also reported discomfort in the shoulder area, further highlighting the importance of fit in spacesuit design [93]. Similar analysis needs to occur with ambulation to assess the effect of suit mobility improvements.

### **2.3 MK III Ambulation Performance**

The MK III spacesuit has been used to experimentally study suited effects on ambulation due to the Z2's relative novelty. In the EVA Walkback Test (EWT), six male subjects were tested with the MK III spacesuit on a treadmill to explore the effects of the MK III spacesuit's weight on planetary ambulation in Lunar (1/6g) and Martian (3/8g) gravity levels. Subjects were tested in three conditions: unsuited and offloaded to selected gravity level; unsuited and offloaded to selected gravity level with the suit weight matched; and suited while offloaded to selected gravity level [104]. This allowed for analysis of suit weight separately from other suit design factors on the

metabolic cost of suited ambulation. Subjects were tested at three speeds above and three speeds below their walk-run transition speed. All subjects also did a 1G baseline unsuited trial and a 10 km suited lunar ambulation. A follow-on integrated suit test (IST) examined the effects of varied suit mass, gravity, and on metabolic cost and kinematics on Lunar suited gait [103] with similar conditions while varying suit pressure and mass. These and similar tests provide insight into how the MK III's design factors affect suited ambulatory performance.

### **2.3.1 Cost of Transport Factors**

Metabolic cost of transport, a measure of how much energy the body is exerting during ambulation calculated through direct calorimetry [74], was collected in these tests across a variety of conditions. Metabolic cost is a direct measure of how hard the body is working to move in the spacesuit. Previous studies have shown that the metabolic cost of transport decreases with gravity [58]. Findings from the EWT and IST were consistent with these previous findings [104, 103]. Unsuited weight-matched metabolic costs were lower than 1G unsuited across all speeds for 1/8G ambulation and similar to 1G unsuited for 3/8G ambulation [104]. This suggests that without suit effects, ambulation on Mars may be metabolically similar to ambulating on Earth. However, the MK III increased the metabolic cost of transport for both gravity environments compared to the unsuited weight-matched condition [104]. At 1/6G, the MK III had a higher metabolic cost than Earth ambulation at lower speeds, but was less metabolically costly at higher speeds [104, 103]. The MK III was very metabolically costly in 3/8G, metabolic cost quickly approach maximal values for low speeds and subjects were unable to run in the suit at higher speeds [104]. The metabolic cost of weight (5%-13%) for both Lunar and Martian gravity levels was significantly dwarfed by the cost of suit design factors (87%-95%) [104]. From these results, its apparent that the MK III's design cannot service ambulation on Mars due to its design factors, but may be sufficient for the Moon.

Other suit design factors partially explained the increased metabolic cost of suited ambulation. The IST found increased suit pressure to minimally increase metabolic cost across all speeds, hypothesized to be due to the MK III's constant volume joints [103]. However, there were some sub-

jective differences in mobility noted across the different pressures, although there was no correlation to subject anthropometry [103]. The effect of suit weight, which encompasses gravity level and suit mass, steadily increased with speed [103]. The percentage of metabolic cost that was not explained by suit weight or pressure decreased as speed increased, but then increased at the fastest speed [103]. Additional factors which can explain the increased metabolic cost can include suit kinematics, stability, and harnessing effects from the gravity offloading, which may be causing more difficulty for ambulation at lower speeds. However, these factors were not isolated in the MK III ambulation experiments. The majority of ambulation during an EVA is most likely done at lower speeds, thereby requiring further understanding of how suit design is affecting mobility at low speeds.

### **2.3.2 Ambulation Biomechanics**

The IST captured little differences in kinematics as a function of pressure, which may be due to the constant volume joints [103]. However, it was noted that at 4.3 psi, the knee joint was limited by the design of the pressurized suit, and that the ankle increased its range-of-motion (ROM) to compensate the limited knee ROM [103]. This shows the importance of the kinematic chain in suited mobility; when a certain motion is inhibited, other joints along the kinematic chain will have to compensate. Similar compensation has led rotator cuff injury in the EMU's HUT [150].

Cullinane et al. [39] found suited MK III ambulation at 1G to reduce heel and toe clearance above ground compared to unsuited ambulation. In addition, the MK III was found to decrease speed, stride length, and step length compared to unsuited ambulation [39]. Cadence and stance time increased with gravity level in the IST, consistent with how metabolic cost increases with gravity level [103]. These findings suggest that the MK III inhibits operator mobility and agility when ambulating.

### **2.3.3 Subjective Feedback**

Subjective feedback allows operators of the MK III to provide their perception of ambulating in the suit. Rating of Perceived Exertion (RPE) and Gravity Compensation and Performance Scale

(GCPS) were consistent with metabolic cost findings in both the IST and EWT; both increased with gravity and speed [104, 103]. Subjects performing the 10 km suited lunar ambulation in the EWT reported “fair” to “moderate” operator compensation required to walk in the MK III on the Cooper-Harper Scale [104]. While mean rating of discomfort was “very low” to “low” on the Corlett-Bishop Scale, discomfort and trauma were noted on the knees and feet of some subjects [104] (fig. 2.1). In addition, muscular fatigue and tightness was also reported in the quadriceps, thighs, glutes, and lower back [104].

Subjective feedback for ambulating in the MK III at 1/6-g suggests that it is mostly acceptable for lunar ambulation. However, the reported trauma and musculoskeletal discomfort are areas of concern. The EWT and IST, along with findings from Cullinane et al. [39], show that the MK III’s design inhibits natural human motion and requires more effort during suited ambulation. It is not enough, however, to design a suit that more closely matches natural human motion; it also needs to work closely with its operator to reduce injury risk from poor fit.



Figure 2.1: Knee (left) and foot (right) trauma identified in the MK III following 10 km walkback evaluation. From Norcross et al. 2009

## 2.4 Spacesuit Fit

Spacesuit mobility needs to have matched spacesuit-operator interaction, primarily driven by spacesuit fit, to ensure the suit works with its operator. Proper spacesuit fit requires both correct sizing and correct indexing between the spacesuit and its operator. In addition, these factors must be maintained not only in a static pose, but through dynamic movements as well.

Static fit refers to the alignment between the operator and the spacesuit, while dynamic fit refers to the coordination of the operator to the spacesuit during motions [133]. Poor static fit leads to empty space around the operator, which allows the operator to move inside and repeatedly contact the spacesuit. However, improving static fit is not as easy as filling this empty space; this would hamper operator mobility and lead to poor dynamic fit and difficulty for the operator to move the suit. In addition, the effect of fit on suited performance is difficult to understand. Difficulty in both sizing the suit and ensuring that suit movements match operator movements may be further improved through body shape modeling.

#### **2.4.1 Spacesuit Sizing Process**

The Apollo EVA spacesuits were custom tailored for each individual, a feat achievable with the small number of astronauts needing EVA suits [65]. However, with a larger and more diverse astronaut corp, custom suits became infeasible. Currently, only the EMU glove is custom made if one which fits the astronaut does not exist [34]. NASA STD-3000 calls for spaceflight hardware to accommodate an anthropometric range from the 5th-percentile female to the 95th-percentile male [99]. The EMU suit was designed to target this range with modular and adjustable components. However, the EMU design only ended up fitting a 40th-percentile female to a 95th-percentile male [77]. In addition, it is not clear what measurement is used to define the population percentiles that the EMU fits.

Even with some adjustable sizing components in the EMU, it takes experienced suit engineers to select and adjust the size of EMU components to best fit the operator. Sizing rings are used in the EMU design to change the length of components like arms and legs [65]. Sizing inserts such as pads can also help position the operator within the spacesuit [34]. The length of restraint straps at convolute joints can be adjusted to change the length of soft components, but this affects joint mobility as the length-diameter ratio is modified [65]. Current suit fit processes do not use any objective measures to define proper fit; a baseline fit is prescribed from anthropometric measures

and then iterated through subjective feedback [49]. Fit is inherently difficult to objectively measure due to the challenges of measuring operator motion inside the suit.

#### 2.4.2 Quantifying Fit

Novel measurement technologies have been explored to measure operator motion inside the spacesuit as traditional optical motion-capture techniques cannot be used through the spacesuit. Pressure sensors can help quantify contact between the operator and spacesuit and highlight hotspots of contact which can indicate poor fit [8, 9, 10]. Inertial-measurement unit (IMU) systems aim to provide some insight into how the operator is moving relative to the suit [19, 50, 130]. Fabric strain sensors have also been developed to predict an operator's body-shape inside the spacesuit [77].

Fineman et al. [50] introduced two objective fit metrics which can help characterize poor static and dynamic fit in the spacesuit: difference in knee angle ROM between the suit and operator, and the relative coordination metric [51]. The relative coordination metric allows for the identification of whether the suit or the operator is driving the other component. Fineman et al. [50] measured these metrics with IMUs placed on the lower torsos of both the operator and the spacesuit. Three subjects walked in a spacesuit with different levels of padding, meant to mimic three different levels of fit. Two subjects had reduced knee ROM compared to unsuited ambulation. One subject had no significant differences in metrics between padding levels but reported better responsiveness with higher levels of padding. Another subject had the lowest knee ROM with no padding, aligning with their feedback that higher levels of padding are harder to control. Results from this study show how some performance metrics can measure the effects of varying fit, but also how fit is very subjective.

Suit fit engineers have commonly reported a dynamic fit problem where the heel lifts out of the boot during heel-off, as shown in Figure 2.2. This was also reported by one subject in Fineman et al. [50]. Data collected from Fineman's study shows that during heel-off, the suit appears to be driven by the operator at the calf. While this may suggest heel-lift, it does not corroborate the subjective reports of a gap between the operator's heel and the spacesuit's heel

as it cannot directly measure this gap. Fineman et al [50] suggests that boot fit may be very important to ambulating in the MK III spacesuit.



Figure 2.2: Heel-lift occurring during heel-off, as subjectively reported in the MK III. The poor fit and indexing in the boot and lower torso allows the heel to lift inside the boot during heel-off

#### 2.4.3 Body Shape Characterization to Improve Fit

NASA's Anthropometry and Biomechanics Facility (ABF) has focused on characterizing the human body as it relates to spacesuit fit. Linear measurements are traditionally used in sizing algorithms to determine a baseline suit fit. These linear measurements are then compared to linear measurements in the suit's design to determine appropriate sizing components. However, linear measurements do not always accurately represent a person's body shape [91]. Three-dimensional scanning can help accurately characterize body-shape to allow for virtual fit testing against 3D models of the suit. Boundary manikins can be generated which represent the extremities of accommodated anthropometry, and overlaid on 3D suit models to determine fit [91]. Virtual fit check metrics may include penetration depth, contact areas, and overlap volume [77]. Monte-

Carlo simulations of vast databases can also be virtually tested to find fit problems that may occur outside the boundary manikins [77].

However, static body shape may not be enough to ensure dynamic fit. It is well known that parts of the body change shape during movement. Capturing 3D-scans in multiple poses also allows for the development of a parametric models that can estimate how body shape changes with a specific movement; for example this can be used to check for shoulder clearance around the HUT [78]. This can greatly improve dynamic fit as it ensures the HUT accommodates the shoulder throughout its entire motion. However, this methodology is limited to poses where the subject can pause between motions due to technological limitations for capturing dynamic body shape changes.

Body shape changes can also occur from exposure to an altered-gravity environment. The ABF found on average posture to increase by a maximum of 3%, hip circumference to decrease by a mean of 7%, and thigh circumference to decrease by a mean of 10% during microgravity spaceflight [77]. EMU sizing incorporates a 2.54cm increase in torso length to accommodate this change [138].

Information from virtual fit testing can be incorporated into spacesuit design by informing where the internal geometry may need to be expanded or contracted to better fit the target population [77]. This process was used to validate the design of the Z2 suit. However, it is virtually impossible to incorporate personal preferences of fit into this process; currently a threshold is implemented to determine acceptable levels of ease or compression [77]. In addition, modifying design to accommodate findings from fit can only be done to a certain extent; there are limitations on modifying the structure of an existing design while still meeting the same engineering requirements. There are also no clear metrics for translating virtual fit testing into spacesuit component design, and current methodologies are limited to modifying the design of existing components rather than designing new components from the ground-up.

## **2.5 Summary**

Ambulating on another surface and gravitational environment presents many challenges of its own, including changes in preferred gait patterns. Wearing a stiff, pressurized spacesuit further

increases the effort required to walk. While constant volume joints may reduce pressurization effects, unquantified factors such as poor operator-spacesuit interaction may also be leading to injury. Spacesuit fit is hard to characterize due to limited knowledge of in-suit motion and challenges including limited suit sizing components, limited suit design flexibility, an incomplete understanding of body shape changes, and lack of quantifiable metrics to validate fit. Poor fit can reduce performance and lead to injury. Ambulation specific fit issues, such as heel-lift, have been subjectively identified in the MK III but not fully quantified. While there has not been a large scale study on injuries in the MK III, these fit issues are similar to the injury mechanisms leading to injury in the EMU.

Body-shape models have been proposed as a way to better fit operators to spacesuits. Static body shape models allow for correctly sized spacesuit components to be selected and spacesuit component designs to be validated for accommodation of a target population. Dynamic body shape models will ensure that dynamic fit is ensured throughout suit motions, but current technology is limited to capturing low-frequency motions. In addition, there is no established framework for integrating dynamic body-shape models into the spacesuit design process. Suit components designed around dynamic body shape models have not yet been tested for increased fit and comfort compared to traditionally designed and fitted suit components.

## Chapter 3

### Investigative Approach

The following gaps were identified from the previous research, as outlined in the literature review presented in the previous two chapters, and motivate the direction of this thesis.

- **Gap 1:** Few efforts to quantify fit discrepancies

- \* Subjective reports are currently used to identify fit discrepancies. While objective fit metrics can indicate decreased performance from poor fit, they cannot identify or confirm specific indexing discrepancies between the operator and spacesuit to support these specific reports.

- **Gap 2:** Limited knowledge on dynamic body shape changes due to motion

- \* Current modeling of dynamic body shape relies on 3D capture of subjects pausing through the motion and interpolation of body shape between pauses. Technological challenges make it difficult to optically capture dynamic body shape changes where the subject cannot pause between the motion, such as during walking. Therefore, the lack of data makes it difficult to model these dynamic body shape changes.

- **Gap 3:** No existing framework for incorporating dynamic body-shape models into the spacesuit design and fit process

- \* It is unclear how dynamic body shape models can be incorporated into both the design of spacesuit components, as well as used to virtually fit test proposed spacesuit

components. Current efforts have proposed ways to modify currently designed space-suit components, but not ways in which spacesuit components can be designed from scratch around dynamic body shape models.

- **Gap 4:** No studies to quantify the effect of using dynamic body-shape models over linear measurements on fit and mobility
  - \* Spacesuit components designed around body shape models have not been tested against traditionally design spacesuit components to show that they result in better fit and mobility.

This proposed thesis will investigate the applicability of dynamic body shape models to improve fit and mobility for planetary EVA suit design. To limit the scope of the work, the proposed work will focus on fit and mobility of the spacesuit boot. The MK III spacesuit currently uses a pressurized modified hiking boot with a convoluted ankle joint and boot sizing inserts. The boot is an important component for MK III ambulation and MK III boot fit has been identified as a key issue in suit fit, especially with the subjectively reported instances of heel-lift [50]. While the thesis will focus on the foot-boot interface design, the novel contribution lies in the development of a experimental and design framework to translate body-shape changes into spacesuit design variables. The proposed hypothesis of this work is therefore:

**Integrating dynamic body shape changes into the spacesuit boot design process will mitigate factors that lead to injury and improve compatibility between the operator and the spacesuit.**

The proposed thesis will encompass the following specific aims:

- **Specific Aim 1:** Quantify instances of heel-lift in spacesuit gait
  - \* **Motivation:** Heel-lift was subjectively reported as a potential symptom of poor fit during gait in the MK III, but was never quantified. Quantifying the frequency and magnitude of heel-lift can help understand the interactions between the human's foot and the spacesuit boot.

- \* **Summary of Work:** Vertical accelerations of the spacesuit's lower leg and operator's tibia were analyzed from IMU data collected on in the MK III suit by Fineman et al. [50]. Differences in heel-off times between the human and spacesuit were used to characterize heel-lift instances. Drift correction techniques were implemented and evaluated to reduce error in integrating acceleration data to positional estimates. Results from both these analyses, however, suggest that IMUs may not be appropriate for quantifying heel-lift magnitude and frequency.
- **Specific Aim 2:** Predictively model dynamic changes in foot morphology during gait
  - \* **Motivation:** The foot changes shape during the loading process of stance phase. Modeling these changes as they relate to subject anthropometry and kinematics will allow for prediction of dynamic foot shape during stance phase.
  - \* **Summary of Work:** A novel dynamic foot scanning system was developed to capture 4D foot scans from subjects walking on a treadmill. Dynamic foot scans were captured from thirty subjects as they walked on the treadmill. A predictive statistical shape model was developed to predict dynamic foot shape with an accuracy of 5.2 mm. From the model, the arch was found to drop in height through stance phase, and rise just prior to toe-off. An additional analysis to assess the relationship between arch height measures and subject anthropometries found little correlation, and therefore suggested that dynamic arch height measurements are highly subject specific.
- **Specific Aim 3:** Define and validate a design process integrating dynamic foot morphology data for a novel spacesuit boot
  - \* **Motivation:** Existing knowledge on foot mobility can provide mobility requirements for a planetary spacesuit boot. Insight from the dynamic foot shape model can be integrated with these mobility requirements to develop a boot design that accommodates the mobility and dynamic shape of the boot.

- \* **Summary of Work:** Mobility of the foot was characterized from the existing literature. A biomechanical design framework was developed to integrate these mobility requirements with the dynamic foot shape model developed in Specific Aim 2. This framework was then used to inform the design of a novel spacesuit boot by implementing a novel lacing feature which accommodates variability in arch height. The pressure bladder for a novel spacesuit boot accommodating this design feature was constructed, and tested to achieve a pressurization of 3.0 psi.
- **Specific Aim 4:** Evaluate the prototype planetary spacesuit boot design for fit, comfort, and mobility
  - \* **Motivation:** The planetary spacesuit boot design developed in Specific Aim 3 will be tested for improved fit and comfort as compared to a current MK III spacesuit boot design and a non-pressurized standard work boot. This will directly test the hypothesis of this thesis.
  - \* **Summary of Work:** A pressurization interface around the subject's calf was constructed for both spacesuit boots to be tested. The test subjects performed heel-lift and walking motions in the all tested boots. A force sensor was integrated into the boots to measure heel contact through the motions. Subject discomfort and exertion was evaluated for each of the boots through surveys.

### 3.1 Expected Outcomes

This thesis presents a process to design spacesuit components with improved fit and comfort. This process starts with understanding human-spacesuit interaction, then modeling dynamic body-shape changes at the area of interest, applying the body-shape changes to spacesuit design, and testing the resultant spacesuit component. This thesis outlines how this process has been applied to the spacesuit boot in the context of planetary walking. It is expected that the findings from the specific aims can be translatable to other spacesuit components of interest, which can follow a

similar process to improve fit and comfort. Future work will be required to assess how the findings from this thesis may need to be modified for applications to other spacesuit components.

## Chapter 4

### Specific Aim 1 : Challenges in Quantifying Heel-Lift during Spacesuit Gait

#### 4.1 Introduction

Ground-based testing of the Mark III Advanced Space Suit Technology Demonstrator EVA Suit (MK III) has resulted in subjective reports of heel-lift, where the operator's heel rises inside the boot before the boot's heel lifts off the ground at heel-off[50]. Heel-lift can be represented as a lag between the operator's and spacesuit's heel-off times, and is an indicator of improper fit; the statically-determined indexing between the operator's and spacesuit's ankle joints does not allow for dynamic alignment during heel-off. Since the foot freely moves within the boot during heel-lift, this could lead to injury through excessive contact or ankle joint overuse when taking a step. Foot contact injuries and discomfort were reported during simulated planetary walkback testing with prototype boot designs[34]. Designing a planetary spacesuit boot to mitigate heel-lift requires a quantitative understanding of its presence and magnitude. However, heel-lift has only been subjectively reported by spacesuit operators and has yet to be quantified through in-suit motion measurement techniques.

Various sensor technologies have been used to estimate relative motion between the spacesuit and operator, including pressure sensors[34], strain sensors[145], and inertial measurement units (IMUs)[19, 50]. IMUs measure acceleration, angular velocity, and magnetic field; estimating orientation from these values. IMU Spacesuit applications include Fineman et al.'s[50] analysis of in-suit lower-body angular velocities of subjects walking with the MK III spacesuit, and Bertrand et al.'s [19] estimation of in-suit upper-body joint angles during isolated joint motions. IMUs can detect

heel-off points during gait[52, 116], and therefore may be able to identify heel-lift instances where spacesuit heel-off lags operator heel-off. However, IMUs can be subject to error in their orientation estimates due to the magnetic field inside the spacesuit environment, and integration drift when calculating linear displacement and velocity quantities from acceleration measurements. Digital filtering methods, zero-velocity (ZVUs), and zero-position updates (ZPUs) have been used in the biomechanics field to correct for integration drift at every step [48, 116] but these methods have not been evaluated in their ability to be robust against spacesuit-environment induced error.

Therefore, this work aimed to evaluate the ability of IMUs, ZVUs, and ZPUs to quantify the frequency and magnitude of heel-lift in the spacesuit. Heel-off times were detected using spacesuit lower leg and operator shank IMU data during suited walking trials. Delayed spacesuit heel-off times compared to operator heel-off times were identified as potential occurrences of heel-lift. Then, ZVUs and ZPUs were evaluated for their ability to reduce integration drift and reliability quantify the heel-lift magnitude.

## 4.2 Methods

### 4.2.1 Data Collection

Experimental data collected by Fineman et al.[50] was reanalyzed for this study. Subject naming was kept consistent with Fineman et al.[50] for cross-reference of results, with subjects numbered 2-4 as Subject 1 did not complete all trials. IMUs were placed on corresponding locations on the lower body of the spacesuit and operator, and different levels of internal padding were placed at the knee and hip (fig. 4.1). It is assumed that the IMUs' x-axis was aligned with the long-axis of the shank and SLL; this axis was considered the vertical task axis. Three subjects walked in the MK III spacesuit along a 10m walkway in each of four conditions: unsuited, MK III with no padding (configuration 0), MK III with one padding layer (configuration 1), and MK III with two padding layers (configuration 2. All subjects wore the same size MK III lower body assembly, but Subject 3 wore a BOA-laced boot with fit adjustment at the tongue and heel, while other subjects

wore a standard strap-laced boot with only tongue fit adjustment. This work only analyzed a total of 216 suited trials, each with data from the left and right sides of the operator and spacesuit, yielding 432 datasets to analyze. Data from Subject 2's left leg during configuration 2 was not included due to data loss from the IMU.

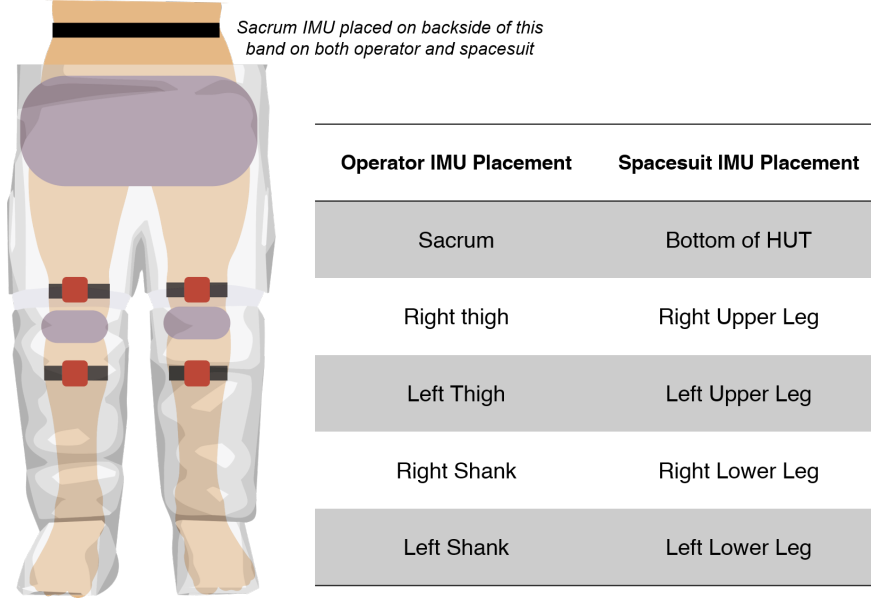


Figure 4.1: Location of IMUs (red squares, placed both the spacesuit and operator) and padding (gray). The sacrum IMU is placed on the back of the operator and spacesuit, where the upper-most black band is located, and is therefore out of view in this diagram. The table on the right outlines the IMUs corresponding locations between the operator and spacesuit.

#### 4.2.2 Data Analysis

The IMUs' vertical acceleration along the shank and SLL's long axis, and the IMUs' pitch angle data were analyzed. It was assumed that the shank and SLL have a rigid connection to their respective ankle joints. Therefore, the difference between the shank's and SLL's vertical position taken after the operator's heel-off time is the magnitude of heel-lift. Data analysis focused on isolating each individual step from the dataset, detecting heel-off points for the operator and spacesuit, and then implementing drift correction techniques to measure the vertical position of the shank and SLL.

Individual steps in each trial were identified to begin analysis. The shank and SLL IMUs' pitch angles were smoothed using a 10-sample window moving average filter. Individual steps for

each trial were then identified by detecting peaks in each IMU's pitch angle, corresponding to the max posterior flexion/extension of the shank/SLL during swing phase. Each step was defined as the time between each step's max extension to the following step's max extension. The first and last peaks of the trial were removed from further analysis to ensure only complete steps were analyzed.

Foot-flat phase, where the foot is flat between toe-strike and heel-off, was identified to discriminate heel-off events. This phase is characterized by near-zero anterior-posterior acceleration; since the foot is flat on the ground, there is very little vertical movement of the shank[116]. Raw shank and SLL IMUs' vertical acceleration data was preprocessed for foot-flat detection by detrending to remove bias by removing the best straight-fit line from the data vector. A 30-sample window moving average filter, equivalent to 0.23 seconds, was then used to remove noise, within the range used for walking-speed estimation[25].

Discrete wavelet transforms (DWT) were used to detect gait events from acceleration signals[71]. A 3-level DWT was applied to the preprocessed shank and SLL anterior-posterior acceleration signals. A Symlets 2 wavelet was then used as the mother wavelet for the transform, due to its high performance in detecting initial-contact and final-contact points during stance phase[71]. After transforming to wavelet space, a threshold was applied where values below 2% of the maximum wavelet coefficient were set to zero. The wavelet coefficients were then reconstructed back into a signal and used to detect foot-flat phase.

Foot-flat phase was detected by looking for the zero regions in the shank and SLL's acceleration's derivative<sup>10</sup>. A threshold of  $0.01m/s^3$  was set to account for small amounts of noise in the DWT signal. Acceleration points within this threshold were identified as zero-acceleration points. Zero-acceleration points less than 3-samples long were removed, since foot-flat phase is expected to be much longer. Fig. 3 shows an example of isolating foot-flat phase from DWT transformed signals. The difference in shank and SLL heel-off times was used to detect instances of heel-lift; a positive value corresponds to operator heel-off prior to spacesuit heel-off, suggesting heel-lift. Heel-off lag times  $<-0.2s$  and  $>0.2s$  were manually inspected, and if detection times were visually

noted to be misaligned with the zero-acceleration period, these steps were removed from analysis. A total of 32 of the 1381 steps met the criteria for removal.

The vertical acceleration signals from the IMUs are subject to integration drift when converted into positional estimates using double-integration. The raw vertical acceleration signals were preprocessed by a 10 Hz low-pass filter to remove high-frequency noise[13]. Zero-velocity (ZVU) and zero-position updates (ZPU) were used to reduce integration drift and improve the accuracy of the positional estimate of the shank and SLL. It is assumed that the shank and SLL's vertical velocities were zero just prior to heel-off, when the operator and spacesuit are in stance phase. Using this assumption, a linear correction is applied retroactively for each step between heel-off times. At the identified heel-off times, the vertical velocity was set to zero, and the vertical velocity during the step prior to heel-off was subtracted by the velocity reported at heel-off weighted based on the distance from the heel-off timepoint. The following step's vertical velocity was then corrected to the heel-off velocity. This process is summarized in eq. 4.1:

$$v'_{x,i} = v_{x,i} - v_{HO} * \frac{t_i - t_{TS}}{t_{HO} - t_{TS}} \quad (4.1)$$

where at timestep  $t_i$ ,  $v'_{x,i}$  is the corrected velocity,  $v_{x,i}$  is the original velocity,  $v_{HO}$  is the velocity at heel-off,  $t_{HO}$  is the previous step's heel-off timepoint, and  $t_{HO}$  is the current step's heel-off timepoint. Integrating the corrected velocity signal to obtain the IMU's position can similarly be subject to integration drift. It was assumed during stance phase that both the operator's foot and the spacesuit boot are flat on the ground and therefore the shank and SLL are not moving vertically. ZPUs can use this to correct for drift by zeroing the position estimate for both the SLL and shank at heel-off. The shank and SLL were assumed to be rigidly connected to their respective ankle joints. Heel-lift magnitude can be then defined as the vertical displacement difference between the shank and the SLL at the SLL's heel-off timepoint.

Drift is not completely eliminated with the outlined methods. An upper bound was calculated to inform the time limit past the heel-off correction point where heel-lift magnitude can be quantified with confidence that the magnitude is not largely due to drift. While drift is not a linear process,

an assumption was made that calculating the drift magnitude between two known timepoints, and dividing by the elapsed time, would be a reasonable approximation to quantify how drift accumulation. During stance phase, it was expected that both the SLL and shank would have the same vertical position at toe-strike and heel-off. During swing phase, it was expected that both IMUs would return to the same vertical position after each step. Drift magnitude was calculated for each detected step by subtracting the post-ZVU/ZPU position values at the beginning and end of stance phase and swing phase from each other, and then dividing by time of each phase, to average drift rate. This rate represents the amount the IMU's positional estimate has drifted over each phase following correction from ZVU/ZPUs, when it is expected to return to zero. Analyzing the distribution drift rates across all trials allowed for the upper time-bound to be defined where drift magnitude is minimal and can ensure accuracy in the calculated position values.

### 4.3 Results

Figure 4.2 shows the distribution of heel-off lag measurements across conditions, subjects, and sides. Subject 2 experienced spacesuit-delayed heel-off in 97 (20 left, 77 right) out of 382 (151 left, 231 right) total steps. Subject 3 experienced spacesuit-delayed heel-off in 305 (155 left, 150 right) out of 410 (204 left, 206 right) total steps. Subject 4 experienced spacesuit-delayed heel-off in 45 (21 left, 24 right) steps, and operator-delayed heel-off in 226 (87 left, 139 right) steps out of 481 (237 left, 244 right) total steps.

Mean drift rates after correction for both the SLL and shank IMUs are presented in table 4.1. An upper confidence bound of 0.03 s (1/32 cm/s) was found to take a heel-lift measurement with an accuracy of 1cm, based on the mean shank IMU swing phase. Average step duration across all trials was  $1.6 \pm 0.2$  s; therefore drift accumulated over 1 cm on average within 2% of the step duration.

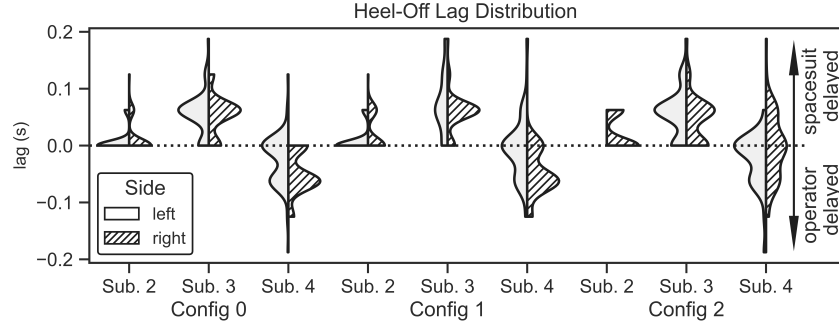


Figure 4.2: Heel-off lag distributions between all subjects and configurations, with discrete heel-off lag measurements being represented as black dots. Positive lag values are indicative of spacesuit-delayed heel-off, while negative lag values are indicative of operator-delayed heel-off

Table 4.1: Drift rate estimations (mean +/- std dev) of raw, filtered, and post-ZVU/ZPU positional estimates for IMUs mounted on the spacesuit lower leg assembly and shank

Phase	IMU	Raw	ZVU/ZPU
Stance	Shank	$43 \pm 63 \text{ cm/s}$	$5 \pm 6 \text{ cm/s}$
	SLL	$241 \pm 130 \text{ cm/s}$	$16 \pm 11 \text{ cm/s}$
Swing	Shank	$67 \pm 59 \text{ cm/s}$	$32 \pm 16 \text{ cm/s}$
	SLL	$265 \pm 103 \text{ cm/s}$	$66 \pm 40 \text{ cm/s}$

Heel-lift magnitude was not calculated due to the operator-delayed heel-off lag noted in Subject 4, and high drift rates following correction resulting in a low upper time-bound for calculating heel-lift magnitude after heel-off.

#### 4.4 Summary

This study aimed to evaluate the use of IMUs with ZVUs and ZPUs to quantify heel-lift in spacesuit gait. Methods were demonstrated to determine heel-off points on the shank and SLL IMU; where a lag in the spacesuit's heel-off point compared to the operator's heel-off point would suggest heel-lift. All subjects experienced varying amounts of spacesuit-delayed heel-off across conditions, with no noticeable effect from padding. Subjects 2 and 4 had more counts of spacesuit-delayed heel-off on their right compared to their left side (Subject 2: 33% vs. 13%, Subject 4: 57% vs. 37%), suggesting a looser boot fit on their right side. Heel-lift was subjectively reported only by subject 26. Only subject 4 experienced operator-delayed heel-off. Examples of both operator-delayed and spacesuit-delayed heel-off are shown in fig. 4.3.

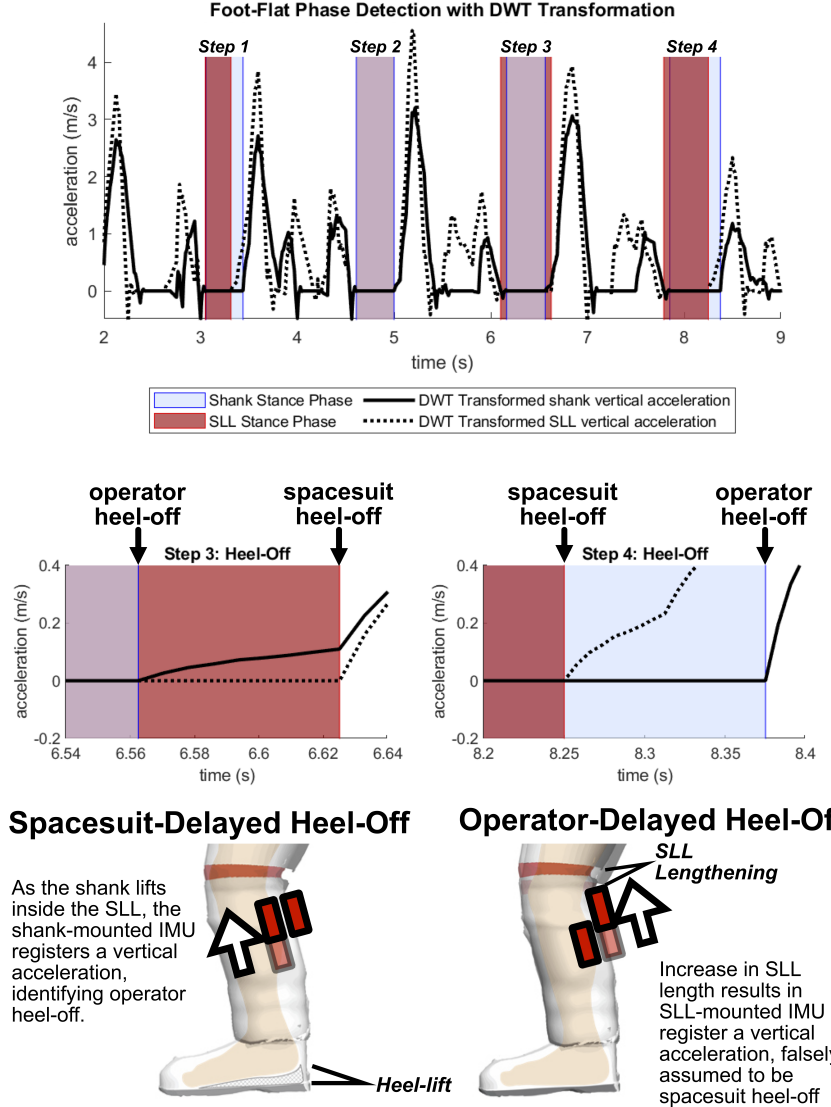


Figure 4.3: (Top): DWT IMU vertical acceleration data for shank and SLL. Shaded regions represent the detected foot-flat phases of zero-acceleration regions for each step. (Middle) Zoomed-in view of the foot-flat phase for two steps, with annotated spacesuit and operator heel-off points. When the shank IMU registers a vertical acceleration in foot-flat phase prior to the SLL IMU (middle-left), this could suggest heel-lift (bottom-left). When the SLL IMU registers a vertical acceleration in foot-flat phase prior to the shank IMU, this would ordinarily suggest that the SLL experiences heel-off prior to the operator (middle-right). However, there may be pressure forces which allow the SLL to extend, registering a vertical acceleration for the SLL-mounted IMU and falsely suggesting that the spacesuit is experiencing heel-off (bottom-right).

integrated along non-bending components such as the SLL [65]. Therefore, the initial assumption that the SLL is rigidly connected to the boot is broken. False-positive vertical accelerations due

to segment lengthening are not a concern for the shank-mounted IMU, as the shank and ankle are rigidly connected and the IMUs are assumed to be rigidly strapped to their segments. While soft-tissue artifacts may be present, they are likely of a much smaller magnitude. The SLL may be expanding in length for Subject 4 at heel-off, causing the IMU mounted on the SLL to register a positive acceleration prior to the operator. Subject 4 wore the same size suit lower assembly as other subjects but had larger crotch and knee heights. As such, there would be more room in the lower leg assembly for the soft goods to expand, providing a possible explanation for why only Subject 4 experienced operator-delayed heel-off.

A tighter boot fit, where the heel stays indexed in the boot, allows the operator to overcome expansion forces that push the SLL down, resulting in the SLL extending upwards and registering as operator-delayed heel-off. In contrast, loose boot fit will not allow the operator to overcome these forces, and will push the boot down, keeping it on the ground and registering as spacesuit-delayed heel-off. Fineman et al [50] summarized that Subject 4 had synchronous motion of the shank and SLL between heel-off and toe-off; Subjects 2 and 3 had motion driven by the suit, suggesting heel-lift. Data from this study similarly suggests that Subjects 2 and 3 experienced more instances of spacesuit-delayed heel-off than Subject 4. Therefore, Subject 4 may have had a tighter boot fit as indicated by operator-delayed heel-off, and operator-delayed heel-off may serve as an indicator for tighter boot fit.

Findings from this study suggest that current IMU technology and drift correction techniques alone may not be appropriate for quantifying the presence and magnitude of heel-lift in the spacesuit environment. Drift evaluation showed that the SLL-mounted IMUs had higher drift rates than the shank-mounted IMU. Potential sources of increased drift could be effects from the SLL segment's soft-goods expansion and contraction [50, 65], resulting in different frequency components compared to the shank's movement. While ZVUs and ZPUs did substantially reduce drift in stance and swing phase, drift was still present in this study. Heel-lift magnitude measurements could not be taken with confidence that magnitude differences would be due to heel-lift. Future work may explore the extent of soft-goods expansion on spacesuit kinematics analysis, which may affect positional

estimates from optical motion capture. IMUs have been shown to measure spacesuit angular kinematics with a root-mean-squared error of 4.8-5.8 degrees[19] and were used to characterize relative angular coordination within the suit[50], but have not been evaluated for accuracy in spacesuit positional estimates as conducted in this study. Suit components should only expand longitudinally, and should therefore not affect angular estimates[65]. Other sensing modalities or improvements to IMU mounting may be more appropriate in quantifying the vertical displacement that defines heel-lift.

Characterization of in-suit motion will be required to develop comfortable and safe planetary EVA spacesuits. This study highlighted the challenges of using IMUs to measure in-suit motion, concluding that IMUs may not be appropriate for measuring in-suit displacement at the magnitude expected during heel-lift. The primary assumption that the SLL was rigidly connected to the ankle joint was not supported; the observed operator-delayed heel-off suggests that the SLL is vertically extending during gait. Fineman et al [50] hypothesized that lower-body relative coordination may be affected by boot fit issues. Future work can characterize SLL extension throughout the gait cycle, further understanding the forces acting on the SLL due to fit. Sensor technologies can also be evaluated to study heel-lift, such as resistive or capacitive force sensors mounted under the heel to directly measure heel contact, or strain sensors mounted between the human and suit to measure displacement. Such methods can be used to evaluate spacesuit components susceptible to injury, such as the gloves or upper torso[34]. IMUs can be mounted directly to the boot to isolate ankle kinematics from SLL lengthening and accurately detect heel-off points using the presented methods and assumptions. Force plates can directly identify spacesuit heel-off points, therefore not requiring suit-mounted IMUs. Developing and evaluating various in-suit motion measurement techniques will help improve spacesuit design and fit, reducing the risk of injury and ensuring mission success for future planetary EVAs.

## **Chapter 5**

**Specific Aim 2: Predictively model dynamic changes in foot morphology during gait**

### **5.1 Introduction**

Designing a new spacesuit boot to be more comfortable and not be subject to fit issues like heel-lift, requires a thorough understanding of foot shape. However, foot shape is known to be highly variable throughout the population, including by sex [154, 83, 84], age [139], and weight [114]. This variability is often not captured in terrestrial footwear sizing, as current fitting standards only use foot length, foot width, and arch length to fit to standardized shoe sizes [14]. Furthermore, terrestrial footwear is commonly designed around lasts, shoe molds that are sized and shaped by each manufacturer with no common standard. This leads to variability in footwear shapes and sizes [72, 146], making it hard for consumers to find a proper fit and resulting in users having to wear ill-fitting footwear with suboptimal comfort and being at risk of occupational injury during ambulation [41]. Footwear fit and comfort has shown benefits in increasing biomechanical performance [115], reducing the risk of movement-related injury [98], and is often the number one factor for consumers to select footwear [92]. Therefore, the issue of footwear fit and comfort is not just limited to spacesuit boots, both terrestrial footwear and spacesuit boots should account for the wide variety of foot shapes to improve fit.

In addition to foot shape variability in the population, the foot also changes shape while being loaded during gait. The current methodology of designing terrestrial footwear uses static lasts, assuming that the foot consists of rigid segments. Assumptions of rigid foot segments during foot

loading have shown inaccuracies in estimation of ankle joint mechanics [157, 76]. Evidence has been presented on articular motion within the foot as it is loaded [86, 153], and that foot loading affects linear foot measurements, such as when transitioning from sitting to standing [155, 105] or during the stance phase of gait [81, 15, 60]. The dynamically changing measurements suggest morphological changes occurring, all of which may not be captured in static linear and circumferential measurements. Thus, footwear should also be designed to account for these dynamic foot shape changes.

Statistical shape models (SSMs) can explain morphological differences across populations and during motion by identifying shape modes which account for variance from the mean shape. These have been developed for whole-body digital human modeling applications to study population and individual variance in body shape [5, 12, 119, 108, 109]. Parametric SSMs are extensions which use correlations between subject anthropometric data and SSM deformations to help predict body shape for new individuals in the population [108, 109]. The ABF at NASA developed parametric SSMs to characterize shoulder shape deformation across the shoulder's range-of-motion, predicting shape as a function of shoulder orientation, to validate HUT design [78, 77]. However, the technology used to capture the body scans for this SSM could not capture the dynamic natural motion of the shoulder; subjects had to pose their shoulder at specific orientations while a scan was taken.

The aforementioned efforts to capture foot measurement changes over the gait cycle did capture 4D foot images [15, 60], but these efforts focused on extracting changes in foot measurements and not volumetric predictions of foot shape. SSMs have recently been applied to characterize static foot shape across a population [37] and recognize foot-shape deviations [131, 129], but these efforts were not predictive. Previously developed systems were based on a catwalk, requiring subjects to correctly hit the scanning area for a successful data capture, which may not be representative of natural cadence. However, the systems used to capture 4D foot shape are very expensive and cannot be used around a treadmill, which allows for subjects to fall into natural gait. Therefore, no SSMs have been developed from previous capture of 4D foot scans to predict dynamic foot shape.

Therefore, the objectives of this specific aim are:

- Develop a low-cost 4D scanning system capable of capturing foot shape around a treadmill
- Create a predictive model of foot shape changes across the dorsal surface during stance phase
- Identify specific areas of the foot that change shape during stance phase
- Correlate changes in foot shape across large-scale population foot measurements

## 5.2 DynaMo: Dynamic Body Shape Capture with Intel RealSense Cameras

A low-cost 4D scanning system, DynaMo, was developed to capture dynamic foot shape during gait. Human body shape can be captured with a variety of methodologies, including laser lines, structured light, photogrammetry, and millimeter waves [40]. However, these technologies require expensive modules and have limited ability to capture dynamic changes in body shape. Motion capture with specific markers is commonly done through camera-based motion tracking [151] These systems for marker tracking are often cost prohibitive and unable to capture surface morphology.

Therefore, the DynaMo software library was developed to use multiple commercial depth cameras, the Intel RealSense DXX Depth Cameras (Intel, Santa Clara CA), retailing between \$150-\$200, to capture dynamic body shape changes. The Intel RealSense Depth cameras use two stereo image sensors along with a structured light projector to capture depth maps at 90 frames-per-second; each pixel in a depth map records the distance from the camera to the world. DynaMo includes functions to calibrate a capture volume, using a checkerboard to identify a common origin between multiple depth cameras (fig. 5.1). DynaMo calculates a common point cloud from the depth maps of all the connected cameras, outputting a point cloud for every frame captured by all connected cameras (fig. 5.2). Functions were also developed to track the position of reflective markers in the scene. The development of DynaMo was published in a journal paper [21].

A post-hoc accuracy analysis was conducted on the DynaMo software and Intel RealSense D415 cameras. A shoe last with a corresponding 3D digital model was placed in the capture volume between all cameras, and scanned 10 times. The last was removed and replaced in the

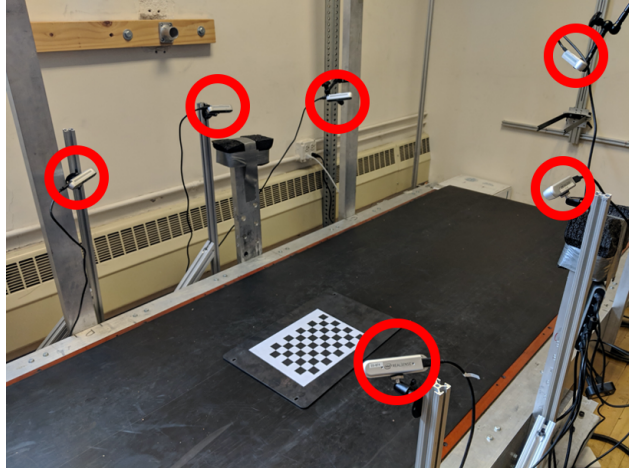


Figure 5.1: Capture setup of 6 Intel RealSense D415 Depth Cameras (circled in red) placed around a treadmill. The checkerboard shown was used to calibrate the cameras using the DynaMo package.

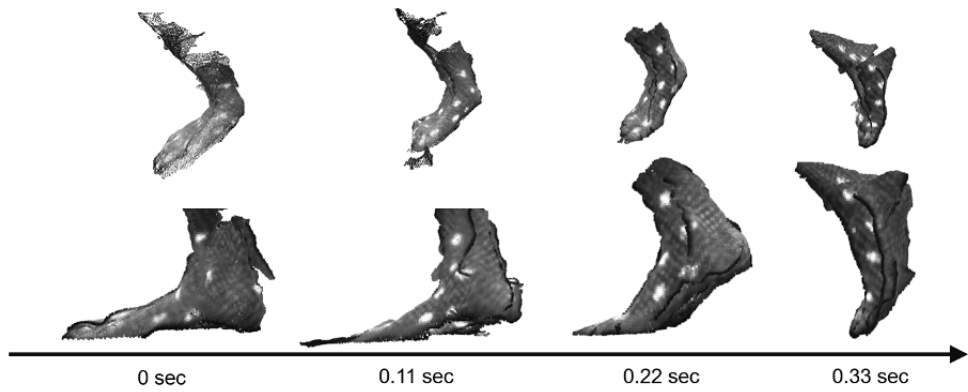


Figure 5.2: Sample frames, shown in 10 frame intervals (bottom), collected by DynaMo showing dynamic shape capture of the foot (top) at 90 frames-per-second, and the capture of reflective markers on the foot shown as white dots

volume between each scan. Root-mean-squared error was then calculated between each resulting 3D scan, and the 3D digital model, and was found to be 2.5 /pm 0.5 mm.

### 5.3 Development of a Predictive Dynamic Foot Shape Model from Statistical Shape Modeling

The DynaMo software [21] allowed for a capturing of foot shape to develop a parametric SSM. This system captures foot morphology changes during loading and unloading on the foot's dorsal surface, but does not capture of the foot's plantar surface. A parametric SSM was developed which can characterize and predict dynamic foot morphology at specific points during stance phase across the subject population.

#### 5.3.1 Methods

##### 5.3.1.1 Subjects

A total of 30 healthy subjects (15 men and 15 women, ages  $23.1 \pm 3.7$ ) participated in this study. Subjects were recruited in a stratified sample into one of six groups (5 subjects per group) to maximize variance in population foot length. Height was used as the grouping factor since height is well correlated to foot length [56]. The general population may not know offhand their exact foot length, and shoe size varies by manufacturer and does not correspond directly to foot length [72, 146]. Groups consisted of 5th-35th, 35th-65th, and 65th-95th height percentiles for each sex. Height percentile values were taken from the ANSUR II survey [57]. Population recruitment groups are summarized in *tbl. 5.1*.

Table 5.1: Enrollment groups based on reported height. 5 subjects were enrolled in each group

Sex	5th-35th percentile Height	35th-65th percentile Height	65th-95th percentile Height
Female	4'11"-5'3"	5'3"-5'5"	5'5"-5'8"
Male	5'4"-5'8"	5'8"-5'11"	5'11"-6'2"

Prior to recruitment, subjects completed a prescreening survey to ensure they were adequately healthy by the American College of Sports Medicine guidelines [120], and between the ages of 18-65. Subjects provided their sex and height, and were only enrolled in the study if their population group was not fully enrolled.

### **5.3.1.2 Experimental Procedures**

The experimental protocol was approved by the University of Colorado Institutional Review Board. Procedures were explained to each subject and written consent was obtained prior to participation. Subjects' height and weight were recorded with a tape measure and scale, respectively. Subjects' foot length, foot width, and arch length were measured with a Brannock device (The Brannock Device Company, Liverpool, NY) [14]. Both foot length and arch length were measured in centimeters. Foot width was measured as an ordinal size (e.g. A, B, C, D, E), and then converted to a linear measurement in centimeters (The Brannock Device Company, Liverpool, NY).

Six Intel RealSense D415 Depth Cameras (Intel, Santa Clara, CA) were placed and calibrated around a custom-built level treadmill in the University of Colorado Boulder Locomotion Laboratory, as shown in fig. 5.1. The treadmill was set to an average walking pace of 1.4 m/s [24]. Reflective markers were placed on the subject's right foot and a black sock over their left foot to aid in right foot identification. Subjects first walked for one minute to warm-up and fall into a natural cadence. The operator then collected 10 seconds of data to capture approximately 10 steps. The data were reviewed to ensure the subject stayed in frame from heel-strike to toe-off during capture. If needed, the subject's placement was shifted and data was collected again, up to two times.

### **5.3.1.3 Data Processing**

Figure 5.3 provides an overview of the data processing workflow; all steps are summarized in the paragraphs below.

For each subject, a single candidate heel-strike to toe-off event was manually identified across all captures by taking into account point cloud quality due to the high computational power required

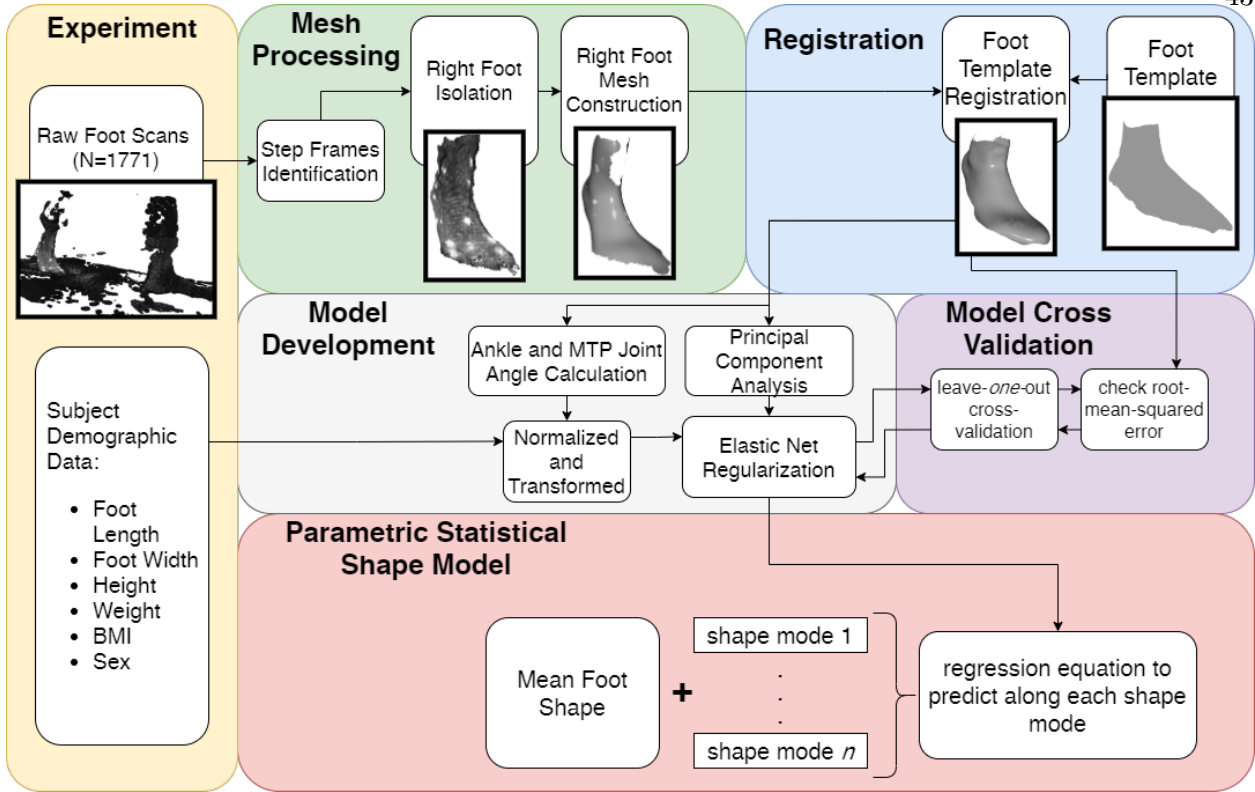


Figure 5.3: Flowchart of processing steps for statistical shape model creation

to process all heel-strike to toe-off events. Events with holes greater than 1cm that appeared across more than one frame were rejected. The depth images captured by each depth camera were processed into point clouds using the DynaMo package [21]. From each point cloud, the right foot was isolated and transformed into a triangle mesh [122, 53, 18, 159]. Since every depth image was captured independently by the cameras, the amount and location of points which represented the foot were not consistent. Registration of all scans to a common template represents every scan by an equal number of points, and ensures any missing points not meeting the rejection criteria are properly interpolated. The right foot meshes were then iteratively registered using a three-step fitting process to an averaged high-quality static template scan, provided by Dr. Matthew Reed from the University of Michigan Transportation Research Institute [117]. First scans were roughly aligned using a point-to-plane iterative-closest-point algorithm [36], implemented in Open3D [159]. Next, the radial-basis function fitting algorithm from the GIAS2 software package [158] was run twice using a thin-plate spline to approximate the foot surface [108, 78]. The mid-stance scan from each

subject was registered first to the template, and then the registration process was run both forwards towards toe-off and backwards towards heel-strike, on a scan-by-scan basis, using the previously registered scan as a template for the next scan. Accuracy was checked by comparing registered scans with the processed scans by finding corresponding points between both, and calculating the root-mean-squared error (RMSE) between the corresponding points.

Anatomical landmarks were approximated from the registered scans using the foot features of the registration template [140]. The first metatarsal head, fifth metatarsal head, and second toe landmarks were used to align all scans to be centered at the second metatarsal head, with the forward axis pointing towards the second toe. Landmarks around the metatarsal-phalangeal (MTP) joint and ankle joint were used to calculate ankle, MTP, and foot kinematics for each subject's scans with respect to the joint angles at the subject's mid-stance scan. Relevant joint angles include dorsi/plantarflexion, ankle inversion/eversion, ankle internal/external rotation, MTP dorsi/plantarflexion, foot inversion/eversion, and foot internal/external rotation angles.

#### 5.3.1.4 Model Construction

Principal component (PC) analysis is a dimensionality-reduction method commonly in constructing SSMs [118, 108, 37, 131]. The first PC represents an axis containing the largest variance in the dataset, and each subsequent PC describes the largest variance orthogonal to the previous component's axis. Therefore, PCs allow for a new, smaller set of orthogonal variables to be defined which represent the variance in the dataset.

Let  $N$  equal the number of total scans in the dataset, and  $n = 29873$  equal the number of vertices in each registered scan. The scikit-learn module [111] was used to incrementally calculate the maximum  $N$  PCs which represent the dataset. Each scan in the dataset is represented in the PC model with  $N$  PC scores. All PC scores are centered around 0, which represents the mean foot scan of the dataset containing all subjects. Each PC represents a shape mode in the SSM, where each score represents a deviation from the mean foot along the shape mode axis. The resultant PC model can be used to inverse transform a vector of length  $N$  PC scores into a  $29873 \times 3$  vector, which repre-

sents the location of the vertices in the foot shape. Not all PCs were retained in the model since the first few PCs explain a majority of the variance, while additional PCs may be accounting for noise.

Subject demographic data and calculated joint angles were incorporated into the SSM by developing multivariate linear regression models based on these features. This was used to predict each PC score, which can then be inverse-transformed into a foot shape. Subject demographic data and joint angles were independently unit normalized and power-transformed across the whole dataset to aid in regression development [156]. An elastic net regularization algorithm [160] was run for each multivariate regression to calculate normalized feature coefficients for each PC score's regression. Two different sets of predictors were created, one with all subject demographic data and calculated joint angles, and one with the highly cross-correlated predictors of arch length, body-mass index, and height were removed. Six potential models were built as combinations between the number of PCs predicted which explained 95%, 98%, and 99.7% of the variance, and the two predictor sets.

### **5.3.1.5 Model Validation**

All six models were validated for performance using leave-one-out cross-validation, where scans from each subject were set as the validation set, and models were trained on the remaining dataset. Model performance during validation was quantified with the root mean squared error (RMSE) and Hausdorff distances of the predicted foot shape to the corresponding registered scan. A two-way RMANOVA analysis was run on the error distributions to test the effect of constructing a predictor with the different number of PCs, and between using the two variable sets. The chosen model was retrained on the whole dataset before being analyzed.

### **5.3.2 Results**

A total of 1771 scans were analyzed across all 30 subjects. The average number of scans collected for each subject's stance phase was  $59 \pm 3.7$ , with a range of 52-69 scans due to inter-individual differences in stride length. Figure 5.4 shows a set of raw and registered scans from one

subject. All processed scans were registered to the template with a mean registration RMSE of  $1.0 \pm 0.6$  mm, and a mean Hausdorff distance of  $25.5 \pm 13.4$  mm.

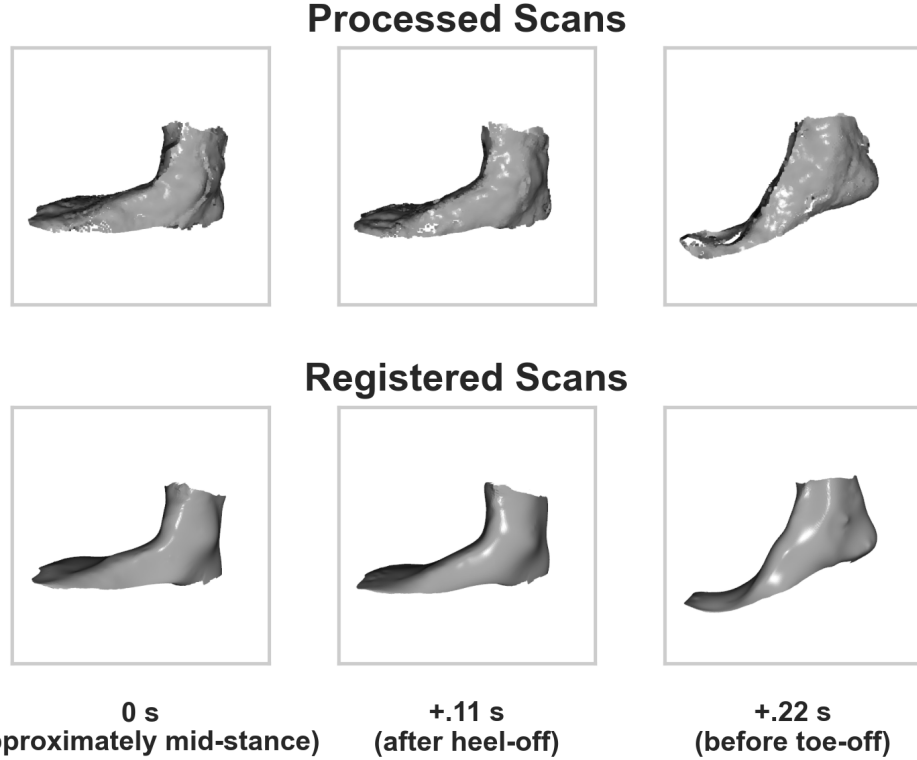


Figure 5.4: Processed and registered scans of one subject during heel-off, shown 10 frames (0.11 seconds) apart.

The PCA analysis of all registered scans found the first 8 PCs to represent approximately 95% of the variance, the first 27 PCs to represent approximately 98% of the variance, and the first 105 PCs to represent approximately 99.7% of the variance. (Fig. 5.5) shows the distribution of cross-validation RMSEs and Hausdorff distances for each of the six models tested. Aligned-Rank Transform [152] was used to compare models as error distributions did not meet assumptions for normality. Significant differences were found in RMSE and Hausdorff distances between predicting different numbers of PCs (RMSE:  $F=7037$ ,  $p<0.001$ ; Hausdorff distances:  $F=4577$ ,  $p<0.001$ ), predicting between the two variable sets (RMSE:  $F=6.4$ ,  $p=0.012$ ; Hausdorff distances:  $F=4.4$ ,  $p=0.036$ ), and for the interaction (RMSE:  $F=3.0$ ,  $p=0.05$ ; Hausdorff distance:  $F=5.3$ ,  $p=0.005$ ). An ART-C post-hoc test [45] with Bonferroni correction found significant differences between all

but one pair of models; detailed results are presented in supplementary information. Therefore, the model predicting 8 PCs with the selected variable set was chosen for its simplicity and performance.

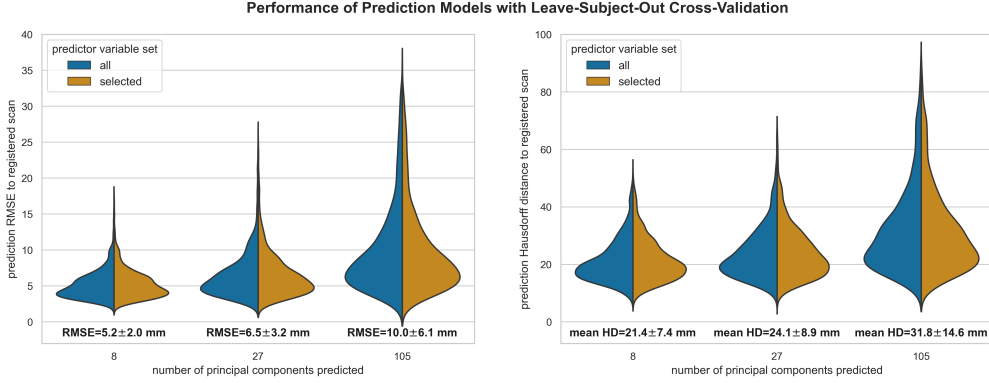


Figure 5.5: Distribution of mean root-mean-square (RMSE) error and mean Hausdorff distance (HD) across the various prediction models leave-subject-out cross-validation results. Model error values and standard deviation are shown below each distribution

Each retained PC is a shape mode. (Fig. 5.6) shows the chosen model's normalized regression coefficient values for each shape mode. The coefficients for the sex predictor are not shown as they were predicted to be zero for every shape mode.

(Fig. 5.3.2) shows each shape mode's axis represented on the mean foot, highlighting which areas of the foot are affected by deformations in each shape mode. (Fig. 5.3.2) shows the  $\pm 2$  standard deviations of deformation along each shape mode overlaid on the mean foot. Supplementary information includes correlation between predictors, ratio of total variance each retained PC accounts for, and a link to an interactive web tool to visualize the model. All data from this project is available online.

Figures 5.3.2 shows each shape mode's axis represented on the mean foot, highlighting which areas of the foot are affected by deformations in each shape mode, and the  $\pm 2$  standard deviations of deformation along each shape mode overlaid on the mean foot.

### Normalized Regression Coefficients per Shape Mode

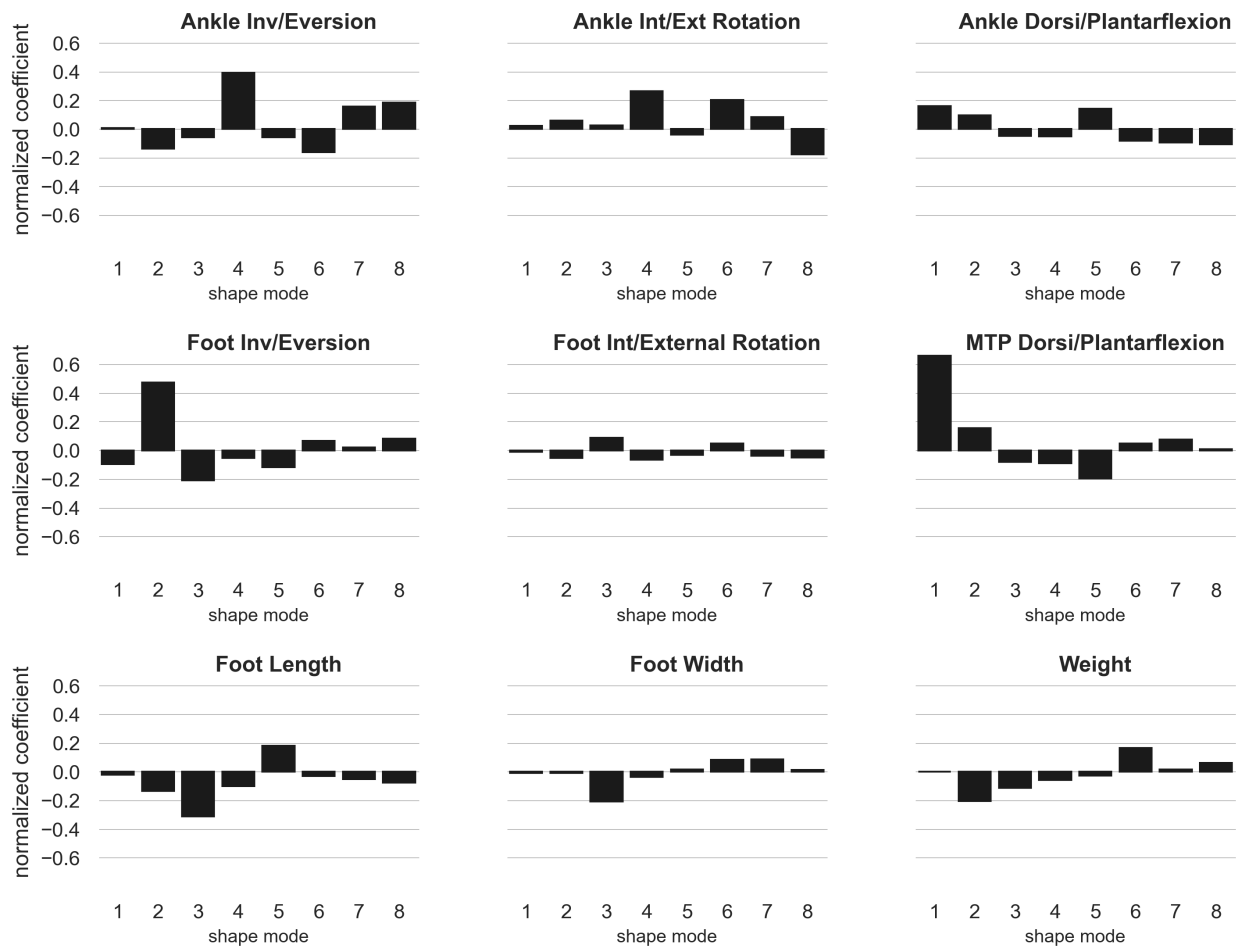
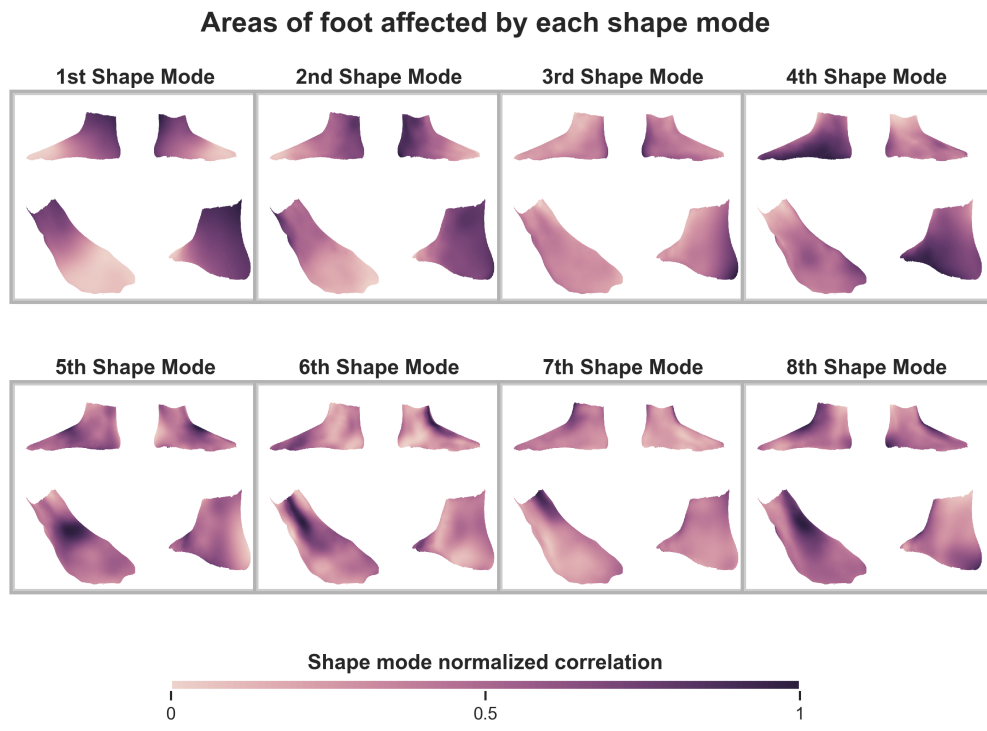
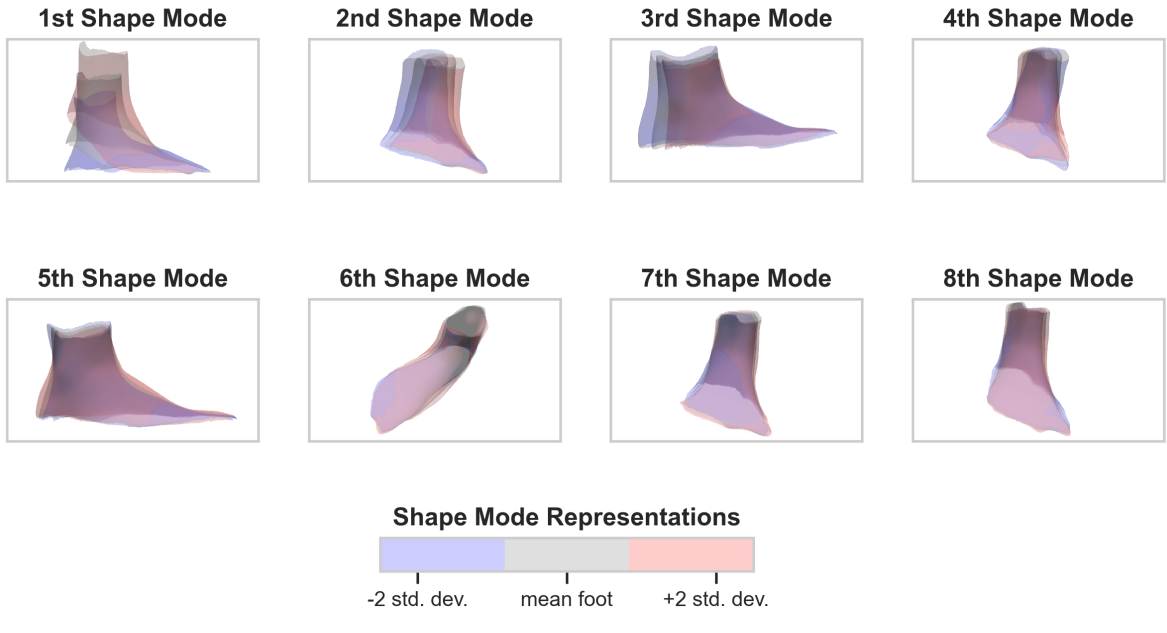


Figure 5.6: Each graph represents the predictor's effects on the shape mode by visualizing the model's normalized coefficients. Larger absolute values indicate a larger effect from the predictor on the shape mode.



### Deformations along each shape mode's axis



[B]

[A] Each shape mode's principal axis represented as a heatmap overlaid on the mean foot and shown from 4 different point-of-views. The darker regions represent vertices which are most correlated with the shape mode's principal axis, and therefore see deformations in the shape mode.

[B] Foot shape deformation at +2 and -2 standard deviations along each shape mode's principal axis, overlaid on the mean foot. The point-of-view is set to highlight the major variance along each shape mode's axis.]  
 [A] Each shape mode's principal axis represented as a heatmap overlaid on the mean foot and shown from 4 different point-of-views. The darker regions represent vertices which are most correlated with the shape mode's principal axis, and therefore see deformations in the shape mode. [B] Foot shape deformation at +2 and -2 standard deviations along each shape mode's principal axis, overlaid on the mean foot. The point-of-view is set to highlight the major variance along each shape mode's axis.

#### 5.3.3 Foot Shape Changes

This study was designed to construct and evaluate a parametric SSM in explaining and predicting dynamic foot morphology changes across the subject population. The model was able to predict dynamic foot shape across the subject population with an average RMSE of  $5.2 \pm 2.0$

mm and mean Hausdorff distance of  $21.4 \pm 7.4$  mm. The disparity between RMSE and Hausdorff distance is due to scan edges, which have inherently high noise from depth camera capture. For context, if all possible RMSE prediction error was accumulated to only affect length and width, it would be higher than the half-size step of the American shoe sizing system [88], but less than inter-brand variability of shoe length and shoe width [146]. Further, this error is lower than the RMSEs of other parametric SSMs that predicted static standing child body shape (mean=10.4mm) [108], dynamic shoulder deformation (mean=11.98mm) [78] and child torso shape (mean=9.5mm) [109]. Note though, that the presented model may have lower prediction errors due to the foot being a relatively smaller section of the body to model. Grant et al's model reconstructed internal foot bones with much lower RMSEs and Hausdorff distances from sparse anatomical landmarks (RMSE: 1.21-1.66 mm, mean Hausdorff: 3.21-7.19 mm) [59] but was trained with higher resolution MRI images. Other efforts to create statistical foot shape models did not incorporate parametric prediction of foot shape [37, 131].

Foot motion during stance is dominated by MTP and ankle dorsi/plantarflexion [85], captured in the first shape mode (fig. 5.3.2). Shape changes in frontal and transverse planes are captured in the second and fourth shape modes, respectively (fig. 5.3.2). Movements captured in these shape modes are well correlated to the expected movement of foot during stance phase [85]. The second and fourth shape modes are slightly affected by foot length, which may suggest inter-individual effects in foot inversion/eversion, ankle inversion/eversion, and internal/external rotation during gait. There is a slight correlation between these angles and foot length (see supplementary figures), which may be due to differences in cadence when walking at the treadmill's set speed. Individuals were given time to acclimate to the treadmill's set speed, but the speed may not have been their preferred walking speed.

Foot length scaling is captured in the third shape mode (fig. 5.3.2). Foot length shrinks when moving positively along the third shape mode (fig. 5.3.2), and thus has a negative effect from foot length. Negative effects from foot width and weight may be due to their correlation to foot length (see supplementary figures).

Longitudinal arch height is a significant factor in static [131, 37] and dynamic foot shape [129]. Due to limitations in the field-of-view of the cameras around the treadmill, arch height was not able to be directly measured. However, the instep area was found to rise along the fifth shape mode's axis (fig. 5.3.2), which is representative of the longitudinal arch apex. This was positively affected by foot length and negatively by MTP dorsi/plantarflexion (fig. 5.6), suggesting that the instep height increases with foot length, and decreases through heel-off as the MTP dorsiflexes. Jurca et al. found a similar relationship between static instep height and foot length, although there is still a wide variety of instep height in the population [73]. The drop in instep height is most likely related to the decrease in medial-longitudinal arch (MLA) angle, attributed to the windlass mechanism and measured through radiographs and optical motion capture [66, 27, 134]. Similarly, midfoot girth was previously found to decrease during stance phase compared to statically standing when taking this measurement over dynamic foot scans [60]. The presented model provides volumetric insight into where the drop in instep height occurs by identifying it in a shape mode, as well as allowing for its predictability from foot length and MTP dorsiflexion.

The heel was found to vary in the third and fifth shape mode's axis, varying from a rounded to a sharper shape along both axes. As the heel lifts off the ground at heel-off, the soft-tissue unloaded during gait and changes morphology [54]. At heel-off, there is foot eversion and MTP dorsiflexion [85], explaining the negative effects on the third and fifth shape modes, respectively (fig. 5.6).

Girth changes at the ankle, midfoot, and medial MTP joints are captured in the second and sixth shape modes (fig. 5.3.2). Girths increase just prior toe-off with ankle internal rotation in the sixth shape mode, and eversion in the second and sixth shape modes (fig. 5.6). Girths are also increased with increased subject weight. The foot is stiffened through tension in the MTP joints in order to prepare for toe-off [66], and the MTP joints are known to move relatively within the foot during gait [153, 86] which may be resulting in the increased girth at the MTP joint. A similar mechanism may be occurring at the ankle joint during ankle inversion and internal rotation, where tension from muscle activation prior to toe-off may cause increased girth.

The model can inform last and footwear design recommendations for increased fit and comfort. Lasts are typically designed to shape the shoe for both fit and fashion, and are derived from static foot dimensions for a given size [88]. Previous work has proposed the use of 3D foot scans to inform last design [124], and even generate predicted individual shoe lasts [7]. The 3D meshes predicted by the model can generate lasts in various size grades and representative of shape changes during stance phase. For example, lasts can be constructed with a deformable or removable instep area, matched to the model’s predicted reduction in arch height for a given foot length. Lasts could also feature a swappable heel element to ensure that rearfoot morphology is accommodated as the heel is off-loaded. Digital footwear design tools could also directly import the predicted meshes generated from this model for virtual fit tests: interaction models between the footwear design and the dynamic foot shape could ensure fit is consistent through motion. Shape changes identified from this model can also inform footwear design. For example, the instep height drop may be accommodated with tensioned lacing, ensuring the foot is captured and cannot shift upward inside the shoe during heel-off. In addition, a heel counter can secure the changing morphology of the heel during heel-off, preventing heel rise within the shoe. While such elements are already found in many commercially available shoes, the presented model validates their importance and provides a framework for iterating on their design.

#### 5.3.4 Study Limitations

A number of limitations in this study should be noted. The elastic-net method is able to retain cross-correlated predictors, but still requires some bias in the dataset to predict scenarios where cross-correlated predictors are independent [160]. Therefore, the presented model may not be valid for predicting changes in morphology from independent changes in joint angles outside of stance phase, or from variance in foot width or weight compared to foot length not captured in the subject population. The model did not capture sex differences in foot shape; studies found that these differences after scaling for foot length were not significant [81, 16, 37], or were small in magnitude [154, 83]. No data was collected to analyzed foot shape differences due to ethnicity

[73]. Data at the toes was noisy, necessitating smoothing the template's toes to ease fitting. Plantar foot shape was not captured, which is also known to vary with foot shape and loading [94]. Future advances in scanning technology may improve data quality and allow for capture of arch shape and plantar shape for further analysis.

### 5.3.5 Study Conclusions

The observed girth changes at the ankle joint, medial malleolus, midfoot, and MTP joint can be directly mapped to spacesuit footwear design recommendations to reduce instances of heel-lift. During heel-lift, the heel rises inside the boot, resulting in the midfoot rotating upward around the MTP-joint much like after the heel-off phase in gait. This can only occur if there is empty space above the midfoot; if the boot's internal shape were perfectly fit to the foot's shape, the foot would not be allowed to move inside the boot. Unlike some terrestrial footwear which can rely on the elasticity of uppers to continuously capture the foot, the stiff nature of a pressurized spacesuit boots does not allow for its upper to continuously conform to the foot if the foot changes shape. The study showed that midfoot girth decreased as the MTP joint is dorsiflexing after heel-off in the fifth shape mode. Therefore, a spacesuit boot should have a mechanism to conform to this volume change to reduce empty space above the midfoot and therefore reduce instances of heel-lift. Heel counters are also designed into many terrestrial boots to ensure the heel stays index through motion; a well-designed heel-counter could also help reduce heel-lift. Rearfoot morphology changed from a rounded shape to a sharper shape with MTP joint dorsiflexion in the fifth shape mode, suggesting that a heel-counter may need to account for this shape change to properly capture the heel. A combination of midfoot capture and an improved heel-counter that account for these morphological changes can work together to reduce instances of heel-lift in the spacesuit boot.

## 5.4 Analysis of Dynamic Instep and Arch Height Changes

The dynamic foot shape model provides insight into how regions of the foot change shape due to motion or anthropometry. One of the primary findings from the model was the decrease

in arch height during stance phase, following by an increase through heel-off. However, the nature of a SSM is that it only outputs foot shapes and not linear or circumferential foot measurements. Therefore, the magnitude of arch height change was not characterized in this model. Characterizing arch height changes will assist in the spacesuit boot design, as this measurement will provide a baseline for engineering a conformable upper which reduces empty space above the midfoot and thereby may reduce heel-lift.

Arch height, however, is not a primary measurement in terrestrial footwear fit.

Lasts are traditionally made in a single reference size, and then either geometrically, arithmetically, or proportionally scaled larger and smaller to match other user sizes based on foot length [88]. This process results in other foot dimensions being scaled with the same proportion as foot length. However, arch height has little correlation with foot length [67]. Arch height is not a measurement used in the grading of shoe sizes, as such customers are not able to select shoes which fit their arch with quantitative fit metrics. Instep height, which is taken near the foot's arch, may be targeted in last design, but is also not used in grading. Furthermore, foot measurements defining shoe sizes are taken statically, and do not account for the dynamic changes in foot shape due to the foot's loading during gait.

The arch changes shape dynamically during gait, thus exacerbating difficulty in accommodating its shape during movement. Medial longitudinal arch (MLA) shape changes are thought to be caused by several mechanisms.

Hicks used radiographs to show that the foot's arch drops and decreases in angle while it is loaded during early and mid-stance, and rises and increases in angle during late stance [66]. They hypothesized that a stiff plantar fascia results in a windlass mechanism, where the plantar fascia is pulled towards the toes as the toes dorsiflex during late stance phase. This shortens the arch and raises its height. Additionally, Ker et. al hypothesizes that the arch behaves like a spring, where it is compliant and stiff during early and mid-stance, and then recoils in late stance to increase in height and assist in propulsion [75]. They also observed this arch height drop during early and mid-stance. Similarly, optical motion capture techniques have shown that the MLA angle increases and arch

height drops in during early and mid-stance, followed by the MLA angle decreasing and arch height rising in late-stance [27, 30, 85, 134]. The arch's dynamic motion can be attributed to a combination of the windlass and arch-spring mechanisms, providing a physical explanation to the arch's dynamic motion [148, 149]. The rise and fall of the arch are reflected as shape changes in the foot's instep area; this was found to be the largest variation in foot shape between loaded and unloaded feet [129].

Customers aiming to find footwear that fits their foot shape may face difficulties due to the lack of arch or instep height as a fit metric and the dynamic nature of the arch itself. Arch and instep height variation can be accommodated for in footwear through lacing and upper design. Customers therefore may need to try on various shoes while searching for an upper design that matches their arch and instep height. Customers may also adjust the fit of the arch and instep in each shoe they try on with lacing until they are satisfied with their fit. Lacing modifies how the shoe's upper sits on the wearer's foot, frequently implemented above the wearer's arch and instep. Lacing can provide a level of customization to arch and instep fit, especially when compared to an elastic shoe upper [69]. Proper lacing can also ensure comfort and performance during activities [63, 64, 115]. Furthermore, tensioned lacing could be used to ensure that dynamic fit is maintained as the arch moves through gait [115]. Investigating how both static and dynamic arch height may relate to other foot measurements could improve footwear design, such as by scaling lasts more accurately to accommodate arch height and provide customers with a guide in selecting shoes that fit all aspects of their foot shape.

To address this gap in footwear design, understanding the magnitude of foot shape changes at the arch may be used. The arch sits at the middle of the foot, just under the instep region. Therefore, it is expected that any change in arch height and MLA angle would affect instep height. There is also opportunity to investigate if dynamic arch height changes are affected by the subject's static foot measurements, and if the instep height measurement is analogous dynamically to the arch height measurement. The objective of this research is to evaluate whether dynamic instep height changes can be correlated to static foot measurements. This research hypothesizes that 4D

scanning can be used to quantify instep height changes, and that dynamic instep height change is correlated to static instep height, foot length, and foot width.

#### 5.4.1 Methods

Instep height measurement was evaluated as an appropriate measure to assess static and dynamic arch height in static scans. A strong correlation between these measurements allows for comparison to arch height measures since instep height is measured near the location of the MLA. Instep height measurements were first correlated to arch height measurements using a subset of the 3D static foot scan measurement dataset from [73] (Swedish Ethics Review Authority reference No. 2019-03243). The dataset was down-sampled to only include length classes in the 4D scan dataset used for the aforementioned dynamic foot shape model. Instep height measurements were taken for each foot scan by taking the height of the frontal cross-section at 55% of foot length from the heel [73]. Arch height measurements were taken at the frontal cross-section at 45% of foot length from the heel [73]. From this cross-section, the height from the ground to the foot is taken at 25% of the foot's width at this cross-section from the lateral side. Pearson correlation coefficients were computed between the instep height and arch height within this dataset.

As the 4D foot scans did not include the foot's plantar surface, a new method for measuring instep height was defined, summarized in fig. 5.7. A virtual landmark, labeled as the middle metatarsal head, was defined as halfway between the medial and lateral metatarsal heads. Then, a triangle was defined on the scan's sagittal plane, with its base defined as the vector from the pterion to the middle metatarsal head. The triangle's height was defined as the orthogonal distance from this vector to the instep landmark; this height was recorded as the scan's instep height. While the instep height landmark may not be perfectly aligned with the pterion-middle metatarsal head vector, this method ensures that the instep height measurement is always taken perpendicular to the base of the defined triangle in the foot's sagittal plane. Despite the data set limiting the measurement technique from following the traditional methods of measuring instep height from

the literature [73], this method does represent the height of the foot at the instep area when the plantar surface of the foot is not available as a reference.

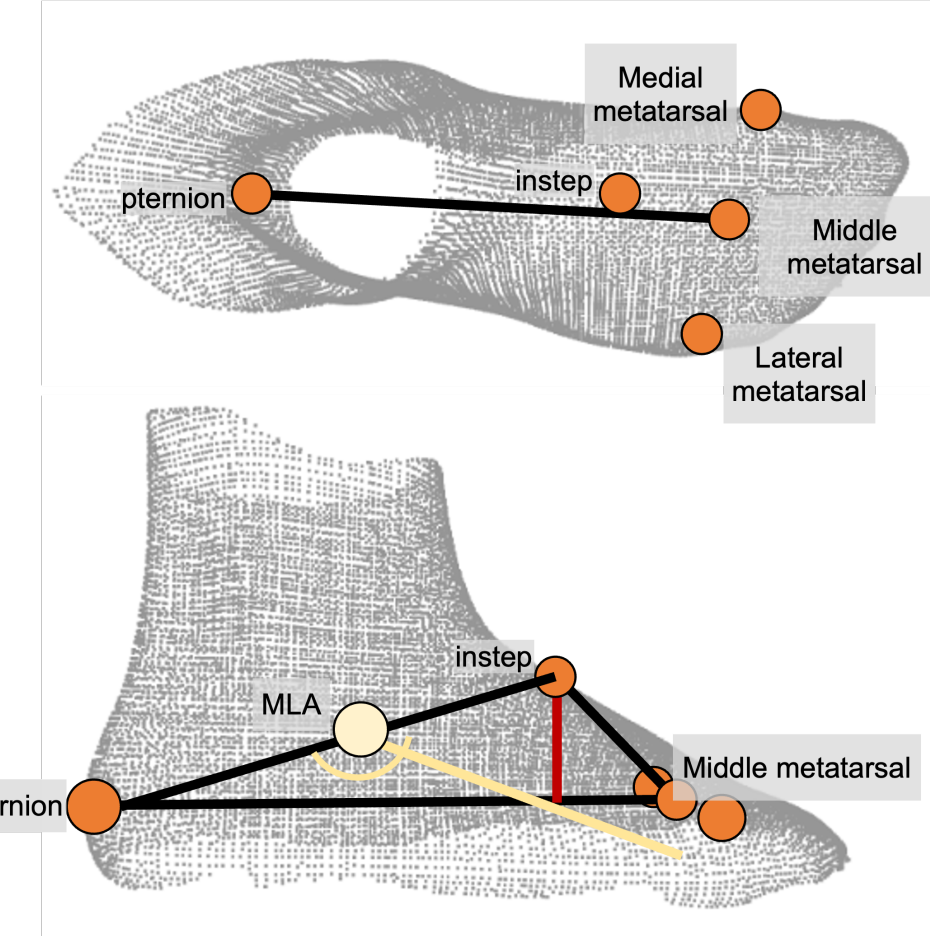


Figure 5.7: Landmarks and vectors used for instep height measurement, shown in top and side views. The principal foot axis is defined from the pterion to the middle metatarsal head landmark (top). A triangle is defined with a base between the middle metatarsal head and the pterion, and an upper vertex at the instep landmark (bottom). The height of this triangle (red) is taken as the instep height. The MLA location is also shown for comparison.

For each subject, the instep height measurement over stance phase was filtered with a 2nd order Butterworth low-pass filter, with a cutoff of 15 Hz, to reduce measurement noise. Mid-stance instep height was defined as the instep height taken halfway between heel-strike and toe-off for all subjects, representative of the static instep height. The late-stance instep height measurement was noted as the highest instep height measurement between mid-stance and toe-off. The difference between these two instep height measurements was calculated for each subject as the dynamic instep

height change. The correlation coefficient was computed for each scan within each subject between instep height and MTP joint angle. The MTP joint angle was chosen for correlation analysis as the hypothesized windlass mechanism for arch height rise is dependent on the MTP joint angle [66]. Correlation coefficients were also computed between all subjects' dynamic instep height change and their foot lengths, foot widths, and static instep heights. Subjects' maximum instep height changes were compared to subjects' foot lengths, foot widths, and static instep heights to identify if there are any trends which predict the maximum instep height change.

#### 5.4.2 Results

Analyzing Volumental's static scans found a correlation coefficient of 0.70 and 0.71 was found between instep height and arch height for females and males, respectively. Instep height was calculated for subjects with dynamic scans and compared to their MTP joint angles. The relationship between selected subject's MTP joint angle throughout stance phase, and their measured instep height, is shown in fig. 5.8. For most subjects, the instep height drops from early to mid-stance, and then rise in late stance with the MTP joint angle. Correlation coefficients between the calculated instep height and MTP joint angle from dynamic scans for each subject are also noted in fig. 5.8. Twenty-five of the thirty subjects had high correlations ( $r^2=0.73\pm0.10$ ) between their instep height and the MTP joint angle. These subjects had a mean instep height difference of  $15mm\pm4mm$ . The remaining five subjects (Subjects 2, 16, 21, 22, and 29) had low to no correlation ( $r^2=0.11\pm0.36$ ) between their instep height and the MTP joint angle across the gait cycle. These subjects' data was manually examined for anomalies, but none were found.

Maximum instep height change was found to be  $53.7 \pm 4.44$  mm for the 25 subjects with high correlations between instep height change and MTP joint angle.tbl. 5.2 shows the correlation coefficients between the maximum instep height changes and foot length, foot width, and static instep height for these subjects.

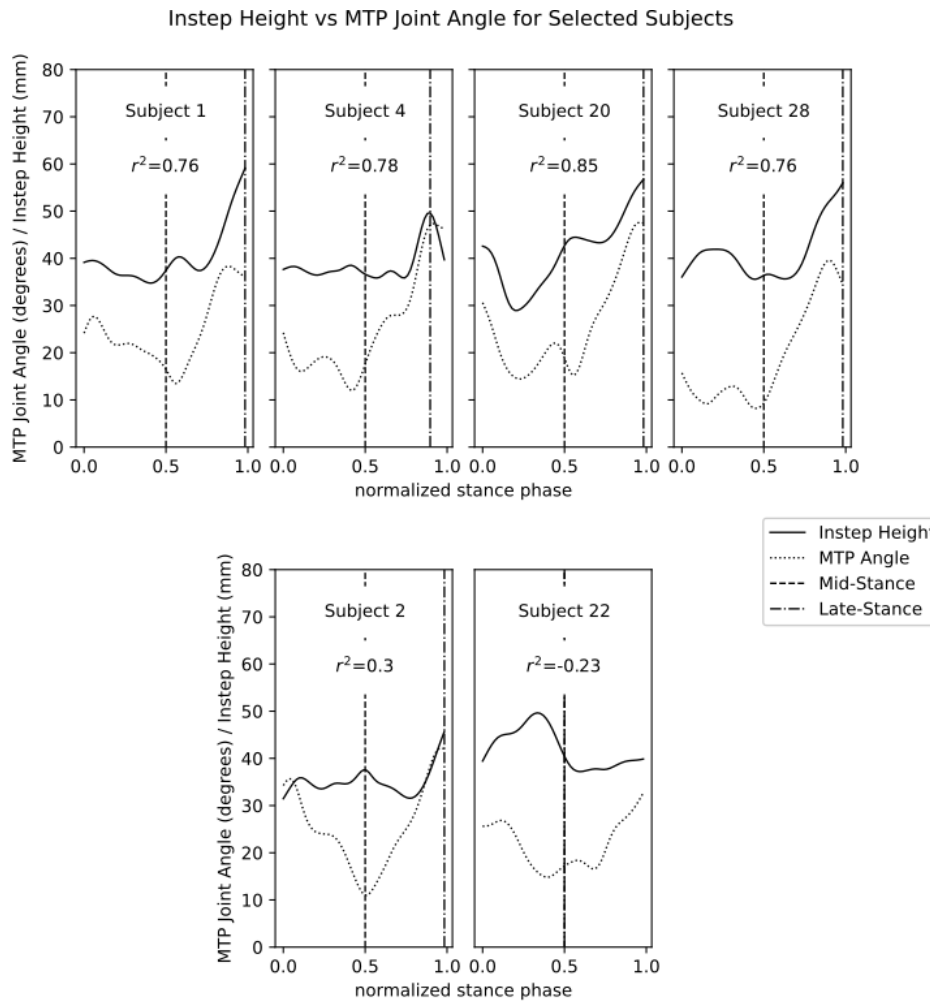


Figure 5.8: Correlation between selected subjects instep height and MTP joint angle over stance phase. Subjects with high correlation between their MTP joint angle and instep height are shown on the top row. Subjects with lower correlations between their MTP joint angle and instep height are shown on the bottom row. Locations of where mid-stance and late-stance instep height values are taken for each subject are highlighted as vertical lines. The Pearson correlation coefficient for each subject is shown on their graph.

Table 5.2: Pearson correlation coefficients between maximum instep height change and subjects' anthropometric measurements

Anthropometric measurement	Correlation to maximum instep height change
Foot Length	0.18
Foot Width	0.18
Static Instep Height	-0.16

### 5.4.3 Translating Instep and Arch Height to Footwear Design

A new measurement technique was proposed to analyze 4D foot scans for changes in instep height due to the dynamic nature of the MLA during gait. This technique provides a normalized

Five of the thirty subjects did not have a strong correlation between their instep height and the MTP joint angle. No anomalies with the instep height measurement were identified after manually reviewing the subject's 4D scans. In addition, manually reviewing the subject's MTP and ankle joint kinematics also did not reveal any differences. These subjects' static instep heights were also similar to subjects whose instep height had a strong correlation to the MTP joint angle. Since instep height was found to be highly correlated to arch height, these subjects' arch height also cannot explain why they have low correlations to the MTP joint angle during stance phase. However, some of these subjects (Subjects 2, 21, and 29) still have a rise in instep height in late stance that is characteristic of the arch height rise due to the windlass and arch-spring mechanisms [66, 75]. The low correlation suggests that for these subjects, instep height changes may be occurring primarily due to the arch spring hypothesis rather than the windlass hypothesis [75]. On the other hand, subjects 16 and 22 had little to no change in instep height. The five subjects in the group without a strong correlation between instep height and MTP joint angle may have a foot structure that responds differently compared to the other subjects', or their arch may not be aligned with the location at which the instep height measurement was taken.

Static arch height has been previously shown to have low correlation to foot length [67]. In this study, no strong correlations were found between instep height changes and other foot anthropometric measurements, suggesting that the instep height change is another mode of variation in foot shape. In addition, there were some subjects in this study who did not have a strong correlation between arch height and MTP joint angle. Both findings suggest that arch and instep height varies inter-individually.

This finding has many implications for footwear design. Geometric, proportional, and arithmetic last grading techniques vary the dimensions of the master last by a percentage of the last, by fixed proportions in various dimensions, or by a fixed increment in various dimensions, respectively. However, these grading techniques cannot consider the variability of static arch height and dynamic instep height, as this variability seems to be different for everyone. Therefore, adjustable mechanisms at the instep area to personalize fit may be necessary to allow footwear to fit a large popula-

tion properly. In addition, these mechanisms should be adaptable to the dynamic changes in instep height during gait. A fixed instep area might result in the foot lifting within the shoe, also known as heel-lift, just before heel-off when the instep height has dropped and there is empty space in the shoe.

The tongue and shoelaces can provide adjustment at the instep area independent of shoe size. Shoe lacing provides tension over the tongue of the shoe [63, 112], which ensures that the tongue stays snug on your instep area. Findings from this study show that the tongue should accommodate at least 20 mm of movement to fit most subject's instep height changes. Individuals can adjust the lacing to best accommodate their static instep height. Shoe lace tension can also be adjusted by varying the number of eyelets and lacing pattern used by the individual [63, 64]. Therefore, shoelace tension can be adjusted by an individual to match their dynamic instep height and arch function. An individual with large instep height changes during stance phase could have higher-tension lacing to ensure the tongue can rise in late stance and then collapse again during the following step's mid-stance phase. Alternatively, an individual with low instep height changes may not need to tension their shoelaces as high. Therefore, shoelaces can allow individuals from this study with high correlation between their instep height and MTP joint angle, and those with low correlation between their instep height and MTP joint angle, to adjust shoe fit to their foot shape and dynamic nature. Advanced shoe lacing concepts have also been shown to reduce in-shoe motion, which could be due to their superior tension provided by these concepts [115, 97]. These concepts could also be providing an easier mechanism for the wearer to adjust the tension appropriately; these wearers could adjust the tension to their liking in an easier fashion to ensure that they are minimizing in-shoe motion while still maintaining comfort.

It should also be noted that the dynamic instep height measurement may not be only due to the MLA. It has been suggested that the foot's transverse arch can also change in curvature due to load, and also affect the foot's stiffness [142]. As the transverse arch is also located close to the region of the foot where the instep height is measured, it may also have a dynamic component that is contributing to the rise of the instep during gait. Further studies of the transverse arch mechanics may be needed to confirm this.

## 5.5 Summary

A 4D scanning system was developed to capture dynamic foot shape changes, and was used to collect data for development of the model. To the authors' knowledge, this is the first parametric foot SSM that captures and reconstructs dynamic motion. The model was able to identify specific changes in foot morphology as they related to subject and kinematic parameters, and suggest spacesuit boot design techniques to reduce instances of heel-lift.

The dynamic shape changes around the arch were further studied, as the arch is a challenging to fit properly. The instep height measurement was found to closely correlate to the arch height measurement. A new method of measuring instep height on dynamic foot scans without a plantar surface was developed. Strong correlations were found between the MTP joint angle and the instep height, reinforcing the dynamic nature of the MLA angle dynamics. However, correlations were low between instep height change and static foot measurements, highlighting the need for adjustable and potentially dynamic lacing integrated into the upper to maintain fit throughout the gait cycle.

## Chapter 6

### Specific Aim 3: Define a design process integrating dynamic foot morphology data for a novel spacesuit boot

Previously designed planetary spacesuit boots have modified terrestrial hiking boots by integrated a pressure bladder, to allow for interfacing with a pressurized spacesuit. These boots were designed through iteration and subjective feedback from wearers. Upon rigorous performance evaluation [121, 50], though, these designs to date have failed to solve the heel-lift problem, necessitating a new approach to boot design.

The design for any new spacesuit component should aim to match the required operator motions for the intended actions, and be sized for the intended population. This allows for the component to provide proper fit and mobility to the wearer. Designing such a component, however, requires an understanding of body segment size and mobility. Combining the novel dynamic foot morphology model with known foot shape and mobility characteristics provides the necessary information to better fit the spacesuit boot to the foot. However, there does not exist a defined process to design spacesuit components that integrates both traditional and novel data to achieve this objective. The design process must therefore be modified to integrate all available data to improve spacesuit fit, comfort, and mobility.

This chapter presents a literature review of existing foot shape and mobility data as it relates to spacesuit boot design. The data is then integrated into a design framework, which is then used to design a novel spacesuit boot with improved fit, comfort, and mobility. Design justifications for com-

ponents of the novel spacesuit boot design are outlined. The construction of a prototype based on the novel spacesuit boot design and a spacesuit boot design based on existing efforts are described.

## 6.1 Existing Knowledge on Foot Shape Mobility

The foot's static shape distribution and mobility have been well characterized through previous analyses [46, 90, 144, 147]. The following sections describe each of these specific foot measures and provide their population-derived nominal values. Figure 6.1 highlights these foot-specific measures.

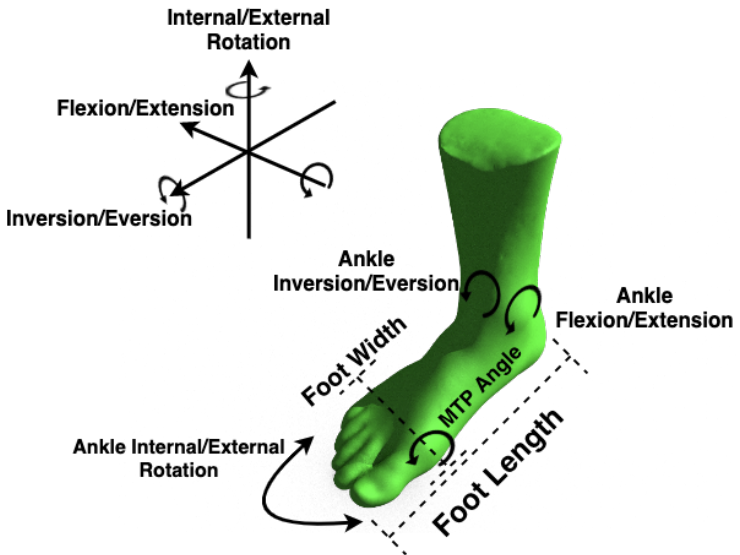


Figure 6.1: Foot-specific measures which directly affect mobility and comfort

### 6.1.1 Linear Anthropometry

The ANSUR II survey collected a number of foot-related measures which can be analyzed to provide a baseline for foot shapes and sizes [57]. Three of these measures are directly related to fit and mobility. Foot length and foot width define the outer bounds of the foot shape. Length is the primary measure used when purchasing shoes, followed by shoe width [88]. In the US sizing system, each half-size corresponds to a 4.23 cm step. Since females generally feature smaller length feet than males, female shoe size is typically 1.5 US shoe sizes more than an equivalent male size

[88]. Figure 6.2 shows that this offset does not sufficiently align the female population to the male population for shoe length. Shoe width sizes are graded with letters (“AA” to “EE”) in the US, offset from a normal “D” in steps of 6.35 mm; a “C” is 6.35mm narrower while a “E” is 6.35mm wider [88]. Shoe width sizes also scale with length; as a longer foot is typically wider [73]. Figure 6.2 shows that the distribution of widths for women is wider than that for men, suggesting that having a common step for both men and women may result in more women not being accommodated in shoe-width. Therefore, when designing a shoe, it is important to consider the target audience’s foot anthropometry outside of the shoe sizing standard and use foot measurements when available.

Arch length denotes the location of the metatarsophalangeal (MTP) joints on the foot. Since power is transmitted through the MTP joints, the alignment of the MTP joints with the ball of the shoe is important to ensure power is properly transmitted during heel-off. Therefore, the arch length measurement is correlated to standard shoe sizes and if larger, will be selected over the length measurement. Figure 6.2 shows that while arch length is correlated to foot length for both males and females, there is still high variability in this relationship. Therefore, arch length is an important measure to consider to ensure proper indexing and dynamic fit between the wearer and spacesuit boot.

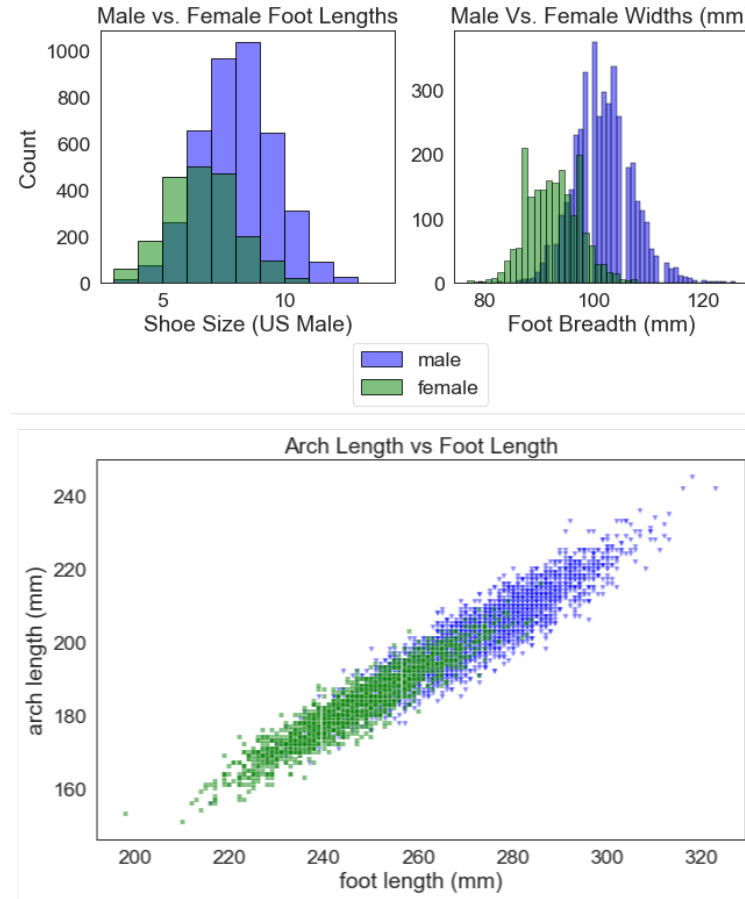


Figure 6.2: (Top-right) Inequality in distribution of equivalent shoe size between male and female. (Top-left) Distribution of male and female foot widths. (Left) relationship between foot length and arch length; visualizations developed from the ANSUR II Dataset

### 6.1.2 Gait Joint Kinematics

The foot's main function during gait is to transmit power against the ground, ensuring that the human pushes off and initiates a step. During each step, the ankle pushes off from the ground to initiate a step. Intrinsic foot muscles help stiffen the foot to assist the push-off from the ankle against the ground [46]. The MTP joint not only exhibits flexion in the sagittal plane, but provides the necessary stiffness to allow for the ankle power to translate into push off [132]. Ankle joint rotation may also help balance and stability during gait, particularly on slopes [147]. Neither the ankle joint nor the MTP joint should be restricted in its movement to enable efficient push-off and stability. However, free movement of the ankle joint can increase the risk of injury from instability

caused by external forces from walking on an uneven surface. Therefore, there is a balance to be struck between allowing for movement while preventing potentially injurious movements.

Nominal values for the foot MTP and ankle joint movement during gait can be derived from the numerous studies conducted on human gait. Voloshina et al. [144] found that during gait on uneven surfaces, the ankle does not flex past  $\pm 20$  degrees. Wannop et al. [147] reported peak foot-floor angles which suggest that on level and sloped surfaces, subjects dorsiflex their ankle up to 40 degrees, and flex their MTP joint up to 60 degrees. The MTP joint has been shown to flex between 70-90 degrees during gait [90]. There is very little ability of the MTP joint to extend or move in the frontal or transverse plane [90]; therefore these motions may want to be limited in the boot's design to prevent injury.

The ankle joint exhibits most of its movement in the sagittal plane. However, the ankle joint can perform inversion/eversion in the frontal plane and internal/external rotation in the transverse plane. Wannop et al. [147] found that subjects wearing a low-top shoe with no additional ankle stability had up to 10 degrees eversion and 15 degrees inversion while navigating a slope. However, excessive inversion/eversion may decrease stability and lead to injury. During gait, the human normally exerts energy to stabilize their ankle in this direction [106]. However, any external force can destabilize the ankle, as commonly seen in basketball or hiking [20]. Therefore, it will be desired that any boot stabilizes the ankle in this motion. In addition, freedom in the transverse plane is desired to allow for positioning of the foot when navigating an uneven surface, aiding in balance [147, 55]. Wannop et al. [147] found the ankle internally/externally rotates +15/-20 degrees on a slope.

## 6.2 Biomechanical Boot Design Framework

The proposed design framework will link traditional linear foot measurements described in the previous section and the dynamic foot shape model (sec. 5) to specific footwear design variables, allowing for the design of a spacesuit boot with an emphasis on improving fit, comfort, and mobility. Note, the framework assumes a gas-pressurized spacesuit boot to maintain compatibility with the current xEMU architecture. Since gas pressurized spacesuits are stiff when

pressurized, they require specially designed joints which allow for flexibility of the stiff structure. The gas pressurized layer does not have the ability to stretch once pressurized, and therefore must be sized specifically to fit the population range.

The framework incorporates two types of design variables, categorized as either population measures or individual measures. Population design variables are used in the general design and selections of materials for the shoe, which will accommodate the range of foot shapes and motions seen by the population. Angular and morphology measurements can inform footwear design for population measurements. These measurements aim to accommodate the shape of the foot, as well as its mobility for the intended activity.

Individual design variables are used to size specific elements which are scaled between sets of boots to fit inter-individual differences. These variables rely on linear measurements of the intended wearer's foots. Individual design variables drive the selection of a shoe size which fits the individual's foot anthropometry.

Figure 6.3 shows how each of these measures is mapped to footwear design variables. In the following sections, the design requirements specific to a planetary spacesuit boot are outlined.

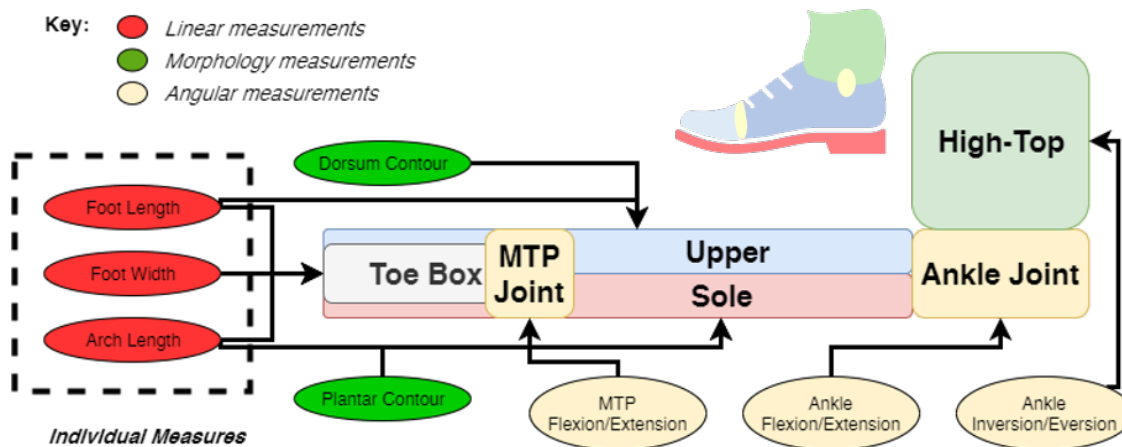


Figure 6.3: Overview and classification of measurements to footwear design variables with representative shoe

### 6.2.1 Mobility

Footwear is flexible at the MTP and ankle joints to allow for effective push-off during gait. Terrestrial footwear normally derives flexibility from the materials used for that portion of the shoe; the shoe is typically made of softer materials or less reinforcement at the joints. Since altering materials property stiffness is not an option for spacesuit design, rolling convolute or toroidal joints could be used in the spacesuit footwear to allow for flexibility at the MTP and ankle joints [65]. fig. 6.4 shows the desired flexibility based on foot-specific measures. These population measures will ensure that the boot provides enough flexion to not constrict natural motion.

The MTP joint should target flexion of +90 degrees and the ankle joint should target dorsiflexion/plantarflexion of +40/-20 degrees. Due to the potential for unstable terrain, a high top style footwear is suggested to stabilize the ankle, similar to a hiking or military style boot. However, it has been shown that a very stiff boot reduces ankle ROM and decreases stability at the knee joint [20], potentially leading to ankle and knee fatigue. By allowing for a internal/external rotation of +15/-20 degrees, and inversion/eversion of +15/-10 degrees, the boot still allows the foot to navigate a sloped and uneven surface without fatigue. The relatively low amount of movement will still allow the ankle to be stabilized and lower the risk of injury.

The only requirements previously stated for boot mobility are in the 2019 NASA SBIR Surface Space Suit Boot Solicitation [100]. The solicitation matches the +40/-20 degrees ankle dorsiflexion/plantarflexion requirement, but presents no requirements for ankle internal/external rotation, inversion/eversion, or MTP joint flexion. The proposed design framework targets higher flexion/extension capability in the ankle joint to match ankle mobility. The framework also specifies a requirement for extension of the MTP joint, limited ankle internal/external rotation, and limited ankle inversion/eversion.

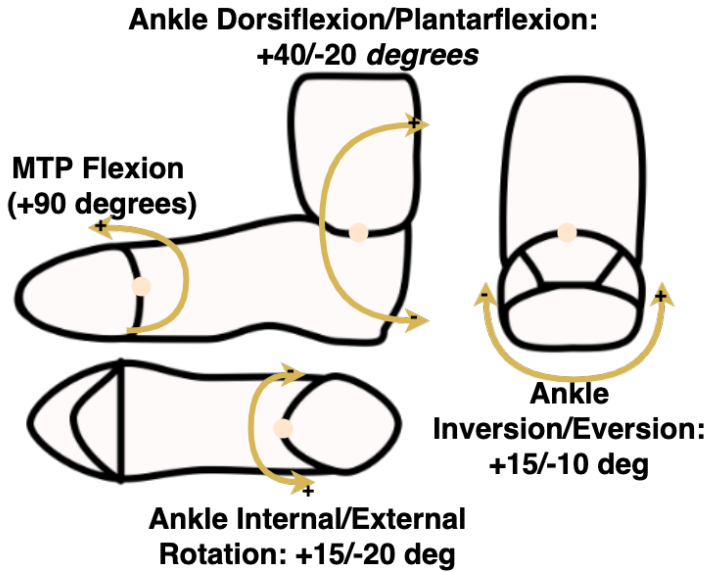


Figure 6.4: Mobility and flexibility of joints needed in the spacesuit boot

### 6.2.2 Toe box

The toe box accommodates the foot forward of the MTP joint. The toes provide the contact for power from the MTP and ankle joints to push off the ground during each step. Therefore, the most important feature of the toe box is contact between the toes and the ground during heel-off. As a result, the toe box can feature more space around the top of the toes for comfort [87]. Since the toe box does not need to provide any additional flexibility, it can be constructed with a less flexible material to allow for adequate support of the boot and foot. In conjunction with the MTP joint, the toe box should also be adjustable such that it can match the arch length of the wearer, allowing for proper fit and indexing of the MTP joint.

### 6.2.3 Upper

The dorsum of the foot is covered by a shoe upper. The shape of the upper needs to conform to the shape of the dorsum to allow for proper driving of the shoe during any activity [47]. Foot shape data taken from a large population will be useful in defining an ideal upper shape that fits a range of persons. The boot upper will also have to conform to the foot shape without causing discomfort during movement. Dynamic foot shape data can quantify how dorsum shape

is changing throughout the gait cycle, allowing for the upper to accommodate any expansion or contraction of the dorsum shape for optimal comfort and support. The instep height measurement is of particular importance, as it represents the height of the foot from the plantar surface to the dorsal surface just in front of the ankle joint. The instep height measurement was found to have both static and dynamic variability from the dynamic foot shape model in Chapter 5. Therefore, the upper should accommodate this variability to ensure fit can be maintained through the gait cycle for a wide range of static instep heights.

Lacing or other closure mechanisms can assist the upper in conforming to and capturing the foot (sec. 5). Closure mechanisms allow for customization by the individual wearing the boot, so each wearer can adjust the boot to their preferred fit. Conforming the upper to the foot will also eliminate any empty space between the foot and above the dorsum, reducing the chance of heel-lift since the foot will no longer be allowed to move within the boot. In addition, this reduces the chance of contact injuries from rubbing between the foot and boot.

The upper and lacing will also play a role in donning and doffing of the spacesuit boot. Traditional boots feature laces along the upper which secure the foot inside the boot during activity, but loosen to allow the foot to slip into and out of the boot. The closure will need to be designed in conjunction with pressure bladder, as the pressure bladder will need to deform in a structured matter when the laces are tightened. The boot can then loosen and allow the foot to be removed.

The upper's location between the MTP and ankle joint, and its requirement to conform to the shape of the foot, may drive the selection of a softer, flexible fabric being used to meet these requirements. This presents a challenge with designing the pressure bladder, as the pressure bladder is inherently stiff under pressure. Therefore, a soft inner layer above the dorsum may be used which allows the stiff pressurized bladder to conform to the individual's dorsum. Since the dorsum still transmits power to push the shoe off the ground, the soft layer still needs to have enough structure to transmit this power. If too soft, the layer will simply act as empty space and the shoe will not respond to ankle flexion during heel-off, potentially resulting in heel-lift.

#### 6.2.4 Sole

The sole in a traditional boot provides traction, support, and protection to the wearer. The sole needs some thickness to accommodate tread for grip on uneven surfaces. In general, the thicker a sole, the stiffer it becomes. As a stiff sole resists bending, it might fight against the motion of the foot and shoe during heel-off. Therefore, the sole needs to be flexible during heel-off without imparting additional forces on the shoe and upper. Dobson et al. [42] found that having a fully flexible sole in coal miner's boots inhibited the natural roll-off of the foot during gait, resulting in less comfort. However, it was not verified if the boot's flexibility at the MTP joint aligned well with the MTP joint, since sole flexibility was done simply by cutting into the sole near the MTP joints. Therefore, it will be imperative to ensure that any flexibility at the MTP joint is either perfectly aligned with the foot, or the flexibility does not inhibit the natural roll off of the foot. The arch length measurement can be used to ensure the MTP joint of a wearer is properly indexed to the sole's flexibility, allowing the MTP joint to act as intended (fig. 6.5).

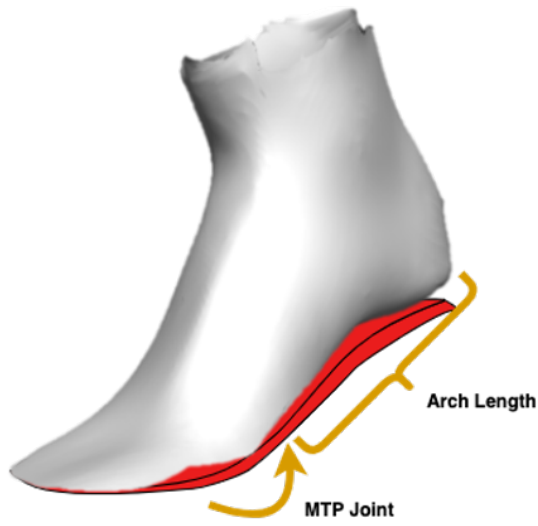


Figure 6.5: Desired sole flexibility (red) needs to be properly indexed to the MTP joint, which can be located by the arch length measurement

### 6.3 Novel Planetary Spacesuit Boot Design

The biomechanical design framework was used to inform the design of a novel planetary spacesuit boot with improved fit and comfort compared to current prototypes. This work's main goal was to reduce the amount of heel-lift in during walking found in current planetary spacesuit boot designs. Therefore, much of the design emphasis focused on providing an upper which was compatible with lacing to accommodate a static and dynamic variability in instep heights, and a heel counter to secure the heel.

The boot is designed to be compatible with gas pressurized spacesuits. When a spacesuit is pressurized, its pressure bladder expands to a stiff shape with increased volume. The stiff structure must be deformed by the wearer to provide mobility, as described in Chapter 2. In addition, this structure is the closest layer in a spacesuit assembly to the spacesuit operator, and therefore plays an important role in fit and comfort. A spacesuit's pressure bladder is typically paired with a restraint layer to control the expansion of the bladder[65]. However, through discussions with spacesuit engineers, the pressure bladder was found to be the most important layer in providing fit, comfort, and mobility. To enable lacing compatibility, the pressure bladder will need to change volume, allowing it to properly tighten around the wearer's foot. Previous efforts at integrating lacing into the boot only focused on running the lacing through the restraint layer [61], and did not have an accompanying conformal pressure bladder. Therefore, the design of the prototype planetary spacesuit boot was restricted to the pressure bladder layer to focus on developing a conformal pressure bladder.

Some design elements from previous planetary spacesuit boot designs were implemented to meet the biomechanical and anthropometric requirements presented in the framework above. The following sections describe the design decisions made for various parts of the prototype planetary spacesuit boot.

### 6.3.1 Ankle Convolute

Current planetary spacesuit prototypes use single-axis convolute assembly with three segments to provide ankle flexion/extension, but not inversion/eversion [121]. A segment consists of a circular piece of fabric; individual segments are assembled with overlap over consecutive segments. While a variety of convolute joint designs are available (see Chapter 5), rolling convolutes were chosen for this boot design after prototyping efforts found these to be the most easily constructed in a laboratory setting. Rolling convolute joints feature a band around each convolute segment, which guide the convolute's rolling and unrolling during motion [65]. When a rolling convolute ankle joint is flexed, one side of the convolute segments roll over each other and collapse, while the convolute segments on the opposite side unroll and expand (fig. 6.6). A longitudinal restraint strap is attached to the convolute segments to ensure that the convolutes do not unfold completely from pressurization (fig. 6.6). The rolling convolute joint also does not require a restraint layer to function, allowing it to be integrated within the scope of this design. It was decided to retain the number of convolutes from the planetary spacesuit prototypes, but recalculate the sizing and placement of the convolute segments to meet the requirements from the biomechanical boot design framework.

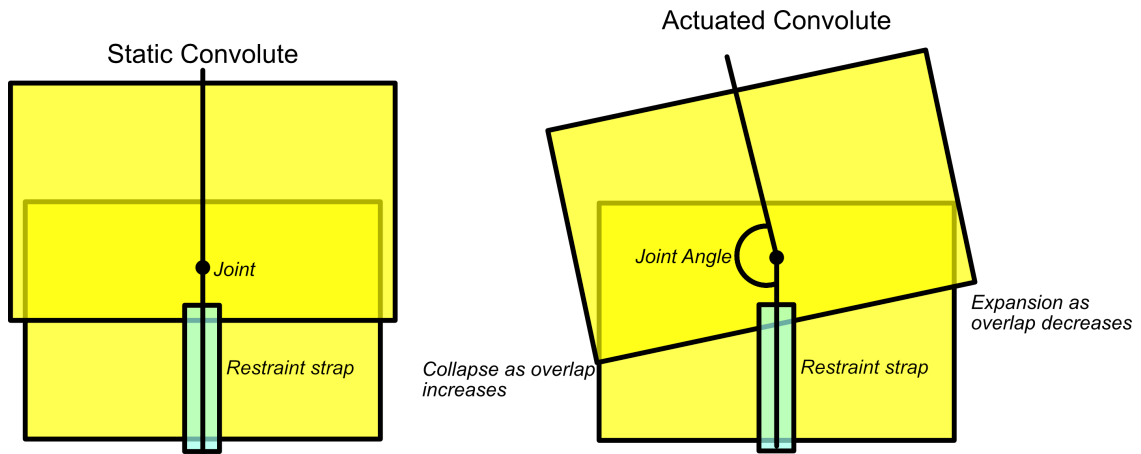


Figure 6.6: Actuation of a convolute joint. The upper convolute segment overlaps the lower convolute segment by a fixed amount, held static at the center by the restraint strap. When the joint is bent, the upper convolute segment rotates around the lower convolute segment. One side of the upper segment rolls over the lower segment, increasing its overlap. The opposite side unrolls from the lower segment, reducing its overlap.

Range-of-mobility for a convolute assembly is limited by the number of convolute segments, height of each convolute segment, and the overlap between each segment. When a convolute assembly is fully actuated, its segments are fully collapsed on one side, and fully extended on the other side. This can be simplified into a triangle, to show the extent to which the convolute assembly is bent (fig. 6.7). The width of this triangle represents the diameter of the convolute assembly. The width and hypotenuse of the triangle are equal as the diameter of assembly is constant for each segment. The height of this triangle is the total actuated height of the convolute assembly when it is fully expanded on one side, and collapsed on the opposite side. A convolute assembly's expanding side can only unroll until it is no longer overlapping the preceding segment (fig. 6.6). Similarly, the collapsing side of the assembly can only roll until each segment reaches the bottom of the succeeding segment. The vertex connecting the base and hypotenuse of the simplified triangle represents the collapsing side of the assembly. The simplified triangle's height represents the expansion of the assembly; as the convolute assembly has a resting height when it is not actuated, the triangle's height only represents the total overlap between all segments.

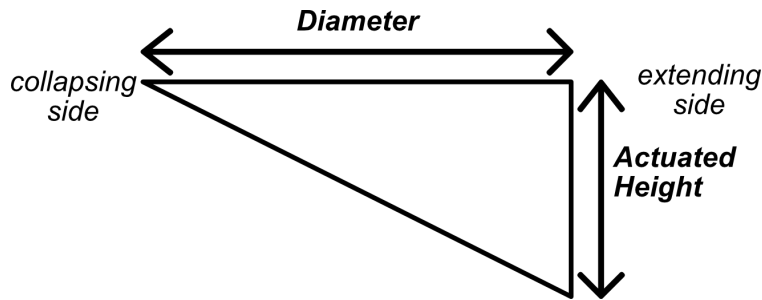


Figure 6.7: Simplified triangle representing a convolute assembly. The left side of the triangle represents the collapsing side of the convolute assembly, while the right side represents the expanding side of the convolute assembly.

The total overlap of the convolute segments can therefore be determined by the diameter of the convolute assembly and the desired range-of-motion (ROM) from this triangle:

$$\text{overlap}_{\text{total}} = \text{diameter} * \tan(\text{ROM}) \quad (6.1)$$

As unrolling and rolling occur simultaneously for each segment, the placement of a convolute segment should be such that its overlap with preceding and consecutive segments is half the segment height.

To determine the individual convolute segment heights, the total overlap is divided by the number of convolute segments minus one, as the total overlap is distributed across all convolute segments. In addition, the final convolute segment in the assembly does not have a succeeding segment to roll over. Therefore, the height of a convolute segment given a desired range-of-motion (ROM) is:

$$\text{height} = 2 * \frac{\text{diameter} * \tan(\text{ROM})}{n_{\text{segments}} - 1} \quad (6.2)$$

Each convolute segment should be placed in the assembly such that it is overlapping the successive segment by one-half of its height.

Circumferential sizing of the ankle convolute assembly was determined by the requirement of the boot to be donned and doffed over the wearer's foot, ankle, and calf. Of these, the heel-ankle circumference was identified as the largest dimension around which the ankle convolute assembly needs be donned/doffed over [57]. The 95% percentile of male heel-ankle circumference, 372 mm, was chosen as the circumference of the ankle convolutes, allowing the convolute assembly to be donned over the foot.

A circumference of 372 mm has a diameter of 184 mm ( $\frac{372}{\pi}$  mm). As the desired dorsiflexion ROM (40 degrees) is greater than the desired plantarflexion ROM (20 degrees), thus the 40 degree dorsiflexion ROM was used for sizing the convolute. Using equation 6.2, the resulting convolute segment height is 100 mm.

A longitudinal restraint strap is needed to ensure the convolutes do not fully expand during pressurization, and to balance the expansion and contraction of the convolutes during joint actuation. This restraint strap fixes the overlap of the convolute segments at the medial and lateral extents of the joint, allowing the assembly to provide plantar and dorsiflexion. The restraint strap should therefore be 200 mm in height, the height of all but one of the convolute segments.

The ankle joint convolute assembly should also be able to be actuated by the operator's ankle joint, whose joint center is at the malleolus. The ankle convolute segments in current planetary spacesuit boots are placed above the instep region, as their vertical height needs to be accommodated. The joint center of the convolute system is at the center of the middle convolute segment. For an ankle joint, this places the joint center well above the malleolus. Therefore, the operator's ankle joint is not indexed properly within the spacesuit boot. Placing the convolute segments at an angle with respect to the plantar-plane of the foot allows the joint segment to be shifted downward (fig. 6.8). A 25-degree tilt was applied to the convolute segments to lower the joint center such that it is closer to the malleolus, improving the indexing of the operator's ankle joint inside the boot.

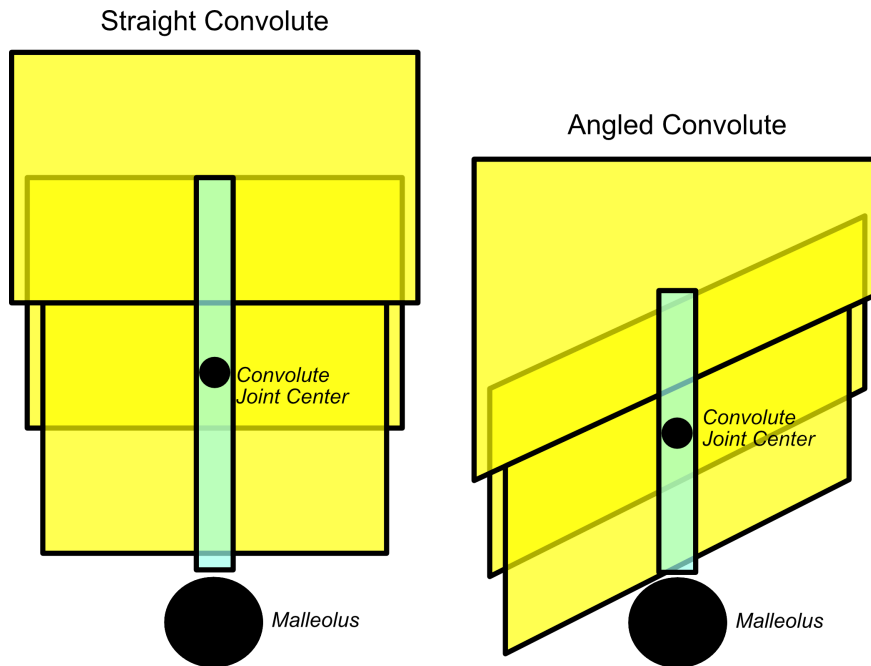


Figure 6.8: Angling the convolutes with respect to the plantar surface allows the joint center of the convolutes to sit much closer to the malleolus, which is the joint center of the ankle.

### 6.3.2 Upper and Toe Box

The upper of the planetary spacesuit boot prototype should allow the foot to drive the motion of the shoe while providing proper fit and comfort, while the toe-box simply accommodates the toes. A last needed to be selected to provide a baseline design for the upper and toe-box. A last is

characterized by its heel-to-toe drop and toe-spring, two sole design features which are very specific to the application of the shoe. As a planetary spacesuit boot is tasked with allowing an astronaut to work and ambulate comfortably across a rough and unknown terrain, parameters from a hiking boot were used to select a last. A male size-9 hiking last was provided for this project from the University of Oregon Sports Product Design Program. This last features a minimal heel-to-toe drop and a toe-spring of 15 degrees. The last features a roomy toe box, where the toe-box is larger than the volume of the toes, for comfort. The last was widened at the ankle to interface to a circumference of 372mm, the same dimension as the ankle convolutes. This allows the ankle convolute assembly to be attached to the upper. The original last and the widening modification are shown in figure 6.9.

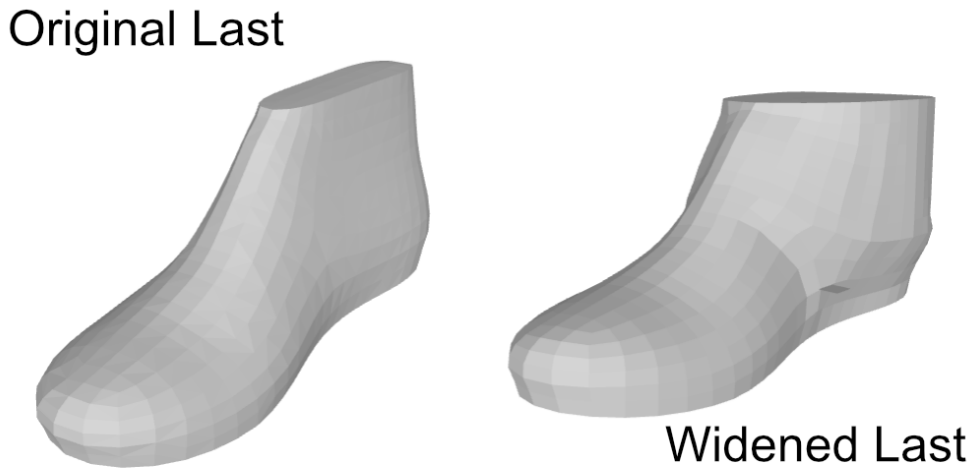


Figure 6.9: Modification of the last to have a wider ankle to accommodate the ankle convolute assembly.

The standard method to generate flat patterns from a last is to place masking tape on the last, cut along seam lines, and flatten the masking tape patterns [96]. The last for this design was 3D printed with ABS. Seam lines for this last's patterns are shown in figure 6.10 . These seams were chosen to ensure the patterns are as flat as possible to minimize folds and creases in the pressure

bladder design. As a result, separate patterns were generated for the sole and toe box, and the upper was split into multiple patterns.

The seam which runs along the foot's length across the upper was used to incorporate lacing into the boot.

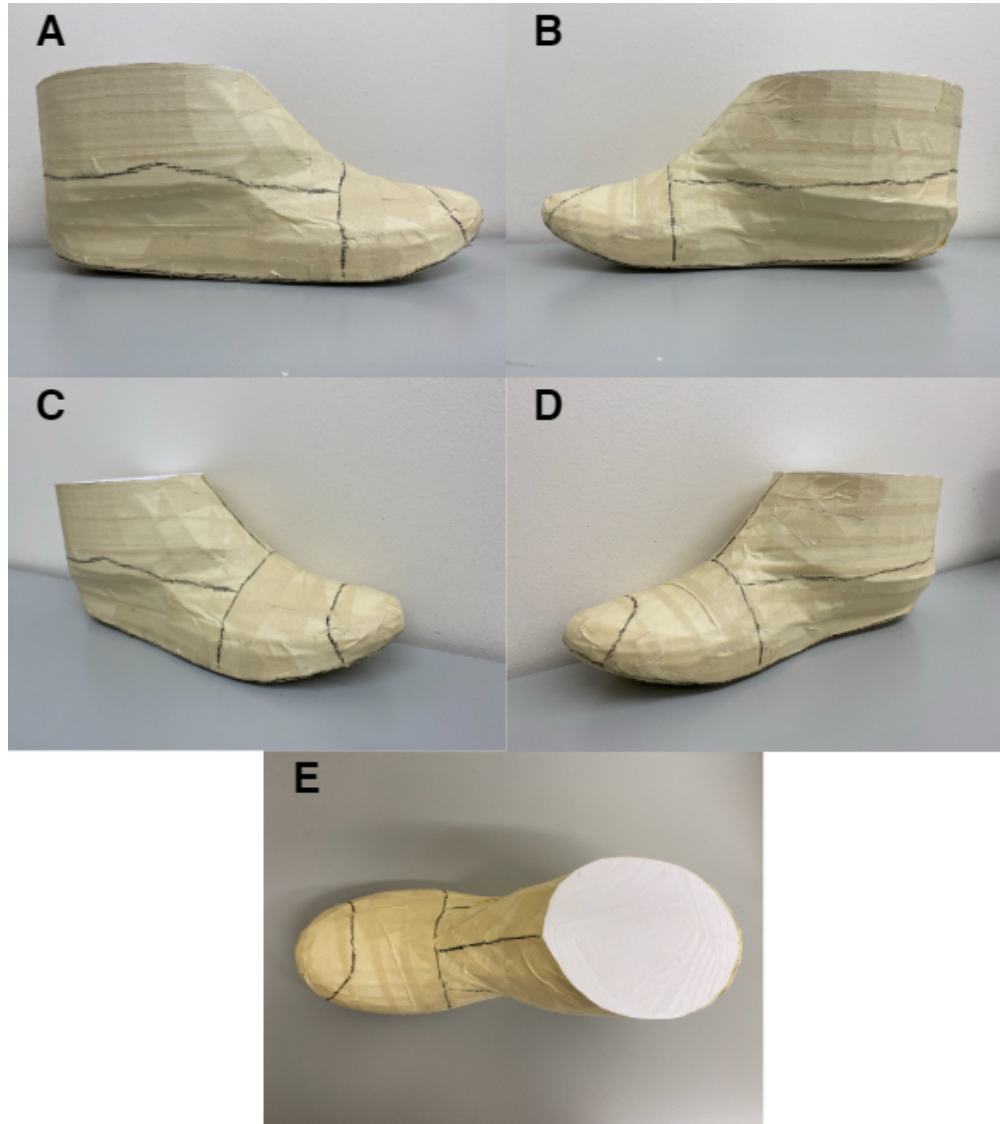


Figure 6.10: Seam lines on taped last. The lateral (A), medial (B), lateral profile (C), medial profile (D), and top-down (E) views are presented

### 6.3.3 Instep Lacing

A rolling convolute was used to make a conformal pressure bladder which accommodates the lacing, and changes its volume as the lacing is tightened. This convolute allow for deformation of the pressure bladder without resulting in folds, which have been shown to cause discomfort [34], and may be unpredictable in their deformation. As the lacing is tightened, the convolute contracts in a prescribed fashion and decreases the distance between the plantar and dorsal surface of the shoe's interior, resulting in a tighter fit. When the lacing is loosened, the convolute is expanded and the volume is increased, resulting in a looser fit.

Initial designs of the lacing convolute had the convolute placed around the entire foot fig. 6.11. Thus, when the convolute is contracted, the distance between the plantar and dorsal surface decreases uniformly across the length of the foot. However, findings from the dynamic foot shape model (see Chapter 5) found that instep height variability mostly occurs towards the ankle joint. Therefore, the lacing convolute design was modified to pivot at the MTP joint. The lacing convolute is designed into the seam between the inferior and superior upper patterns. The overlap for the lacing convolute was designed with a varying height across the length of the upper patterns, as opposed to the constant height of the overlap used for the ankle convolutes. The overlap is 1 cm at the toe-box, and 5 cm near the heel, allowing for the pivot at the MTP joint.

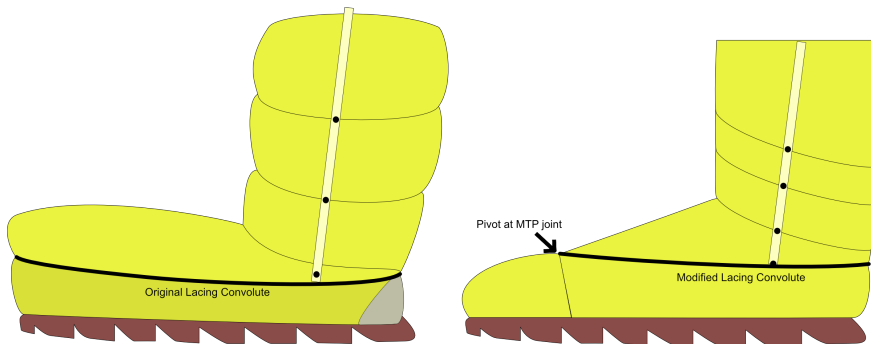


Figure 6.11: Evolution of lacing convolute design. Originally, the lacing convolute ran the length of the boot (left). The lacing convolute was then iterated to pivot at the MTP joint, and provide greater capture closer to the heel

The convolute is paired with a lacing system to allow the wearer to adjust the fit of the upper to their desired tightness (fig. 6.14). In a spacesuit boot, the lacing will need to withstand the pressure forces; the pressure forces will want to expand the boot and loosen the lacing. A BOA lacing system (BOA, Denver CO) was chosen for its strength and fine adjustment, and was provided by BOA. The BOA H4 system consists of a dial, a steel lace, tubing, and low-friction guides; this is the strongest system provided by BOA. The guides are attached in an alternating pattern between the top and bottom layers of the convolute. The lace is run from the dial, through the tubing on the medial side, through the guides, and back through the tubing on the lateral side to the dial. As the dial is tightened, the lacing length is decreased, bringing the guides closer together and contracting the convolute. The lace length is kept constant through the tubing, which fixes the length between the dial and the guides. This is necessary to ensure that no tightening is occurring near the ankle convolute assembly, which would prevent the ankle convolutes from working. Once the lace is tightened to the desired level, the dial can be locked; this prevents the lace from lengthening or shortening.

All lacing adjustment is done when the boot is unpressurized. Adjusting the lacing when the boot is pressurized will require additional effort to compress the air inside the boot. Therefore, adjustment of the boot in an operational setting will require the user to de-pressurize the spacesuit, which precludes adjustment from occurring during an EVA. Therefore, it will be important for users of this system to spend time during training to find their ideal fit prior to performing an EVA.

The placement of the dial was chosen to provide dynamic tightening (fig. 6.14). The dial is placed on the front of the convolute assembly. The tubing is run on the distal side of the convolute assembly. Therefore, when the ankle is plantarflexed, such as during heel-off, the distance that the lace travels increases. Since the lace length is locked, the guides must move closer together to accommodate the lace travel length; this therefore rolls the convolute and tightens the fit. The dynamic tightening accommodates the drop in instep height characterized in the dynamic foot shape model (Chapter 5), ensuring that fit is maintained throughout the gait cycle.

### 6.3.4 Heel Counter

The heel counter is used in footwear to provide a stiffer rear foot support [141], which may prevent the rear of the shoe from deforming and allowing the heel to lift out of the shoe. The placement of the rearmost BOA dial (fig. 6.14) acts as a heel counter, as it is designed to sit above the heel.

An additional heel counter was designed based on the dynamic foot morphology model (Chapter 5). The selected last had a similar shape as seen in the foot model, and was used as a mold for the heel counter. Clay was molded to the heel of the last to provide a template for the heel counter shape. The thickness of the polymer heel counter was determined through iterative testing; polymer thickness was increased until it interfered with donning and doffing. The heel counter is designed to be placed underneath the lacing convolute, as to not interfere with its operation.

Figure 6.12: Image of additional heel counter which was placed inside the boot

### 6.3.5 Sole

The sole of the boot provides support, traction, and protection to the wearer. As the novel spacesuit boot will only be constructed for laboratory testing, a simple sole was constructed to represent the height that a manufactured sole would have. A sole was designed by our collaborators at the University of Oregon Sports Product Design Program to fit the last used for the novel spacesuit boot design. A 3D model of the sole is shown in fig. 6.13.

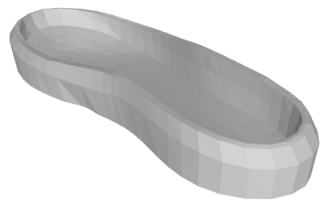
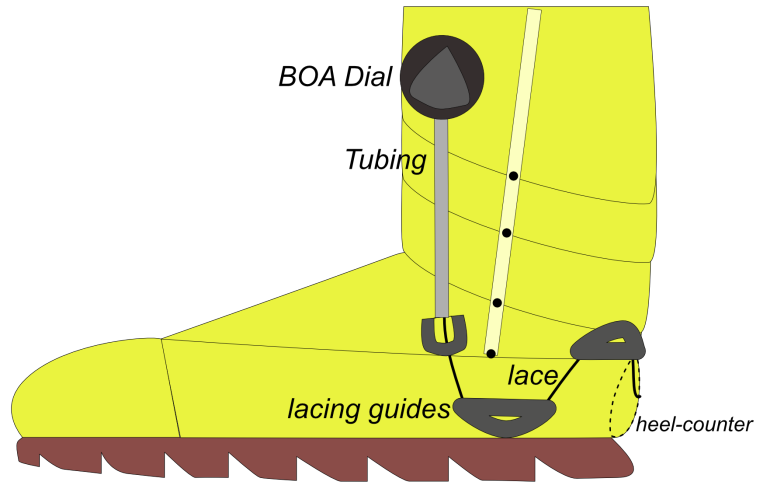


Figure 6.13: 3D view of the sole generated from the last.

### 6.3.6 Summary

The novel spacesuit boot's design summarized in figure 6.14. The various design elements work together to provide adjustability for the wearer through lacing, and secure the heel in place through the lacing and heel counter.

Foot Flat:



When plantarflexed:

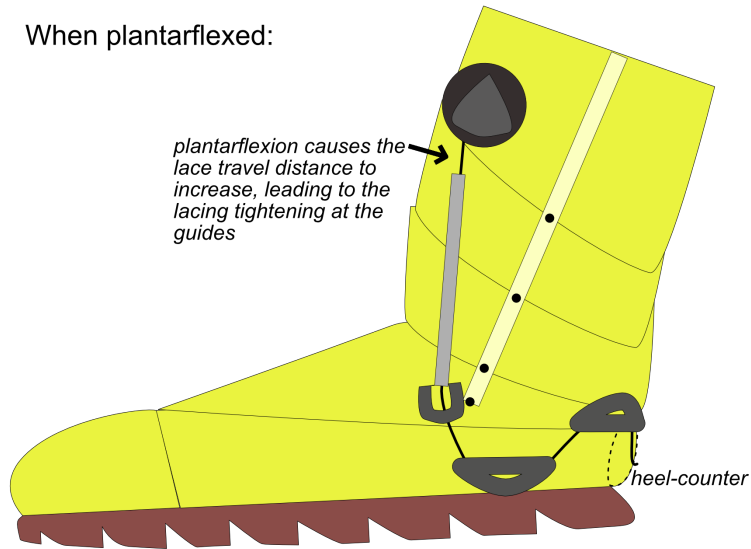


Figure 6.14: Overview of the novel spacesuit boot. Only the medial side is shown, but the lacing is mirrored on the lateral side. The heel counter's location is shown as a dotted line as it is internal to the pressure bladder. When plantarflexed, the distance the lace has to travel is increased and is shown by the arrow. Therefore, the lacing near the guides further tightens.

## 6.4 Novel Planetary Spacesuit Boot Construction

Much effort was required to translate the novel planetary spacesuit boot design into a functional prototype, as shown in figure 6.15. The following sections outline the manufacturing process for constructing the boot prototype.



Figure 6.15: Prototype planetary spacesuit boot constructed with BOA lacing, ankle rolling convolutes, and a heel counter. The heel counter is not visible as it is inside the pressure bladder

A heat-sealable urethane coated nylon (Seattle Fabrics, Seattle WA) was used as the material for the pressure bladder [65]. Discussions with spacesuit engineers suggested 400 Denier nylon for its strength. The material can be made air-tight by heat-sealing with a mini-iron (Clover Needlecraft, Los Angeles CA) which can reach a maximum of 580 degrees Fahrenheit.

Numerous coupons were made to test how long heat was required to achieve a strong seal between the nylon fabric. These coupons had heat applied at 390 degrees Fahrenheit in intervals of 5 sec up to 30 seconds. The coupons were tested on an Instron machine using an ASTM D5034-19 fabric tensile test method. It was found that the coupons with 20 seconds of heat application and up failed at the nylon interface, and not just at the urethane, suggesting a strong bond had been achieved between the fabric.

As only one side of the material is coated in urethane, and the urethane can only be bonded to another layer of urethane, care must be taken in the patterning to ensure that each panel is sealable. It was decided that the urethane-coated side of the patterns will be facing towards the foot, as it is done in current spacesuit construction. Panels were sealed together with another strip of pressure bladder material (fig. 6.16). This technique was applied to each section of the pressure bladder, with specific details regarding construction below.

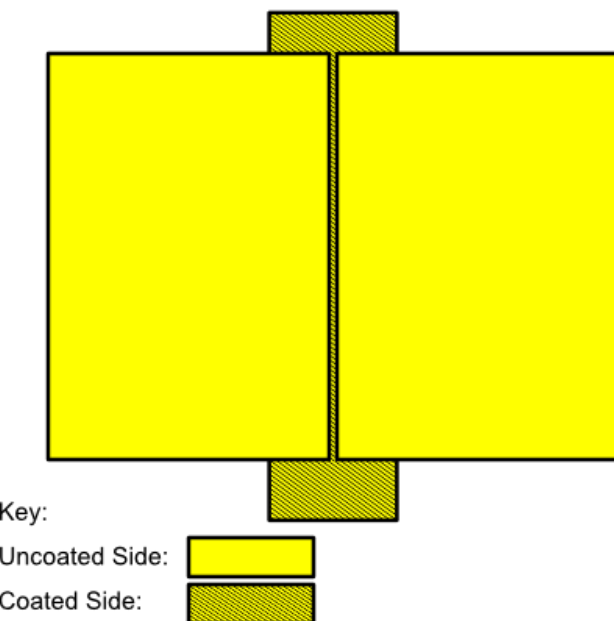


Figure 6.16: Two pressure bladder patterns (left, right) are connected by a single strip of material (middle) at the team. This strip is heat-sealed to both patterns, creating an air-tight seam.

#### 6.4.1 Ankle Convolute Construction

Ankle convolute construction starts with a flat panel for each convolute segment, as summarized in figure 6.17. The convolute assembly was constructed by folding over the top of the

convolute segments for the two convolute segments by one-half of the convolute segment's height to achieve the desired segment height. Then, the bottom of the preceding convolute segment is sewn to the folded-over top of the succeeding convolute segment using a straight stitch at 1.0 mm pitch, at both the overlap itself and 1 cm above the overlap. The stitches are then heat-sealed. This process is repeated for the next convolute segment.

A restraint strap is constructed from a 3/4" in canvas fabric which is folded in half and stitched on one side. Two restraint straps are used for each convolute assembly, and are placed at 25% and 75% of the flat panel convolute assembly's width. This results in the restraint straps lying on the medial and lateral neutral axes of the convolute assembly once it is folded into a cylinder. As a result, these restraint straps will be on the medial and lateral side when the convolutes are fully assembled. The restraint straps are stitched to the junctions in two locations between convolute segments by using a straight stitch at the overlap and 1cm above the overlap.

Once all three convolute segments and the restraint straps are attached, the two ends of the segments are brought together to make the flat panel into a circular convolute assembly. A strip of urethane-coated nylon is then used to seal the seam on the inside. 3D printer filament is used for the bands of the rolling convolute. The filament is inserted into the gap between the stitching at the convolute segment junctions. The filament is trimmed to length at the seam. A 1.5cm strip of canvas material is glued to the bottom of each convolute segment to ensure that the convolute's overlap actuates properly. Without this canvas strip, the succeeding convolute segment was found to expand under pressurization and prevent the preceding convolute segment from rolling over it. The ankle convolute assembly is now ready to be attached to the upper.

### Pattern Trimming

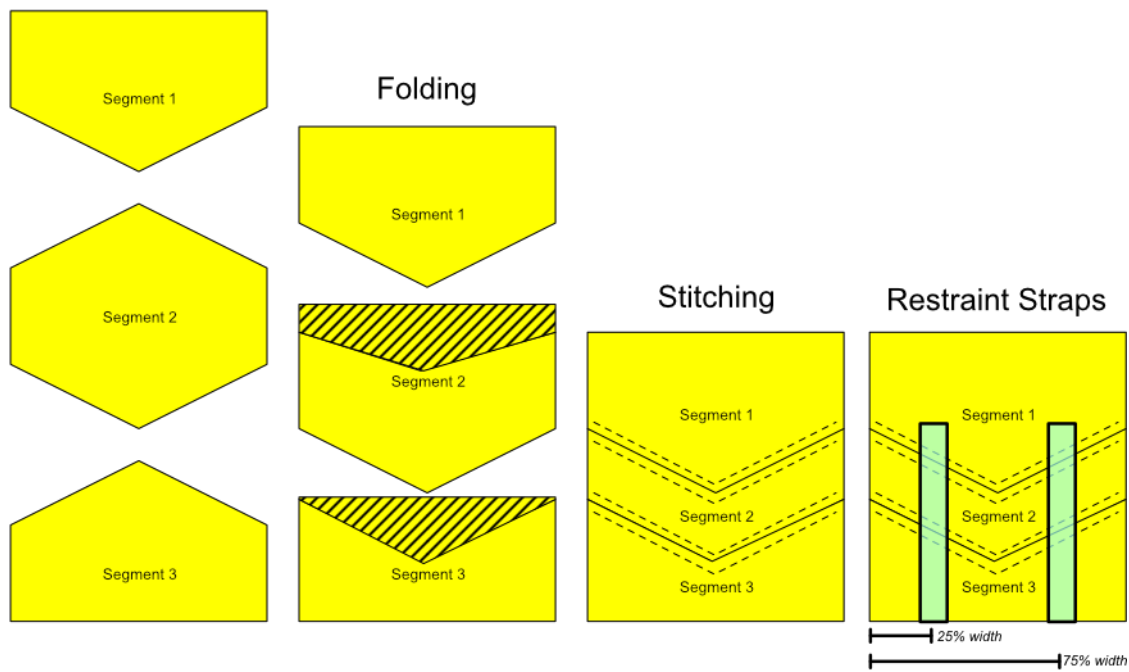


Figure 6.17: Ankle convolute flat pattern construction.

#### 6.4.2 Upper and Toe-Box Construction

Patterns for the upper and toe box expected to interface with the pattern for the sole are extended by 1 cm to provide a seam to attach to the sole (fig. 6.18). This avoids having to use a strip of urethane coated nylon on the interior of these seams, which is at a sharp angle and proved difficult to manufacture.

The patterns for the toe box are simply assembled and sealed together by using strips of urethane-coated nylon at the seams. Construction of the upper needs to account for the instep lacing feature. The inferior upper pattern is extended by the dimensions of the overlap needed for the instep lacing. The top of the overlap is folded over and the superior upper pattern is stitched to the fold. This is done for both the lateral and medial upper patterns. The lateral and medial

upper patterns are attached at the heel with a strip of urethane coated nylon. Then, 3D printer filament is inserted into the gap between the stitches to provide structure to the convolute.

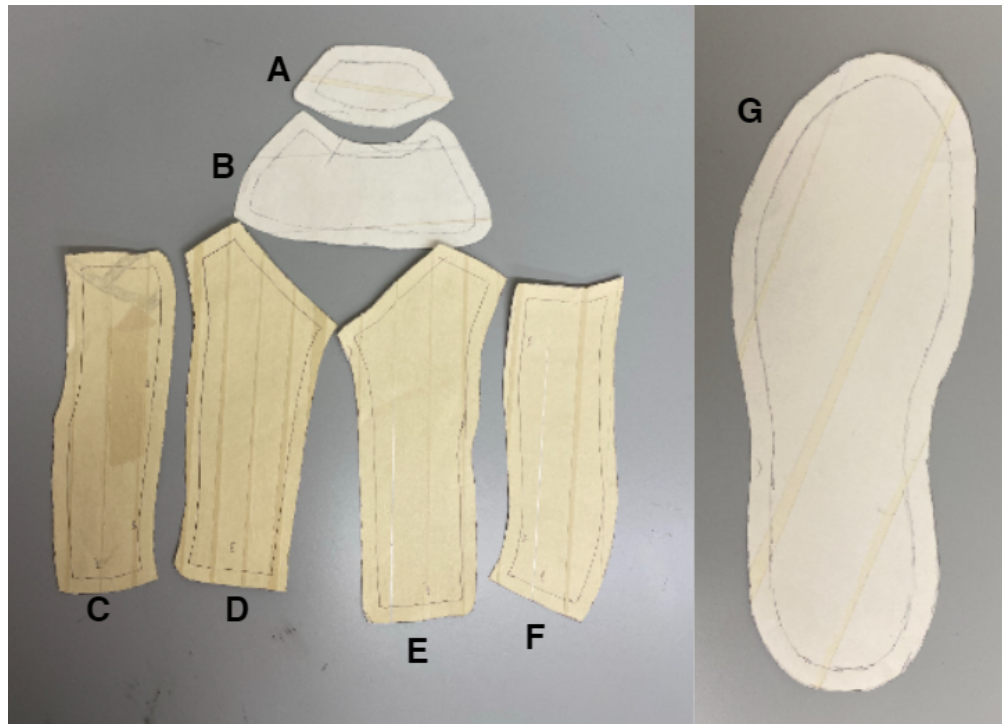


Figure 6.18: Patterns for the upper, toe-box, and sole. These patterns are cut from the last taping process, and flattened onto a piece of paper. New patterns are then traced around the flattened tape patterns, and used to make the respective panels. A 1cm seam is added around each pattern to provide flexibility in manufacturing. Patterns were generated for the forward (A) and rear (B) toe-box, inferior (C) and superior (D) medial upper, inferior (F) and superior (E) lateral upper, and the sole (G).

#### 6.4.3 Sole Construction

Ethylene-Vinyl Acetate foam is a common material used for sole construction in sneakers and daily shoes. Collaborators at the University of Oregon Sports Product Design Program informed us that their prototyping process for most footwear involved using Smooth-On Flex Form-it 17 (Smooth-On, Macungie PA) expanding foam, which provides a similar bounce and deflection as Ethylene-Vinyl Acetate foam.

A mold for the sole was designed to allow for casting from the expanding foam. The sole was provided as a 3D mesh file (fig. 6.13). A negative of the sole was created using the Blender

software, where a rectangular box mesh which was bigger than the sole was placed over it and the difference between the two meshes was taken. A seam was added to this box so that it can be separated into two halves. Three holes were placed in the top half of the box above the centerline of the sole negative, allowing for the foam to be poured in before it cures. In addition, four holes were placed at the corners of the box, allowing the box to be clamped together with bolts and thus sealing the mold. This mold was then 3D-printed out of PLA material, and is shown in fig. 6.19.



Figure 6.19: Two halves of the mold used to cast the sole.

Ease Release 2831 (Smooth-On, Macungie PA) was applied to the 3D mold. The expanding foam was mixed, poured into the mold, and allowed to fully cure as per the manufacturer's instructions. The mold was then unclamped, and the sole was peeled out of the mold. Any flash, excess material from the molding process, was then cut off with a knife.

The pressure bladder is attached to the sole through a welting process. The seam from the attachment of the pressure bladder's upper and sole patterns is sewn to the sole. This process is reinforced with hot glue.

#### **6.4.4 BOA Lacing Integration**

The BOA lacing guides are secured to the pressure bladder and sole through stitching. The guides are first perforated with four holes, and then hand stitched to the pressure bladder and sole. The BOA lacing dial is glued to the top of the upper most convolute segment. The lace tubing is press-fit into the dial and the first set of guides. The lace tubing is also glued to the canvas straps at the bottom of upper-most convolute segment to ensure it stays secure.

#### **6.4.5 Heel Counter**

The heel counter made by casting a thin (3 mm) layer of Elite Double 16 dental polymer (Zhermack SpA, Badia Polesine (RO), Italy). This layer was trimmed to size to fit on the interior of the boot beneath the lacing convolute. The heel counter was secured to the interior of the boot with hot glue and tape.

#### **6.4.6 Pressure Sealing**

While the urethane-coated nylon has an air-tight seam when heat-sealed properly, manufacturing tolerances and wear from use of the boot were found to create leak paths in the prototype spacesuit boot's pressure bladder. It was found that hot glue was an adequate sealant for the pressures used in testing. Therefore, a thin layer of hot glue was applied to all seams in the pressure bladder.

### **6.5 Classic Spacesuit Boot Design and Construction**

To evaluate the design of the proposed novel spacesuit boot, a comparison “classic” spacesuit boot was fabricated, based on current designs to the extent possible (fig. 6.20). Similar construction techniques were used as the prototype planetary spacesuit boot: the same sole was used for both boots, and the upper for both boots was designed around the same last. The convolutes for the classic spacesuit boot were constructed with the same height, and overlap, but the convolutes were left flat to the foot's plantar surface, as they are in current planetary spacesuit boot prototypes [121]. In

addition, the restraint strap was secured to the sole in the absence of the lacing convolute. The upper for the classic spacesuit boot does not have any lacing; the superior and anterior upper patterns were sealed at the seam separating them. This ensure that the two boots are identical except for the three novel features in the prototype boot: angled ankle convolutes, lacing, and a heel counter.



Figure 6.20: Classic spacesuit boot which was constructed with similar techniques as the prototype spacesuit boot, but without lacing, or a heel-counter.

### 6.5.1 Pressurization Test Interface

~~This analysis outlined a framework for designing a new spacesuit boot with an emphasis on fit and mobility during gait. The framework aims to reduce the risk of spacesuit boot injury by developing a process to design a spacesuit boot. It is expected that focusing a design on fit and mobility will reduce the occurrence of heel lift and contact injuries.~~

~~This framework therefore serves as bounding requirements to ensure future spacesuit footwear does not inhibit natural foot motion or cause discomfort due to incompatibilities between foot and shoe shape. The only previously bounding requirement, the 2019 NASA SBIR solicitation for a new surface spacesuit boot, had only one requirement for ankle flexion/extension. This work provides~~

a series of requirements based from previous biomechanics studies on foot motion while walking and hiking to expand upon the provided NASA requirements.

These requirements, along with findings from the dynamic foot shape model in Chapter 5, were translated into a prototype spacesuit boot design. This design features a novel lacing feature which accommodates the static and dynamic variability in instep height. In addition, the prototype boot also features a heel counter, which should assist in ensuring the heel does not slip out of the boot during walking. The prototype boot modifies the ankle convolutes found in current planetary spacesuit boots by tilting their plane towards the heel, thus lowering the joint center to be better indexed with the operator's ankle joint.

The prototype boot was constructed using an urethane coated nylon for the pressure bladder. A sole constructed from expanding foam was integrated into the design. Lacing for the prototype boot was provided by BOA.

A classic planetary spacesuit boot was also constructed, but omitted the novel features of the prototype spacesuit boot. No lacing or heel counter was included in the classic spacesuit boot. Ankle convolutes were left parallel to the plantar surface. However, this boot was constructed using the same last, resulting in similarly shaped patterns. In addition, the sole used for this boot is identical. This ensures that the novel features of the prototype spacesuit boot can be compared to the classic spacesuit boot through evaluation, which is described in Chapter 7.

The novel pressurized spacesuit boot prototype developed in Specific Aim 3 was validated for fit and comfort through subject evaluation. Results of the validation can help answer the main hypothesis of this thesis: a spacesuit boot designed with dynamic foot morphology will provide increased compatibility between the spacesuit and operator. In a terrestrial environment not requiring pressurized spacesuits, EVA tasks are best performed with a work boot. Therefore, an unpressurized laced work boot was used as the gold standard to compare the novel spacesuit boot to. As the novel spacesuit boot features lacing, the unpressurized work boot was compared in both laced and unlaced conditions. A classic pressurized spacesuit boot, not featuring any lacing, was used in the evaluations to compare the novel spacesuit prototype to current spacesuit boot

~~technology. This chapter details the methods for the subject evaluation of all four boots, results, and a discussion on the results as related to each boot's performance.~~

A pressurization interface was constructed to allow a pressurized boot to be worn by a subject during testing. This interface was common between the classic and novel pressurized spacesuit boots. ~~The interface was designed to allow the~~ This interface is not designed to integrate with a spacesuit, but rather for a user to wear a pressurized spacesuit boot without having to wear an entire spacesuit, much like wearing ~~the control work boot~~ a terrestrial shoe. This allows for the performance of the boots to be isolated to the boots themselves, and not to the presence or absence of a spacesuit.

#### 6.5.1.1 Interface layers

A base layer of neoprene is heat-sealed to the upper-most ankle convolute. This neoprene layer is patterned as a staircase (fig. 6.21), with the dorsal side having a height of 3 cm, and the ventral side having a height of 6 cm. This layer has the same circumference as the The dorsal side of this layer is then heat sealed with neoprene sealing tape. This creates a 6 cm diameter for the wearer to don and doff the boot. While this gap is much smaller than the wearer's anthropometry that needs to pass through it, the stretch characteristics of the neoprene allow for the foot, heel, and calf to pass through. As a result, a tight fit was maintained around the wearer's calf once the boot was fully donned.

A neoprene and canvas strap was constructed with velcro backings to assist in creating a seal around the neoprene base layer. After the boot is donned, the canvas strap was wrapped over the neoprene layer around the wearer's calf. The strap was then secured to itself using the velcro backing. The canvas material has minimal stretch, ensuring that the lower neoprene layer does not balloon from the internal pressure of the boot. The neoprene strap is then similarly wrapped over the canvas strap. The stretch of the neoprene strap allows it to compress the lower layers around the subject's calf, creating an even tighter fit. Two additional elastic straps with velcro backings were constructed and placed at the top of the lower straps, further sealing the interface between the boot and the wearer. An overview of the straps is provided in figure 6.22.

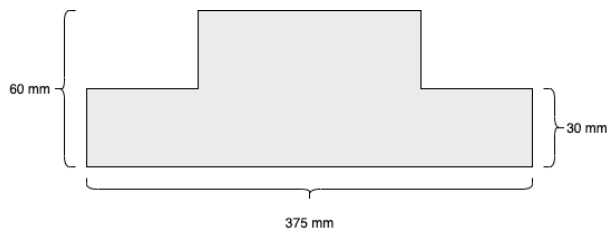


Figure 6.21: Patterning of the base neoprene layer (top) which results in a much smaller opening (bottom, yellow highlight) for the wearer's calf to enter through.

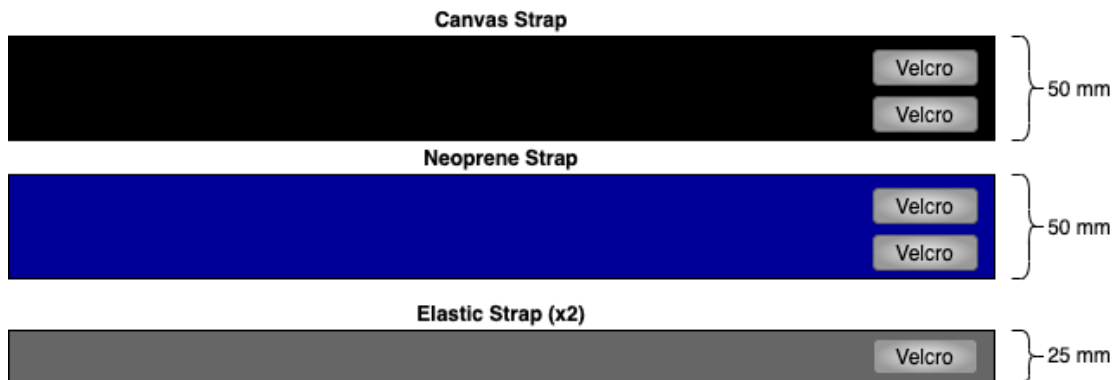


Figure 6.22: Overview of straps used to create a seal around the wearer's ankle.

### 6.5.1.2 Air Feed and Monitoring

Two air lines were integrated into the boots just below the neoprene layer; a supply air line to provide pressurized air and a monitoring air line log the boot's interal pressure with a pressure gauge. Masterkleer Soft PVC Tubing (McMaster-Carr, Elmhurst IL), with a inside diameter of 1/8" and an outside diameter of 1/4", was used for the air lines. A vertical slit was cut in the boot 2 cm below the pressurization interface to allow the air lines to enter the boot. The slit was

then sealed with hot glue. The air lines were oriented along the circumference of the boot's calf to minimize interference with the ankle convolutes.

The boot's monitoring line was connected to a differential pressure manometer (Amprobe MAN30, Amprobe, Everett WA). This manometer provides a gauge readout of the internal air pressure in the boot. The supply line was connected to the lab's air line, which provides air at 100 psi, with a ball valve. The ball valve was adjusted by the test conductor while monitoring the boot's internal pressure through the manometer.

#### **6.5.1.3 Interface Performance**

The pressurization interface was used on all subjects during boot evaluation. Every subject was able to reach a boot internal pressure of 2.5 psi for both boots. Leakage was still present in the boots due to high tolerances from manufacturing the boots by hand.

The EMU operates at 4.3 psi, and future planetary exploration suit concepts have called for suits to be operated at a higher 8.3 psi to reduce the pre-breathe time required for astronauts prior to getting into the suit [80]. The ACES, which was not designed for EVA operations, operated at 3.5 psi [137]. Higher operational pressures may require increased effort to move suit components.

It was originally desired to reach a pressure of 4.3 psi to replicate the spacesuit pressure in current EVA activities aboard the EMU. While the boots were only able to achieve 2.5 psi, this was still deemed sufficient to proceed with testing as the boot's material was fully expanded to its maximal volume. This allows the boots' mechanisms, such as the rolling convolute ankle joint, to function as they would at a higher pressure. A higher pressure would require additional effort from the subject to move the boot, but would activate the mechanisms in the same fashion. Therefore, it was decided to continue with testing as this would still provide insight into the performance of the boot's mechanisms with regards to subject fit and comfort, but results will need to be taken into context with the lower operating pressure.

#### **6.6 Summary**

This analysis outlined a framework for designing a new spacesuit boot with an emphasis on fit and mobility during gait. The framework aims to reduce the risk of spacesuit boot injury by developing a process to design a spacesuit boot. It is expected that focusing a design on fit and mobility will reduce the occurrence of heel-lift and contact injuries.

This framework therefore serves as bounding requirements to ensure future spacesuit footwear does not inhibit natural foot motion or cause discomfort due to incompatibilities between foot and shoe shape. The only previously bounding requirement, the 2019 NASA SBIR solicitation for a new surface spacesuit boot, had only one requirement for ankle flexion/extension. This work provides a series of requirements based from previous biomechanics studies on foot motion while walking and hiking to expand upon the provided NASA requirements.

These requirements, along with findings from the dynamic foot shape model in Chapter 5, were translated into a prototype spacesuit boot design. This design features a novel lacing feature which accommodates the static and dynamic variability in instep height. In addition, the prototype boot also features a heel counter, which should assist in ensuring the heel does not slip out of the boot during walking. The prototype boot modifies the ankle convolutes found in current planetary spacesuit boots by tilting their plane towards the heel, thus lowering the joint center to be better indexed with the operator's ankle joint.

The prototype boot was constructed using an urethane coated nylon for the pressure bladder. A sole constructed from expanding foam was integrated into the design. Lacing for the prototype boot was provided by BOA.

A classic planetary spacesuit boot was also constructed, but omitted the novel features of the prototype spacesuit boot. No lacing or heel counter was included in the classic spacesuit boot. Ankle convolutes were left parallel to the plantar surface. However, this boot was constructed using the same last, resulting in similarly shaped patterns. In addition, the sole used for this boot is identical. This ensures that the novel features of the prototype spacesuit boot can be compared to the classic spacesuit boot through evaluation, which is described in Chapter 7.

## **Chapter 7**

### **Specific Aim 4: Evaluate novel planetary spacesuit boot design for fit and comfort**

The novel pressurized spacesuit boot prototype developed in Specific Aim 3 was validated for fit and comfort through subject evaluation. Results of the validation can help answer the main hypothesis of this thesis: a spacesuit boot designed with dynamic foot morphology will provide increased compatibility between the spacesuit and operator. In a terrestrial environment not requiring pressurized spacesuits, EVA tasks are best performed with a work boot. Therefore, an unpressurized laced work boot was used as the gold standard to compare the novel spacesuit boot to. As the novel spacesuit boot features lacing, the unpressurized work boot was compared in both laced and unlaced conditions. A classic pressurized spacesuit boot, not featuring any lacing, was used in the evaluations to compare the novel spacesuit prototype to current spacesuit boot technology. This chapter details the methods for the subject evaluation of all four boots, results, and a discussion on the results as related to each boot's performance.

#### **7.1 Experimental Design**

The goal of this evaluation was to assess fit and comfort of the novel spacesuit boot, as it compared to the classic spacesuit boot, unlaced work boot, and laced work boot. Fit was primarily assessed through heel performance, as reducing heel lift is a primary focus for planetary EVA boot design. Proper dynamic fit will allow for high heel performance, which would improve upon current planetary spacesuit boot efforts. Subjects in this evaluation performed five heel-raises and

a short walk for each test boot condition. Quantitative measurements were taken during the heel-raises, and surveys were administered after completing the evaluation for each boot. Therefore, this experiment aimed to answer the following hypotheses:

- The novel spacesuit boot design provides equivalent comfort compared to the laced work boot and improved comfort compared to the unlaced work boot and classic pressurized spacesuit boot
- The novel spacesuit boot design provides equivalent heel performance compared to the laced work boot and improved ~~comfort~~-heel performance compared to the unlaced work boot and classic pressurized spacesuit boot

## 7.2 Methods

### 7.2.1 Subjects

Five subjects with a self-reported shoe size between 8-10 US Male (9.5-11.5 US Female) were recruited to participate in this evaluation. Participant foot length, foot width, and arch length were measured with a Brannock device when they arrived in the lab. A summary of participant foot anthropometries is provided in table 7.1.

Table 7.1: Summary of subjects' foot measurements

Subject	Foot Length (cm)	Foot Width	Arch Length (cm)	Sex
FQ	25.5	C	26	F
FT	25.5	D	25	F
RM	25.5	C-D	27	M
TF	25.5	D	25	M
TQ	26.5	D	27	M
Average	25.7 ± 0.4		26 ± 1	

### 7.2.2 Procedures

For each boot condition, subjects donned the test boot on their right foot. The order of the test boots was counterbalanced ~~aeross all subjects—within the pressurized and unpressurized categories; subjects started their trials with the unpressurized boots and then proceeded to the pressurized boots. The lacing was simply removed or added when switching from the laced workboot to the unlaced workboot, and vice versa; this maintained the same boot for both these conditions minus the lacing.~~ Subjects were instructed to bring their own low-top sneaker to wear on their left ~~shoe~~foot; a low-top sneaker does not limit the amount of heel-rise when compared to a high-top shoe, and therefore serves as a control between all test boot conditions.

Subjects started by performing one set of five heel-raises, and were instructed to best synchronize their heel-raises between both feet. They were also instructed to lift each foot independently as high as possible. Subjects were monitored during their performance of the heel-raises, and asked to repeat the heel-rise set if they were not able to maintain balance during the heel-raises, or were not synchronized when initiating the heel-rise. After performing the heel-raises, subjects were then instructed to walk a distance of 4 meters. This distance was limited by the length of supply air line available to pressurize the spacesuit boots.

### 7.2.3 Quantitative Measures

Each of the test boots had two markers placed on their medial side. The first marker was placed on the sole in-line with where the center of the shank would lie in the boot. The second marker was placed on the sole 10 cm forward of the first marker. Silver retro-reflective tape was used as the markers for the work boot as it provided the greatest contrast against the black sole. Black Duck tape was used for the spacesuit boots for contrast against the white sole. Markers were similarly placed on the subjects' left shoe, choosing a color which provided the greatest contrast against their shoes.

For the heel-raises, subjects were instructed to stand centered between two Intel RealSense D415 cameras. These cameras were used to collect video data of the markers' movement for both the left (control shoe) and right (test shoe) sides fig. 7.1. Kinovea software was used to measure the vertical amount of heel-rise with these markers. For each heel-rise set, the distance between the two markers is used to calibrate the video data from the camera's coordinates to the global coordinates. The horizontal axis was defined as the plane of the floor. The Kinovea software tracked the vertical displacement of the first marker to assess heel-rise magnitude with respect to the floor to measure the heel position over time in the vertical plane.



Figure 7.1: Marker locations for the novel spacesuit boot (A), work boot (B), and a subject's left shoe (C). The novel spacesuit boot and left shoe use black Duck tape for markers on their sole. The work boot uses a silver reflective tape for its markers. The Kinovea software's annotations are shown on each of the image: Marker 1 is tracked to provide heel rise magnitude, and the orange line is used to calibrate the coordinate system.

Findings from Chapter 4 showed that IMUs may not be appropriate for detecting instances of heel-lift and characterizing heel performance. Therefore, a force sensitive resistor (FSR 402, Interlink Electronics, Camarillo CA) was embedded in the sole of the test boots fig. 7.2. The FSR was attached to a Raspberry Pi Pico, which measured the voltage across the sensor with a voltage divider. The FSR was supplied with a 3.3V reference voltage. As a force is applied to the FSR, the resistance of the FSR decreases. To align the sign of the FSR voltage to the sign of the heel rise magnitude, the voltage reading was inverted such that applying force to the FSR decreased the voltage.

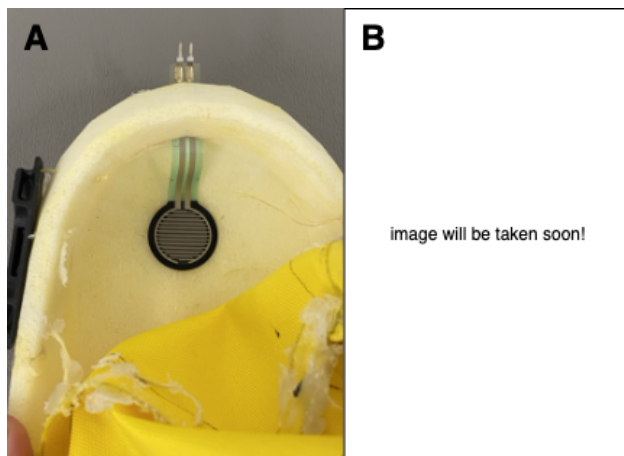


Figure 7.2: Location of the FSR embedded into the sole of the novel spacesuit boot (A) and the work boot (B). The FSR was embedded in the classic spacesuit boot's sole in the same fashion as the novel spacesuit boot

Post-hoc calibration of the FSRs was conducted to characterize the voltage response to force. Calibration was conducted by applying a force from a instrumented force gauge to the sensors, while they were still embedded in the boot. The voltage response of the FSR and the force gauge's output were synced with a custom Python script. Due to sensor breakage, the sensor in the novel spacesuit boot for subjects FT and TF was not calibrated, as it was replaced prior to being used by the other subjects. Calibration results fig. 7.3 showed a similar voltage response for both spacesuit boots, while the work boot's voltage response appears shifted. This may be due to the softer material sole used in the spacesuit boots compared to the work boot. However, for In addition, there was little confidence that the calibration curve is completely representative of a foot on the sensor, as the foot may shift while maintaining contact and this could not be accurately characterized by a

single sensor. Therefore, as voltage is the only reliable measurement to obtain from the FSRs, it was decided to continue reporting FSR voltage as a proxy for heel contact. For all boots, there is a strong inflection point in the response at 0.5V, where voltages below 0.5V covered a wide range of applied force. Therefore, it was decided to characterize a voltage of 3.3V as “no contact”, voltages between 0.5 and 3.3 V as “mild contact”, and voltages below 0.5V as “full contact”.

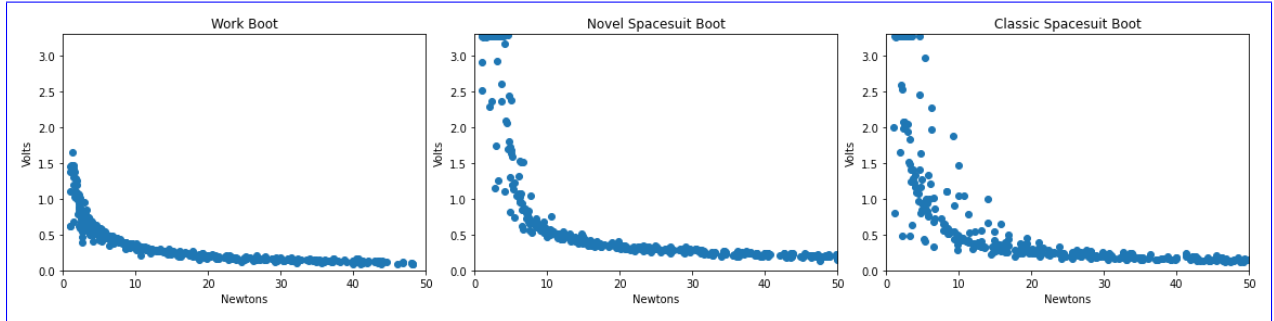


Figure 7.3: Voltage response curves of the FSR to an applied force from a force gauge, for each of the three boots.

A Python script was written to sync the FSR and video data, collecting frames from both cameras and the FSR voltage at the same time. The internal pressure of both spacesuit boots was also logged from the manometer and collected with the FSR and video data, but the reading of the manometer was only updated about once a second. Computational power limited the sample rate of the FSR and video data to 14 Hz. While this is much lower than typical biomechanics sample rates, it is still within the frequency content of gait [13].

While video and FSR data was collected during the short walk, this data was not analyzed due to the video’s limited field-of-view, thus only capturing one step in each walk.

#### 7.2.4 Survey Measures

After completion of the exercises in each boot, subjects filled out a survey assessing heel performance, discomfort, and exertion. Heel performance was defined as the response of the shoe to the subject’s heel. Heel performance was assessed by asking the subject to score the boots’ heel performance on a ranking from 1 (low) to 10 (high). Low heel performance was described as analogous to a flip-flop, where the shoe does not lift when the heel is lifted and there is high

heel-lift. High heel performance was described as analogous to a well fitted sneaker, where the shoe instantly responds to the subjects heel being lifted and there is minimal to no heel-lift. The Corlett-Bishop Discomfort Scale [38] was used to assess subject discomfort; the survey was modified and limited to 10 areas below the knees of the subject. This survey asks subjects to report their discomfort from a scale of 0 (none) to 10 (extremely high) for each of the areas, shown in figure 7.4. The Rating of Perceived Exertion (RPE) [22] was used to assess how much effort was required to perform the motions. This question asks subjects to report the amount of effort required to perform the heel-rise and walking tasks.

After performing the exercises in all four boots, subjects were then asked to rank the boots from best to worst with respect to overall performance and comfort.

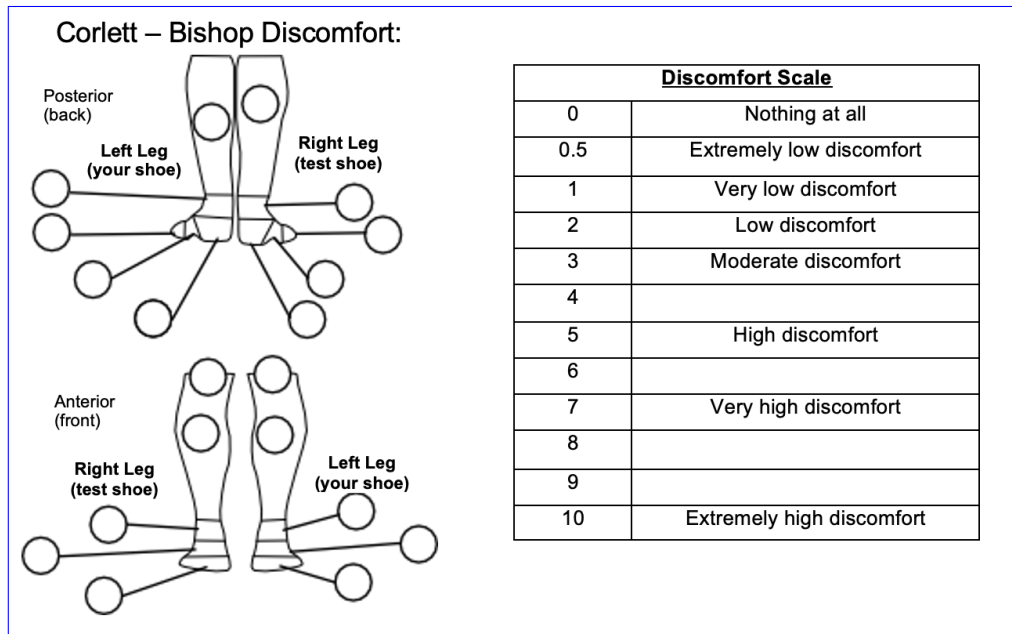


Figure 7.4: Modified Corlett-Bishop Discomfort Scale mapping used for this evaluation, limited to areas below the knee

### 7.2.5 Quantitative Data Processing

Heel position, as measured by the Kinovea software, was used to identify heel-off initiation time and maximum heel-rise magnitude for both the left (control) and right (test) shoe for each boot condition's heel-rise set. For all sets, the first heel-rise was not analyzed. Python's

`scipy.signal.find_peaks` peak detection algorithm was used to identify the peak heel positions for each heel-rise with a width of 5 samples. The left shoe was lifted higher in all heel-raise compared to the right shoe, necessitating differing peak prominence parameters for the peak detection algorithm. A peak prominence of 4 cm was used for the left shoe compared to a peak prominence of 1.5 cm for the right shoe. These prominences were set by observation of the collected data. The heel position at each peak was noted as the maximum heel-rise magnitude for each heel-rise in the set.

Heel-off ~~initiation~~-time was identified for both sides by first inverting the heel-position signal and then identifying the signal peaks with the identical parameters for each side as for the maximum heel-rise magnitude analysis. These peaks are the foot-flat phases of the heel-rise motion for each heel-rise. Then, a moving average filter with a window size of 10 samples was applied to the heel position signal. The filtered signal was then integrated to obtain the heel's velocity. Within the foot-flat phases, a threshold of 1 cm/s, decided on after trial and error, was used to identify when a heel-rise was beginning. The point at which the velocity signal crossed 1 cm/s was identified as the heel-off ~~initiation~~-time for that heel-rise.

The FSR voltage was recorded at each heel-off ~~initiation time~~ time for the right side. The maximum FSR voltage obtained during each heel-rise was obtained by first applying a moving average filter with a window size of 20 samples to the FSR voltage signal. Then, Python's `scipy.signal.find_peaks` algorithm was used to identify peaks with a prominence of at least 0.5 V and a width of 5 samples. As the FSR signal was quite noisy at its peak, a window of 50% of the peak's width from the peak's highest value was isolated. The average FSR voltage in this window was then noted as the FSR peak voltage for that heel-rise.

#### 7.2.6 Statistical Analysis

Bayesian linear regressions were modeled was used to analyze the following metrics across all four shoe conditions:

- heel performance score

- rating of perceived exertion
- left/right difference in heel-rise magnitude
- left/right difference in heel-off time
- FSR voltage at heel-off
- FSR voltage at heel-rise

Mixed-effects linear models were used to estimate these metrics as they are affected by the various boots (fixed effects); subject specific intercepts (random effects) allows for estimation of the group-level effect while controlling for subject-specific effects. Subject-specific intercepts allow for the capture of subjects' internal calibration of surveys, or their individual performance of the heel-rises irregardless of the footwear they are wearing. Each model used in this analysis is of the form:

$$\text{metric} = \beta_{\text{shoe}}x_i + \alpha_{\text{subject}}^n + \sigma \quad (7.1)$$

where  $\beta_{\text{shoe}}$  is the effect of each footwear ( $x_i$ ) on the metric,  $\alpha_O$  are the  $n$  subject-specific intercepts, and  $\sigma$  is the unexplained error of the model. Since the shoe types are categorical,  $\beta_{\text{shoe}}x_i$  can be expanded:

$$\text{metric} = \beta_{\text{Novel Spaceboot}} + \beta_{\text{Laced Workboot}} + \beta_{\text{Classic Spaceboot}} + \beta_{\text{Unlaced Workboot}} + \alpha_{\text{subject}}^n + \sigma \quad (7.2)$$

The model for each of the metric therefore consisted of an estimate of the effect of each footwear and subject specific intercepts for each subject. Bayesian inference was used to estimate the parameters of the mixed effects models as a interval of its likely values. This is done by starting with a prior, defining the model, and sampling from the posterior distribution to obtain each parameter's posterior distribution. This distribution was then presented as the estimate of the parameter's value. The Bambi Python package [26] was used for this analysis.

Bayesian inference starts with the selection of a prior for each of the predictors. The priors for the heel performance score and rating of perceived exertion were selected to be a uniform

distribution with lower and upper bounds set by the limits of the survey scales. This reflects our knowledge that survey scores cannot exceed the bounds of the survey rating. Similarly, a uniform prior with a lower bound of 0 and an upper bound of 3.3 was used for the FSR voltage metrics, as the FSR voltage is always positive and has a maximum of 3.3 V.

There exists no previous work which can directly inform the prior for heel-rise difference and the differences in heel-off time, as affected by various footwear. Therefore, weakly informative priors with wide standard deviations were used as the priors due to our limited knowledge of the specific metric. Previous work has shown that barefoot humans can lift their heels an average of 12 cm [23]. Therefore, the prior for heel-rise difference was set to a Normal distribution with a mean of 0, and a standard deviation of 12. This reflects an expected maximal heel-rise difference of a normal heel-rise on one side, while the other side stays on the ground. A normal distribution with a mean of 0 and a standard deviation of 1 was chosen as the prior for difference in heel-off time, as it was not expected that the time to complete one step would be more than 1 seconds.

Priors for the subject specific intercepts and unexplained error were left for Bambi to automatically select [26]. Once priors are chosen and the model is specified, the model is fit using a Markov Chain Monte Carlo (MCMC) method to sample from the posterior, as implemented in the PyMC3 Python library [123]. Ten parallel MCMC chains were run for each metric's regression, with 6,000 burn-in draws and 12,000 sampling draws per chain. The acceptance target was set to 0.99 to reduce the step size within each iteration, and thereby eliminating divergences from the chain.

The maximal posterior estimate and 95% Bayesian credible interval were calculated from the sampled posterior distribution for each parameter in each model. The posterior distributions for each of the shoe condition parameters were then compared to the novel spaceboot's posterior distribution to assess their comparative performance, presenting the chance of the compared shoe condition resulting in a higher or lower metric response compared to the novel spacesuit boot.

### 7.3 Results

Four out of the five subjects ranked the shoe conditions from best to worst as Laced Workboot, Novel Spaceboot, Unlaced Workboot, Classic Spaceboot. The remaining subject's ranking switched the order of the Novel Spaceboot and Unlaced Workboot. The mean and maximum Corlett-Bishop Discomfort ratings across all subjects for each shoe condition are presented in figure 7.5.

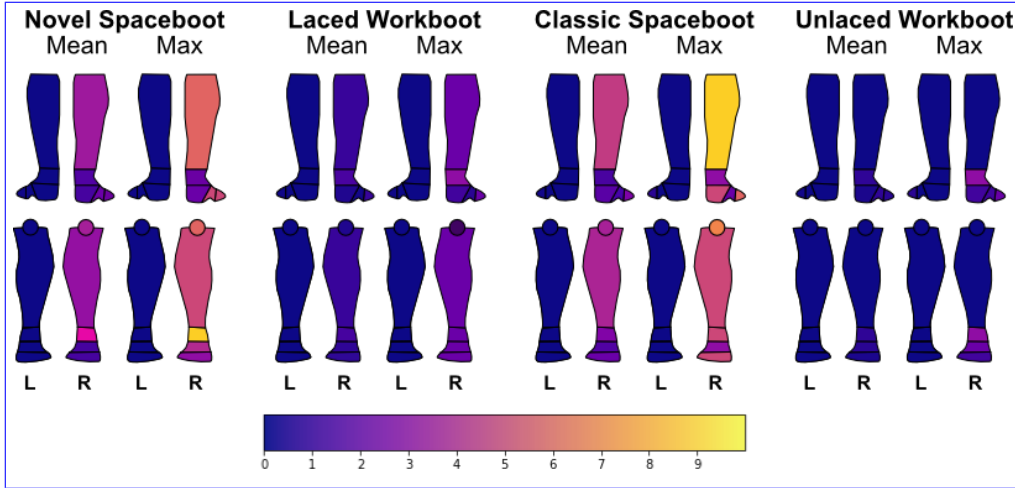


Figure 7.5: Mean and maximum of reported Corlett-Bishop discomfort ratings on both the left (control) and right (test) shoe. Results are presented across all subjects.

The maximal posterior estimate of the heel performance rating for the novel spaceboot was 6.8, compared to 8.4 for the laced workboot, 2.3 for the classic spaceboot, and 2.4 for the unlaced spaceboot (fig. 7.6). The posterior distribution of the laced workboot's heel performance rating was estimated to be higher than the novel spaceboot's 98.6% of the time, while the posterior distributions of the classic spaceboot's and unlaced workboot's heel performance ratings were estimated to be lower 100% of the time.

The maximal posterior estimate of RPE for the novel spaceboot was 12.0, compared to 8.8 for the laced workboot, 14.3 for the classic spaceboot, and 8.4 for the unlaced workboot (fig. 7.7). The posterior distributions for laced and unlaced workboots' RPE were estimated to be lower than the novel spaceboot's 98% and 99% of the time, respectively. The posterior distribution for the classic spacesuit boot's RPE was estimated to be higher than the novel spaceboot's 94.3% of the time.

Figure 7.8 shows an example FSR response and heel-rise measurement from a subject's heel-rise set.

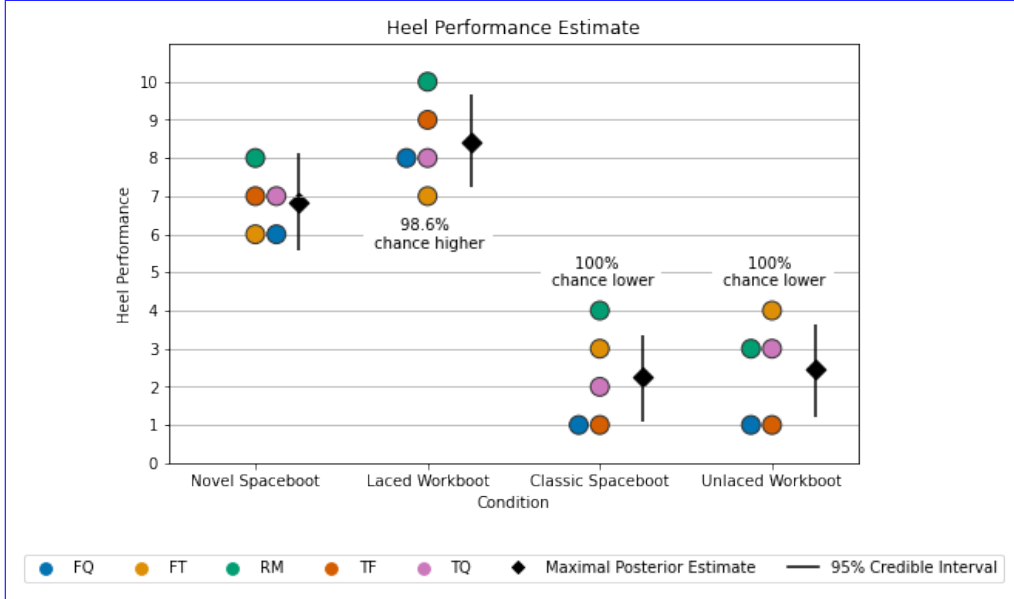


Figure 7.6: Estimate (black) of the heel performance rating across all boot conditions, as compared to the subjects' data. The subjects' data is offset along the x-axis to show all data points. Each boot's posterior distributions' overlap as compared to the novel spaceboot are annotated.

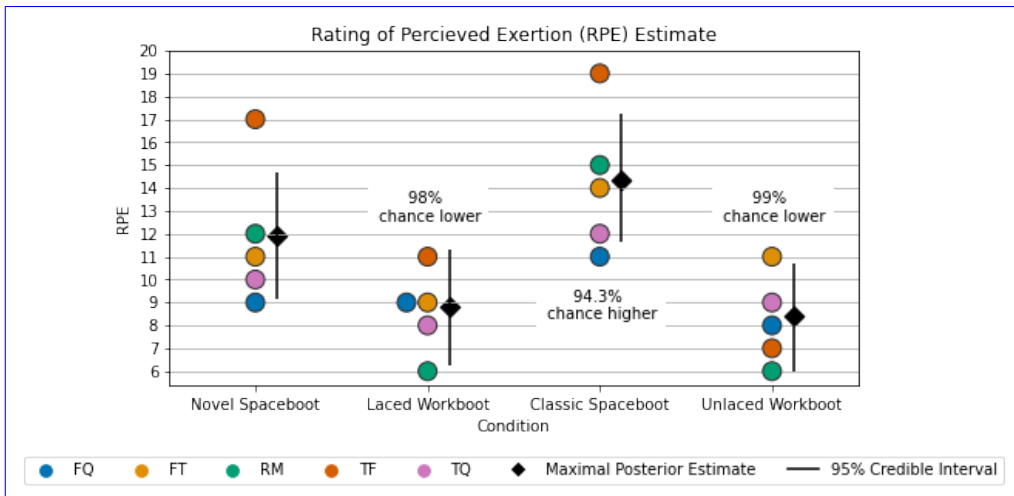


Figure 7.7: Estimate (black) of the rating of perceived exertion across all boot conditions, as compared to the subjects' data. The subjects' data is offset along the x-axis to show all data points. Each boot's posterior distributions' overlap as compared to the novel spaceboot are annotated.

The maximal posterior estimate of the difference in heel-rise magnitude was 3.3 cm for the novel spaceboot, compared to 3.8 cm for the laced workboot, 5.5 cm for the classic spaceboot, and 4.8 cm for the unlaced workboot (fig. 7.9). The posterior distribution for laced workboot's heel lift difference was estimated to be higher than the novel spaceboot's 86.3% of the time. The posterior

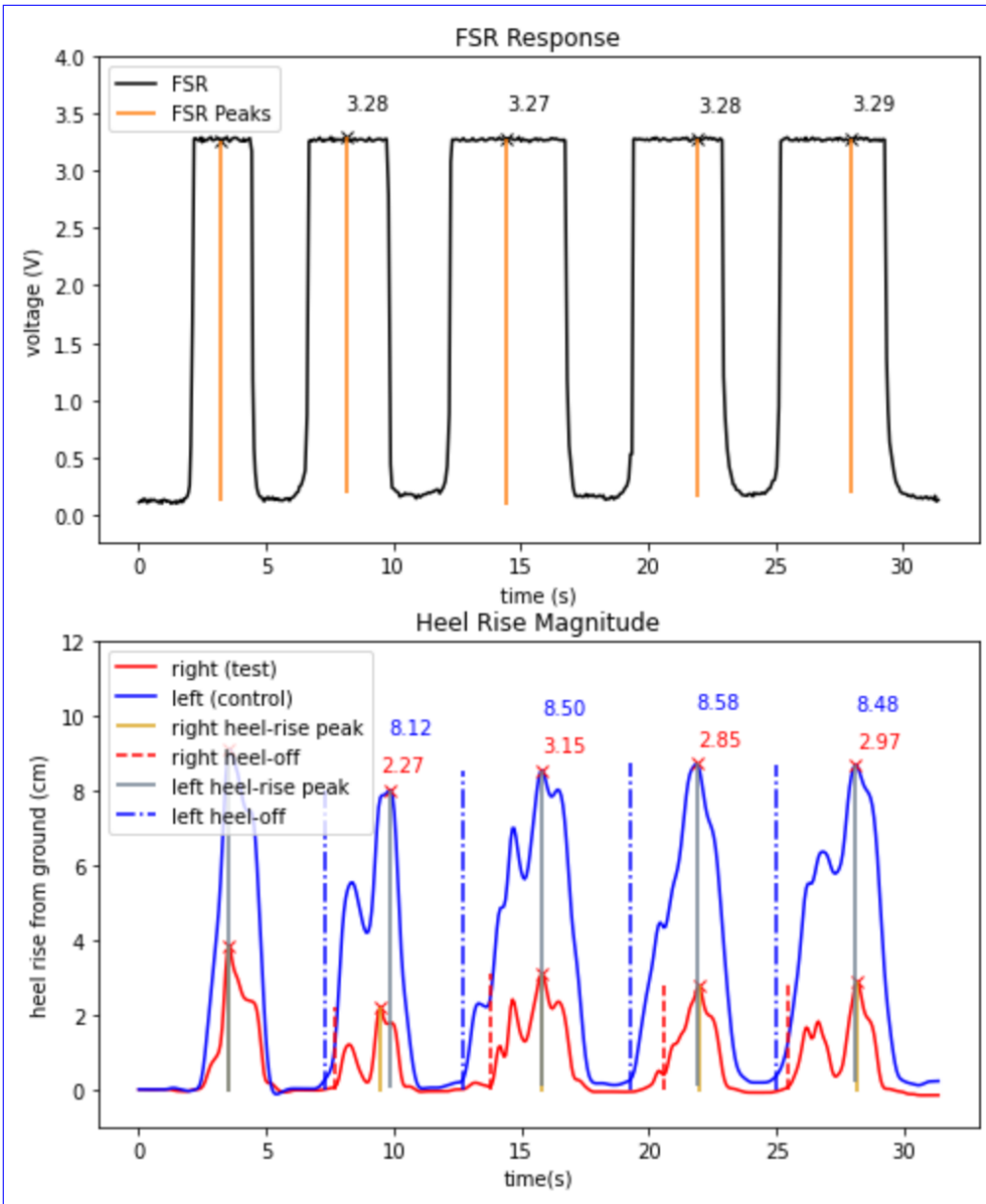


Figure 7.8: Example FSR and heel-rise data trace from a heel-rise set. Detected peaks and heel-off times are shown with the vertical lines

distributions for the classic spacesuit boot's and unlaced spacesuit boot's heel lift difference were estimated to be higher than the novel spaceboot's 100% of the time.

The maximal posterior estimate of the difference in heel-off time was 0.0s for the novel spaceboot, compared to -0.3 s for the laced workboot, -0.5 s for the classic spaceboot, and -0.3 s for the unlaced workboot (fig. 7.10). The posterior distribution for laced workboot's, classic

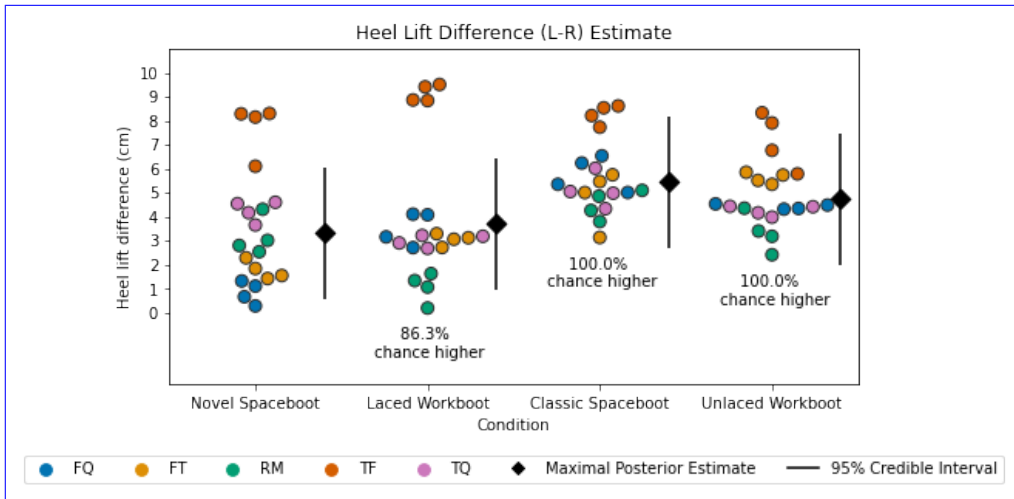


Figure 7.9: Estimate (black) of the difference in heel-rise magnitude across all boot conditions, as compared to the subjects' data. heel-rise magnitude difference is calculated by subtracting the magnitude of the right foot from the left foot. The subjects' data is offset along the x-axis to show all data points. Each boot's posterior distributions' overlap as compared to the novel spaceboot are annotated.

spacesuit boot's, and unlaced workboot's heel-off time difference was estimated to be lower than the novel spaceboot's 100% of the time.

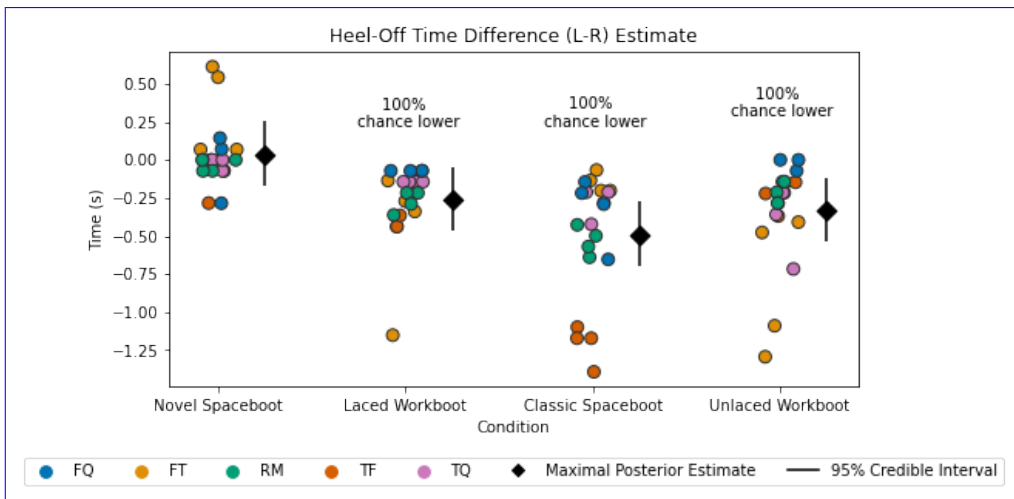


Figure 7.10: Estimate (black) of the difference in heel-off time across all boot conditions, as compared to the subjects' data. The difference in heel-off time is calculated as the left foot's (control) heel-off time minus the right foot's (test) heel-off time. Therefore, negative numbers indicate that the right foot lifted after the left foot. The subjects' data is offset along the x-axis to show all data points. Each boot's posterior distributions' overlap as compared to the novel spaceboot are annotated.

The maximal posterior estimate of the FSR voltage at maximum heel-rise was 2.2 V for the novel spaceboot, compared to 3.3 V for the laced workboot, the classic spaceboot, and the unlaced workboot (fig. 7.11). The posterior distribution for laced workboot's, classic spacesuit boot's, and unlaced workboot's heel-off time difference was estimated to be higher than the novel spaceboot's 100% of the time.

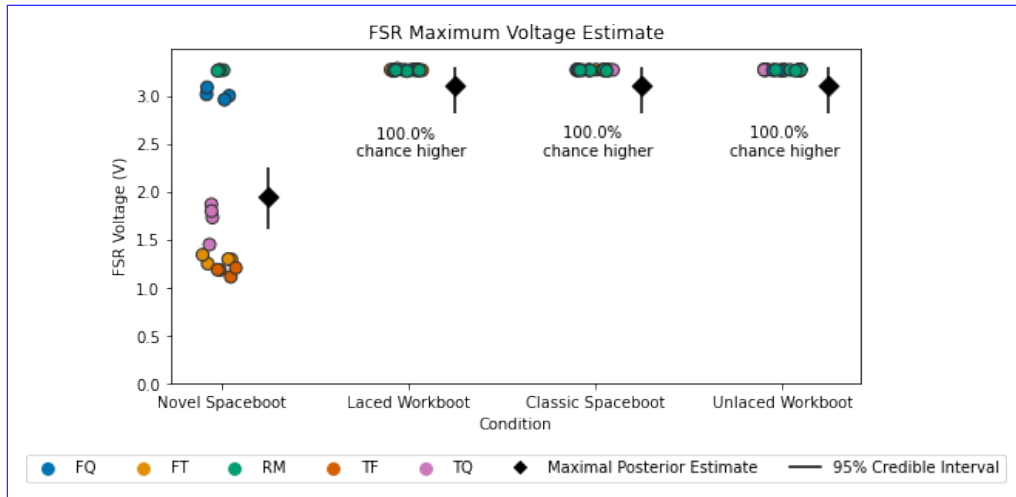


Figure 7.11: Estimate (black) of the FSR voltage at maximum heel-rise across all boot conditions, as compared to the subjects' data. The subjects' data is offset along the x-axis to show all data points. Each boot's posterior distributions' overlap as compared to the novel spaceboot are annotated.

The maximal posterior estimate of the FSR voltage at heel-off for the novel spaceboot was 1.6 V, compared to 1.0 V for the laced workboot, 3.0 V for the classic spaceboot, and 2.3 V for the unlaced spaceboot (fig. 7.12). The posterior distribution of the laced workboot's FSR voltage at heel-off was estimated to be lower than the novel spaceboot's 97% of the time, while the posterior distributions of the classic spaceboot's and unlaced workboot's FSR voltage at heel-off were estimated to be higher 100% and 98.6% of the time, respectively.

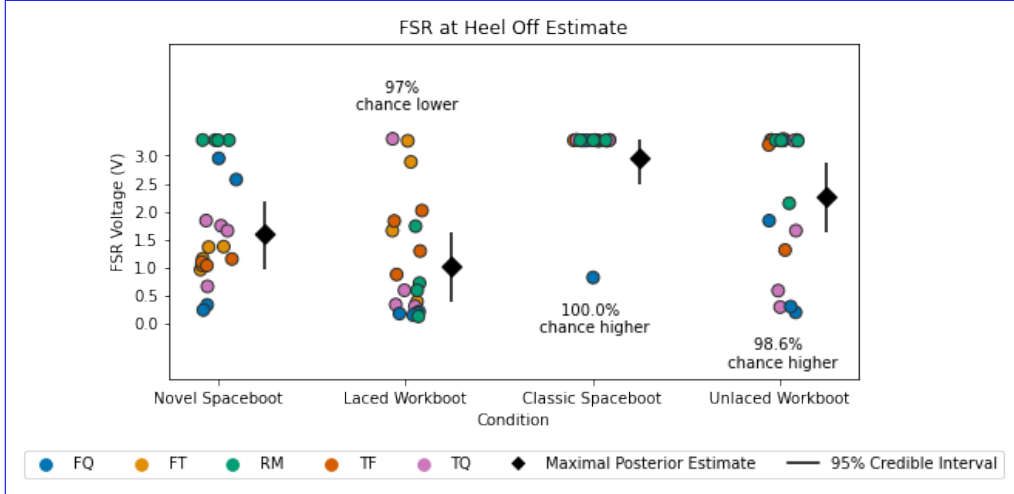


Figure 7.12: Estimate (black) of the FSR voltage at heel-off across all boot conditions, as compared to the subjects' data. The subjects' data is offset along the x-axis to show all data points. Each boot's posterior distributions' overlap as compared to the novel spaceboot are annotated.

## 7.4 Discussion

This study aimed to evaluate the performance of the novel spacesuit boot design against a laced workboot, unlaced workboot, and classic spacesuit boot design. Fit and comfort were the primary focus of this evaluation, with specific metrics chosen to evaluate the heel's dynamic fit in the boot, as well as the boot's overall comfort. It was hypothesized that the laced workboot would perform the best of all in these metrics, following by the novel spaceboot, unlaced workboot, and classic spaceboot. Most subjects subjectively ranked the boots in the same order as the hypothesis, except for one subject.

Select metrics from this study were further analyzed using Bayesian inference for linear mixed models to objectively assess the boots' performance. The linear mixed modeling approach allowed for capture of subject specific effects as random intercepts in the model. This was especially apparent for the heel-rise magnitude metric. Subject TF had much higher heel-rise magnitude across all boot conditions when compared to other subjects, and this subject-specific effect was captured in subject TF's random intercept and the credible intervals for the metric take into account performance within each subject. While the credible intervals may look like they overlap

even if their chance of being greater or less than is close to 100%, observing the data points of each subject shows trends substantiated by the posterior distribution overlap for all metrics.

Comfort and exertion are key metrics in assessing the performance of a spacesuit component [1, 34]. The pressurized spacesuit boots had higher levels of reported discomfort compared to the unpressurized work boots ([f@fig:SA4-CBresults]). Similarly, the pressurized spacesuit boots had higher reported levels of exertion compared to the unpressurized workboots. However, the classic spacesuit boot still had a high (94.5%) chance of an increased RPE rating than the novel spacesuit boot. Since both boots were pressurized to a similar level, the novel spacesuit boot likely results in less exertion due to its design enabling better fit. The highest areas of pressure on both spacesuit boots was the calf, which may be due to the pressurization interface needing to compress the calf to maintain a seal. The novel spacesuit boot had reports of high discomfort at the instep, which may suggest contact between the foot and boot. This is most likely a result of the design of the boot, which attempts to maintain contact with the instep. In addition, one subject complained about discomfort from the BOA dial pressing into their calf. Future iteration may improve the discomfort associated with these contacts by strategically adding padding between the pressure bladder and wearer.

The FSR voltage metrics provide insight into heel-contact at heel-off and at maximum heel-rise. The FSR voltages suggest that both the novel spaceboot and laced workboot maintain some contact with the heel at heel-off (between 0 and 3.3 V), compared to the unlaced workboot and classic spaceboot which are almost always offloaded (at 3.3 V). However, the laced spacesuit boot maintains contact more often, with the majority of data points at 0 V. In addition, the novel spaceboot appears to be the only boot which maintains contact at maximum heel-rise, as evidenced by its FSR voltage at heel-rise being lower than all other boots. This may be due to the interaction of the lacing and the softer sole of the novel spaceboot. The tension of the BOA lacing is kept constant when doffed; since the lower lacing guides are placed on the sole, the sole's motion is matched to the foot's instep where the upper lacing guides run, ensuring that it is brought up during the heel-rise by the tension in the BOA lacing (fig. 7.13). This may also work in tandem

with the designed dynamic lacing aspect of the novel spaceboot (see sec. 6), which lengthens the lace path of the BOA by relatively moving the tubing from the dial to the guides and requires the guides to come closer together to compensate. This is in contrast to the laced workboot's lacing, which does not interact with the sole and therefore has no mechanism to actively raise the sole. Therefore, this and other boots rely on the material properties of the boot itself and not an active tension force to raise the sole. Future work can expand upon these hypotheses by quantifying the magnitude of dynamic lacing lengthening and tension in the BOA system.



Figure 7.13: Video frame of heel-rise by subject FT in the novel spaceboot. As the BOA lace length cannot change, the sole is kept at a constant distance to the instep throughout the heel-rise motion. This ensures that the heel is continuously making contact with the

The heel-off time difference and heel-raise magnitude difference further add to the heel performance characterization by comparing the test boots against the subjects' own control shoes when performing a heel raise. The novel spacesuit boot had the lowest heel-off time difference between the left and right shoes, suggesting that most heel raises were initiated in tandem with the novel spacesuit boot. The other boots all were estimated to have a delay in their heel-off time, with their right foot taking longer to initiate heel-off. This may be an indication of heel-lift; the foot

inside may have lifted but it had not yet resulted in the boot leaving the ground. When assessed alongside the FSR voltage at heel-off for the unlaced workboot and classic spacesuit boot, this further corroborates the heel-lift hypothesis; if the FSR voltage measured at the boot's heel-off is high, then the foot is not making contact with the boot. However, the laced workboot appears to have a delay at heel-off and still maintains contact with the heel, which may suggest that subjects simply have a hard time initiating heel-off. The classic spacesuit boot and unlaced workboot were estimated to have a higher heel-raise magnitude difference 100% of the time compared to the novel spacesuit boot. This suggests that these boots may either have large amounts of heel-lift (as evidenced by the FSR voltage at maximum heel raise), and/or are simply limiting the magnitude of a maximum heel raise. The unlaced workboot has a loose tongue which may allow the foot to further lift out of the boot while performing a heel-raise, while the classic spaceboot may be limited in its mobility. The laced workboot had a 86.3% chance of a higher difference in heel-raise magnitude, suggesting similar or worse performance than the novel spaceboot.

Subjects rated the novel spacesuit boot's heel performance as below that of the laced workboot, but above the classic spacesuit and unlaced workboot. However, the FSR data suggests that only the novel spaceboot maintains some level of contact with the heel during heel-off. Similarly, the heel-raise magnitude difference suggests that the novel spaceboot is the closest match to a subject's control tennis shoe in heel raise magnitude. Therefore, the quantitative data suggests that the novel spacesuit may be better at heel-raises than the laced workboot, classic spaceboot, and unlaced spaceboot.

However, it is important to note that no quantitative measurements were collected during the short walk exercise, and the laced workboot may have performed better here to align with the subjective ratings of heel performance.

## 7.5 Summary

This evaluation compared the novel spacesuit boot against a laced workboot, classic spaceboot, and unlaced workboot. When performing a heel-raise, both the novel spaceboot and laced workboot

appear to maintain contact with the heel at heel-off. However, the novel spaceboot appears to maintain some contact throughout the heel-raise, and allows subjects to achieve their highest performance heel-raise. Survey measurements report the novel spacesuit boot having a lower heel performance than the laced spaceboot, but a higher heel performance compared to the unlaced workboot and classic spacesuit boot. Therefore, the hypothesis that the novel spacesuit boot provides equivalent heel performance compared to the laced workboot, and improved heel performance compared to the unlaced workboot and classic spaceboot is partially true. It is clear that the novel spacesuit boot is an improvement over the classic spacesuit boot and unlaced workboot, but it is unclear whether it is equivalent, better, or worse than the laced workboot as various metrics have shown all these possibilities.

Pressurization appears to have had a greater impact on comfort than originally anticipated. Both the pressurized spacesuit boots had higher discomfort ratings and higher ratings of perceived exertion compared to both unpressurized workboot conditions. The novel spacesuit boot did have a lower rating of perceived exertion than the classic spacesuit boot. Therefore, the hypothesis that the novel spacesuit boot provides equivalent comfort to the laced workboot, and improved comfort compared to the classic spaceboot and unlaced workboot is partially true. The novel spacesuit boot is not as comfortable as the unpressurized workboots, but clearly more comfortable than the classic spaceboot.

Results from this evaluation show that the novel spacesuit boot design is a clear improvement over the classic spacesuit boot design. The novel design was able to achieve much improved heel performance and require less exertion. This highlights the need for a lacing system and heel counter in spacesuit boots to help maintain heel indexing and reduce instances of heel-lift, leading to a level of performance closer to that of a workboot.

## Chapter 8

### Summary

Through many advancements of planetary EVA spacesuit design, operator-spacesuit coordination is still not perfectly matched. Poor mobility and poor fit between the operator and spacesuit are some of the most common factors that can lead to injury. This thesis ~~aims was designed~~ to determine the feasibility of using dynamic body shape models to improve spacesuit component fit and mobility, specifically with planetary spacesuit boots. The spacesuit boot has demonstrated specific problems relating to poor fit, such as heel-lift and contact injuries. The work in the thesis aims to answer the hypothesis:

Integrating dynamic body shape changes into the spacesuit boot design process will mitigate factors that lead to injury and improve compatibility between the operator and the spacesuit.

This thesis investigated the hypothesis through four specific aims, resulting in novel contributions to the field.

~~Table ?? outlines the peer-reviewed conference and journal papers resulting from this thesis work. Table ?? outlines conference presentations and posters from this thesis work. Publications and presentations which are proposed and subject to having their title changed. The thesis first investigated the ability to quantify heel-lift magnitude inside the spacesuit. A contribution was made by observing from IMU data that the lower leg of the spacesuit expands during gait; this observation supports the belief that heel-lift in the boot may be due to forces from the spacesuit, and re-emphasizes the importance of keeping the foot indexed in the boot. In addition, findings~~

from this study suggest that IMUs are not the best tool to quantify heel lift and that drift correction techniques are not enough to reduce drift for positional estimates in the spacesuit context.

~~Peer-reviewed publications~~ Type Title Journal Status Note Detecting Heel Lift in Spacesuit Gait Aerospace Medicine and Human Performance In Prep., expected Nov 2020 Journal Paper DynaMo: Dynamic Body Shape and Motion Capture with Intel RealSense Cameras Journal of Open Source Software Published Journal Paper Dynamic foot morphology explained through 4D scanning Following this study, the dynamic morphology of the foot was investigated with a focus on discovering changes which can improve spacesuit boot design. The thesis contributed here a novel, low-cost dynamic foot scanning system was designed and built to enable capture of foot scans at 90 fps while subjects walk on a treadmill. The thesis also contributed a novel predictive dynamic foot shape model for walking using shape modeling and linear modeling techniques. A further contribution includes an analysis on dynamic instep height, including a new method to measure instep height without a plantar surface, and shape modeling Journal of Biomechanics Under Review Conference Paper A Biomechanical Design Framework to Improve Spacesuit Boot Fit 50th International Conference on Environmental Systems Published Journal Paper Static and Dynamic Distribution of Instep Height Footwear Science Proposed, expected Mar 2021 Journal Paper Design of A Novel Planetary Spacesuit Boot Design Acta Astronautica Proposed, expected Aug 2021 Journal Paper Comfort and Mobility Evaluation of a Novel Planetary Spacesuit Boot Design Aerospace Medicine and Human Performance Proposed, expected Feb 2022 the finding that dynamic instep height is subject specific and cannot be accurately predicted from static anthropometries.

~~Conference Presentations and Posters~~ Type Title Conference Date Talk Using The dynamic foot morphology model was translated into footwear design by first creating a new footwear design framework. This framework contribution tied both traditional footwear measurements and novel footwear measurements, like the dynamic foot morphology data to design spacesuit footwear Footwear Biomechanics Symposium July 2019 Talk Development of a Dynamic 3D Scanning System with Multiple Intel RealSense Depth Cameras International Society

~~of Biomechanics Congress Aug 2019 Poster Quantifying the Heel-Lift during Spacesuit Gait NASA HRP IWS Jan 2020 TBD Dynamic Body Shape Models to Reduce Risk OF EVA Spacesuit Injury NASA HRP IWS Feb 2021 TBD Novel Spacesuit Boot Design Developed from Dynamic Foot Shape Modeling Footwear Biomechanics Symposium July 2021 TBD Spacesuit Boot with Improved Comfort and Mobility Developed from Dynamic Shape Modeling NASA HRP IWS Jan 2022 model, into footwear design variables. The framework was then used in the context of planetary spacesuit boot design to pick parameters for mobility, fit, and comfort that would meet the requirements. The thesis then contributed the design and prototype for a novel planetary spacesuit boot, with a BOA lacing system and heel counter, with the express goal of accommodating the variability in instep height to improve fit and reduce heel-lift.~~

~~All required coursework was completed as of The final contribution of this thesis lies in the evaluation of the novel spacesuit boot against the classic spacesuit boot, a laced workboot, and an unlaced workboot for fit and comfort. This is the first published comparison of a spacesuit boot against a terrestrial boot. This evaluation showed that the novel spaceboot provided improved heel performance and comfort compared to the classic spaceboot, and improved heel performance compared to the unlaced spaceboot. The novel spaceboot provided improved heel performance compared to the laced workboot when investigating heel contact at heel-rise, heel-off delay, and heel-rise performance, and lower heel performance when analyzing heel-contact at heel-off and subjective heel performance ranking. Nevertheless, the novel spacesuit boot provides a great improvement over the classic design and appears to come close to the performance of a gold standard workboot.~~

~~The performance of the novel spacesuit boot design shows the utility of using body shape models to inform spacesuit component design. In this application, a foot shape model first identified specific shape modes which varied throughout stance phase. Of these, it was decided to target the shape mode where the instep height falls during stance phase, and the novel spacesuit boot design features a lacing system to ensure the instep area is captured through stance phase. A heel counter was also added to accommodate changes in the heel shape. As the Spring 2020 semester,~~

Of the 36 required credits, 30 were taken in ASEN, with 12 at the 6000 level. MCEN 5228 (Modeling Human Movement) and APPM 5590 (Statistical Modeling) were taken outside of ASEN. The 6 required math credits were exceeded with taking ASEN 5519 (Experimental Design and Statistical Analysis), APPM 5590 (Statistical Modeling), and ASEN 5044 (Statistical Estimation for Dynamical Systems). As of the Fall 2020 semester, 15 out of the 30 required Doctoral dissertation credits have been taken. The remaining 15 credits will be evenly taken during the Spring 2021, Fall 2021, and Spring 2022 semesters. The teaching practicum has been fulfilled through the mentoring of UROP students in the Summer 2018, Fall 2019, and Spring 2020 semesters. A TA position is also expected in Fall 2021. evaluation shows, these two additions to the spacesuit boot design resulted in a much greater improvement in heel performance and reduction of exertion. Therefore, the work in this thesis supports the hypothesis: integrating dynamic body shape changes into the spacesuit boot design process will mitigate factors that lead to injury and improve compatibility between the operator and the spacesuit.

## 8.1 Future Work

Gantt chart ?? shows the timeline for each specific aim of the thesis and for PhD graduation milestones. This work's effort in translating a foot shape model to spacesuit boot design can serve as a template for other spacesuit components as well. A similar process can be followed to identify dynamic body shape changes in the shoulder, hands, and hips. Then, these changes can be translated into improvements in spacesuit design to accommodate such changes, thus reducing the risk of injury in these areas.

Similarly, this thesis' work is not limited to spacesuit design. This process can be applied to apparel or terrestrial footwear for any application where injury might be a risk.

Future advancements in technology can also work to improve the fidelity of the foot shape model. This thesis' goal is to show the utility of dynamic scanning in modeling body shape changes. Advancements in cameras and computer vision can improve the resolution, framerate, and reliability of such systems to make 4D scanning accessible to more industries.

Finally, this thesis aims to show the importance in understanding all dimensions of human motion when it comes to spacesuit design. The boot designed in this thesis was designed first around the motion and shape of the foot, with the hope that other requirements, such as thermal, dust, and radiation, can be met through additional layers. Novel solutions might be needed to address these problems prior to returning to the Moon.

## Bibliography

- [1] Andrew F J Abercromby, Michael L Gernhardt, and Harry Litaker. Desert Research and Technology Studies (DRATS) 2009: A 14-Day Evaluation of the Space Exploration Vehicle Prototype in a Lunar Analog Environment. Technical Report TP-2012-217360, NASA Johnson Space Center, 2012.
- [2] Isaak P. Abramov, Anatoly Yu Stoklitsky, Arnold S. Barer, and Sergei N. Filipenkov. Essential aspects of space suit operating pressure trade-off. In SAE Technical Papers. Society of Automotive Engineers, 1994.
- [3] Marko Ackermann and Antonie J. Van den Bogert. Predictive simulation of gait at low gravity reveals skipping as the preferred locomotion strategy. Journal of Biomechanics, 45(7):1293–1298, 2012.
- [4] R. Alexander McN. Optimization and gaits in the locomotion of vertebrates. Physiological Reviews, 69(4):1199–1227, 1989.
- [5] Brett Allen, Brian Curless, and Zoran Popović. The space of human body shapes: Reconstruction and parameterization from range scans. ACM Transactions on Graphics, 22(3):587–594, 2003.
- [6] Ryan Z. Amick, Christopher R. Reid, Scott A. England, and Sudhakar L. Rajulu. Characterization of joint resistance and performance degradation of the Extravehicular Mobility Unit Spacesuit: A pilot study. In Proceedings of the Human Factors and Ergonomics Society 59th Annual Meeting, pages 1259–1263, sep 2015.
- [7] Cătălin Amza, Aurelian Zapciu, and Diana Popescu. 3d-printed shoe last for bespoke shoe manufacturing. 290:04001.
- [8] Allison Anderson. Understanding Human-Space Suit Interaction to Prevent Injury During Extravehicular Activity. Phd, Massachusetts Institute of Technology, 2014.
- [9] Allison Anderson, Yigit Menguc, Robert J. Wood, and Dava Newman. Development of the polipo pressure sensing system for dynamic space-suited motion. IEEE Sensors Journal, 15(11):6229–6237, 2015.
- [10] Allison P. Anderson and Dava J. Newman. Pressure sensing for in-suit measurement of space suited biomechanics. Acta Astronautica, 115:218–225, 2015.

- [11] Allison P. Anderson, Dava J. Newman, and Roy E. Welsch. Statistical evaluation of causal factors associated with astronaut shoulder injury in space suits. *Aerospace Medicine and Human Performance*, 86(7):606–613, 2015.
- [12] Dragomir Anguelov, Praveen Srinivasan, Daphne Koller, Sebastian Thrun, Jim Rodgers, and James Davis. SCAPE: Shape Completion and Animation of People. *ACM Transactions on Graphics*, 24(3):408–416, 2005.
- [13] Erik K. Antonsson and Robert W. Mann. The frequency content of gait. *Journal of Biomechanics*, 18(1):39–47, jan 1985.
- [14] ASTM F539-01. Standard Practice for Fitting Athletic Footwear. Technical report, ASTM, West Conshohocken, PA, 2017.
- [15] Bettina Barisch-Fritz, Timo Schmeltzpfenning, Clemens Plank, and Stefan Grau. Foot deformation during walking: Differences between static and dynamic 3D foot morphology in developing feet. *Ergonomics*, 57(6):921–933, jun 2014.
- [16] Bettina Barisch-Fritz, Timo Schmeltzpfenning, Clemens Plank, Tobias Hein, and Stefan Grau. The effects of gender, age, and body mass on dynamic foot shape and foot deformation in children and adolescents. *Footwear Science*, 6(1):27–39, jan 2014.
- [17] Elizabeth Benson and Sudhakar Rajulu. Complexity of sizing for space suit applications. *Lecture Notes in Computer Science (including subseries Lecture Notes in Artificial Intelligence and Lecture Notes in Bioinformatics)*, 5620 LNCS(June):599–607, 2009.
- [18] Fausto Bernardini, Joshua Mittleman, Holly Rushmeier, Claudio Silva, and Gabriel Taubin. The Ball-Pivoting Algorithm for Surface Reconstruction. *IEEE Transactions on Visualization and Computer Graphics*, 5(4):349–359, 1999.
- [19] Pierre J Bertrand, Allison Anderson, Alexandra Hilbert, and Dava Newman. Feasibility of Spacesuit Kinematics and Human-Suit Interactions. In *44th International Conference on Environmental Systems*, Tuscon, AZ, 2014.
- [20] Harald Böhm and Matthias Hösl. Effect of boot shaft stiffness on stability joint energy and muscular co-contraction during walking on uneven surface. *Journal of Biomechanics*, 43(13):2467–2472, sep 2010.
- [21] Abhishektha Boppana and Allison P Anderson. DynaMo: Dynamic Body Shape and Motion Capture with Intel RealSense Cameras. *The Journal of Open Source Software*, 4(41), 2019.
- [22] G. A.V. Borg. Psychophysical bases of perceived exertion. *Medicine and Science in Sports and Exercise*, 14(5):377–381, 1982.
- [23] Annelie Brorsson, Richard W. Willy, Roy Tranberg, and Karin Grävare Silbernagel. Heel-Rise Height Deficit 1 Year After Achilles Tendon Rupture Relates to Changes in Ankle Biomechanics 6 Years After Injury. *The American Journal of Sports Medicine*, 45(13):3060–3068, November 2017.
- [24] Raymond C. Browning, Emily A. Baker, Jessica A. Herron, and Rodger Kram. Effects of obesity and sex on the energetic cost and preferred speed of walking. *Journal of Applied Physiology*, 100(2):390–398, feb 2006.

- [25] Seonjeong Byun, Hyang Jun Lee, Ji Won Han, Jun Sung Kim, Euna Choi, and Ki Woong Kim. Walking-speed estimation using a single inertial measurement unit for the older adults. *PLoS ONE*, 14(12):1–16, 2019.
- [26] Tomás Capretto, Camen Piho, Ravin Kumar, Jacob Westfall, Tal Yarkoni, and Osvaldo A. Martin. Bambi: A simple interface for fitting Bayesian linear models in Python, 2020. *eprint*: 2012.10754.
- [27] Paolo Caravaggi, Todd Pataky, Michael Günther, Russell Savage, and Robin Crompton. Dynamics of longitudinal arch support in relation to walking speed: contribution of the plantar aponeurosis. *217(3):254–261*. *eprint*: <https://onlinelibrary.wiley.com/doi/pdf/10.1111/j.1469-7580.2010.01261.x>.
- [28] J. Martin Carlson. Functional limitations from pain caused by repetitive loading on the skin: A review and discussion for practitioners, with new data for limiting friction loads. *Journal of Prosthetics and Orthotics*, 18(4):93–103, 2006.
- [29] Christopher E. Carr and Jeremy McGee. The apollo number: Space suits, self-support, and the walk-run transition. *PLoS ONE*, 4(8):1–7, 2009.
- [30] Trisha Cashmere, Richard Smith, and Adrienne Hunt. Medial longitudinal arch of the foot: Stationary versus walking measures. 20(2):112–118. Publisher: SAGE Publications Inc.
- [31] G. A. Cavagna, N. C. Heglund, and C. R. Taylor. Mechanical work in terrestrial locomotion: two basic mechanisms for minimizing energy expenditure. *American Journal of Physiology - Regulatory Integrative and Comparative Physiology*, 2(3), 1977.
- [32] G. A. Cavagna, H. Thys, and A. Zamboni. The sources of external work in level walking and running. *The Journal of Physiology*, 262(3):639–657, 1976.
- [33] Steven P. Chappell. *Analysis of Planetary Exploration Spacesuit Systems and Evaluation of a Modified Partial-Gravity Simulation Technique*. Phd, University of Colorado Boulder, 2006.
- [34] Steven P. Chappell, Jason R. Norcross, Andrew F.J. Abercromby, Omar S. Bekdash, Elizabeth A. Benson, and Sarah L. Jarvis. Evidence Report : Risk of Injury and Compromised Performance Due to EVA Operations. Technical report, Human Health and Countermeasures Element, NASA Johnson Space Center, Houston, TX, 2017.
- [35] Chacqueline M. Charvat, Jason Norcross, Christopher R. Reid, and Shane M. McFarland. Spacesuit Glove-Induced Hand Trauma and Analysis of Potentially Related Risk Variables. In *45th International Conference on Environmental Systems*, Bellevue, WA, 2015.
- [36] Yan Chen and Gerard Medioni. Object modelling by registration of multiple range images. *Image and Vision Computing*, 10(3):2724–2729, 1992.
- [37] Bryan P. Conrad, Michael Amos, Irene Sintini, Brian Robert Polasek, and Peter Laz. Statistical shape modelling describes anatomic variation in the foot. *Footwear Science*, 11(sup1):S203–S205, jun 2019.
- [38] E. N. Corlett and R. P. Bishop. A technique for assessing postural discomfort. *Ergonomics*, 19(2):175–182, 1976.

- [39] Conor R. Cullinane, Richard A. Rhodes, and Leia A. Stirling. Mobility and agility during locomotion in the mark III space suit. *Aerospace Medicine and Human Performance*, 88(6):589–596, jun 2017.
- [40] H. A.M. Daanen and F. B. Ter Haar. 3D whole body scanners revisited. *Displays*, 34(4):270–275, oct 2013.
- [41] Jessica A. Dobson, Diane L. Riddiford-Harland, Alison F. Bell, and Julie R. Steele. The three-dimensional shapes of underground coal miners’ feet do not match the internal dimensions of their work boots. *Ergonomics*, 61(4):588–602, 2018.
- [42] Jessica A. Dobson, Diane L. Riddiford-Harland, Alison F. Bell, Caleb Wegener, and Julie R. Steele. Effect of shaft stiffness and sole flexibility on perceived comfort and the plantar pressures generated when walking on a simulated underground coal mining surface. *Applied Ergonomics*, 84:103024, apr 2020.
- [43] J. M. Donelan and R. Kram. Exploring dynamic similarity in human running using simulated reduced gravity. *Journal of Experimental Biology*, 203(16):2405–2415, 2000.
- [44] Bret G. Drake and Kevin D. Watts. Human exploration of mars, design reference architecture 5.0. Technical report, NASA Johnson Space Center, Houston, TX, 2010.
- [45] Lisa A. Elkin, Matthew Kay, James J. Higgins, and Jacob O. Wobbrock. An aligned rank transform procedure for multifactor contrast tests.
- [46] Dominic James Farris, Luke A. Kelly, Andrew G. Cresswell, and Glen A. Lichtwark. The functional importance of human foot muscles for bipedal locomotion. *Proceedings of the National Academy of Sciences*, 116(5):1645–1650, jan 2019.
- [47] Daniel Feeney, Brett Vladika, Jay Dicharry, and Bradley Davidson. Upper configurations can affect endurance, agility, and power performance. *Footwear Science*, 11(sup1):S96, jun 2019.
- [48] Raúl Feliz, Eduardo Zalama, and Jaime Gómez García-Bermejo. Pedestrian tracking using inertial sensors. *Journal of Physical Agents*, 3(1):35–42, 2009.
- [49] Richard A. Fineman, Andrew F J Abercromby, Amy Ross, and Leia A. Stirling. Cognitive Task Analysis of Mark III Fit Checks for the Development of Human-Spacesuit Performance Metrics. In *Proceedings of the 47th International Conference on Environmental Systems*, Charleston, SC, 2017.
- [50] Richard A. Fineman, Timothy M. McGrath, Damian G. Kelty-Stephen, Andrew F. Andrew, and Leia A. Stirling. Objective metrics quantifying fit and performance in spacesuit assemblies. *Aerospace Medicine and Human Performance*, 89(11):985–995, nov 2018.
- [51] Richard A. Fineman and Leia A. Stirling. Quantification and visualization of coordination during non-cyclic upper extremity motion. *Journal of Biomechanics*, 63:82–91, 2017.
- [52] Carl Fischer, Poorna Talkad Sukumar, and Mike Hazas. Tutorial: Implementing a pedestrian tracker using inertial sensors. *IEEE Pervasive Computing*, 12(2):17–27, apr 2013.
- [53] Martin A. Fischler and Robert C. Bolles. Random sample consensus: A Paradigm for Model Fitting with Applications to Image Analysis and Automated Cartography. *Communications of the ACM*, 24(6):381–395, 1981.

- [54] C. G. Fontanella, A. Forestiero, E. L. Carniel, and A. N. Natali. Analysis of heel pad tissues mechanics at the heel strike in bare and shod conditions. *35(4):441–447.*
- [55] John J Fraser, Mark A Feger, and Jay Hertel. Midfoot and Forefoot Involvement in Lateral Ankle Sprains and Chronic Ankle Instability. Part 1: Anatomy and Biomechanics. *The International Journal of Sports Physical Therapy*, *11(6):992–1005*, dec 2016.
- [56] Eugene Giles and Paul H. Vallandigham. Height Estimation from Foot and Shoeprint Length. *Journal of Forensic Sciences*, *36(4):13129J*, 1991.
- [57] Claire C. Gordon, Cynthia L. Blackwell, Bruce Bradtmiller, Joseph L. Parham, Patricia Barrientos, Stephen P. Paquette, Brian D. Corner, Jeremy M. Carson, Joseph C. Venezia, Belva M. Rockwell, Michael Mucher, and Shirley Kristensen. 2012 Anthropometric Survey of U.S. Army Personnel: Methods and Summary Statistics. Technical report, ARMY NATICK SOLDIER RESEARCH DEVELOPMENT AND ENGINEERING CENTER MA, Natick, MA, dec 2014.
- [58] Alena Grabowski, Claire T. Farley, and Rodger Kram. Independent metabolic costs of supporting body weight and accelerating body mass during walking. *Journal of Applied Physiology*, *98(2):579–583*, 2005.
- [59] Tamara M. Grant, Laura E. Diamond, Claudio Pizzolato, Bryce A. Killen, Daniel Devaprakash, Luke Kelly, Jayishni N. Maharaj, and David J. Saxby. Development and validation of statistical shape models of the primary functional bone segments of the foot. *PeerJ*, *2020(2):e8397*, feb 2020.
- [60] Stefan Grau and Bettina Barisch-Fritz. Improvement of safety shoe fit - evaluation of dynamic foot structure. *Footwear Science*, *10(3):179–187*, sep 2018.
- [61] Dave Graziosi, Bobby Jones, Jinny Ferl, Steve Scarborough, Linda Hewes, Amy Ross, and Richard Rhodes. Z-2 Architecture Description and Requirements Verification Results Abstract. In *46th International Conference on Environmental Systems*, Vienna, jul 2016.
- [62] Timothy M. Griffin, Neil A. Tolani, and Rodger Kram. Walking in simulated reduced gravity: Mechanical energy fluctuations and exchange. *Journal of Applied Physiology*, *86(1):383–390*, 1999.
- [63] Marco Hagen and Ewald M. Hennig. Effects of different shoe-lacing patterns on the biomechanics of running shoes. *27(3):267–275*.
- [64] Marco Hagen, Ann Kathrin Homme, Tim Umlauf, and Ewald M. Hennig. Effects of different shoe-lacing patterns on dorsal pressure distribution during running and perceived comfort. *18(3):176–187*.
- [65] Gary L. Harris. *The origins and technology of the advanced extravehicular space suit*. American Astronautical Society, San Diego, CA, 2001.
- [66] J.H Hicks. The mechanics of the foot II. The plantar aponeurosis and the arch. *Journal of Anatomy*, *88(1):25–30*, 1954.
- [67] Matthew Hill, Roozbeh Naemi, Helen Branthwaite, and Nachiappan Chockalingam. The relationship between arch height and foot length: Implications for size grading. *59:243–250*.

- [68] B. Holschuh, J. Waldie, J. Hoffman, and D. Newman. Characterization of structural, volume and pressure components to space suit joint rigidity. In SAE Technical Papers. SAE International, 2009.
- [69] Youlian Hong, Lin Wang, Jing Xian Li, and Ji He Zhou. Changes in running mechanics using conventional shoelace versus elastic shoe cover. 29(4):373–379.
- [70] Y. P. Ivanenko, R. Grasso, V. Macellari, and F. Lacquaniti. Control of foot trajectory in human locomotion: Role of ground contact forces in simulated reduced gravity. Journal of Neurophysiology, 87(6):3070–3089, 2002.
- [71] Ning Ji, Hui Zhou, Kaifeng Guo, Oluwarotimi Williams Samuel, Zhen Huang, Lisheng Xu, and Guanglin Li. Appropriate mother wavelets for continuous gait event detection based on time-frequency analysis for hemiplegic and healthy individuals. Sensors (Switzerland), 19(16):1–18, 2019.
- [72] Ales Jurca and Saso Dzeroski. Length dispersion of shoes labelled with the same size in the UK shoe-size system. Footwear Science, 5(SUPPL. 1):2–5, 2013.
- [73] Ales Jurca, Jure Žabkar, and Sašo Džeroski. Analysis of 1.2 million foot scans from North America, Europe and Asia. Scientific Reports, 9(1):1–10, 2019.
- [74] Glen P Kenny, Sean R Notley, and Daniel Gagnon. Direct calorimetry: a brief historical review of its use in the study of human metabolism and thermoregulation. European Journal of Applied Physiology, 117:1765–1785, 2017.
- [75] R. F. Ker, M. B. Bennett, S. R. Bibby, R. C. Kester, and R. McN. Alexander. The spring in the arch of the human foot. 325(6100):147–149.
- [76] Sarah E. Kessler, Glen A. Lichtwark, Lauren K.M. Welte, Michael J. Rainbow, and Luke A. Kelly. Regulation of foot and ankle quasi-stiffness during human hopping across a range of frequencies. Journal of Biomechanics, page 109853, 2020.
- [77] K. Han Kim, Karen Young, Elizabeth Benson, Sarah Jarvis, Linh Vu, Yaritza Hernandez, and Sudhakar Rajulu. Human modeling tools for spacesuit and hardware design and assessment. In Sofia Scataglini and Paul Gunther, editors, DHM and Posturography, chapter 46, pages 613–625. Academic Press, jan 2019.
- [78] K. Han Kim, Karen S. Young, Yaritza Bernal, Abhishektha Boppana, Linh Q. Vu, Elizabeth A. Benson, Sarah Jarvis, and Sudhakar L. Rajulu. A Parametric Model of Shoulder Articulation for Virtual Assessment of Space Suit Fit. In Proceedings of the 7th International Conference on 3D Body Scanning Technologies, pages 201–207, Lugano, Switzerland, nov 2016.
- [79] Joseph J. Kosmo and Amy Ross. Space suit mobility evaluations in lunar/mars gravity environments. JOURNAL OF AEROSPACE, 107:535–542, jul 1998.
- [80] Joseph J. Kosmo, William E. Spenny, Rob Gray, and Phil Spampinato. Development of the NASA ZPS Mark III 57.2-kN/m<sup>2</sup> (8.3 psi) space suit. JOURNAL OF AEROSPACE, 1988.
- [81] Makiko Kouchi, Makoto Kimura, and Masaaki Mochimaru. Deformation of foot cross-section shapes during walking. Gait and Posture, 30(4):482–486, nov 2009.

- [82] Rodger Kram, Antoinette Domingo, and Daniel P. Ferris. Effect of reduced gravity on the preferred walk-run transition speed. *Journal of Experimental Biology*, 200(4):821–826, 1997.
- [83] I. Krauss, S. Grau, M. Mauch, C. Maiwald, and T. Horstmann. Sex-related differences in foot shape. *Ergonomics*, 51(11):1693–1709, nov 2008.
- [84] Inga Krauss, Gordon Valiant, Thomas Horstmann, and Stefan Grau. Comparison of female foot morphology and last design in athletic footwear—are men’s lasts appropriate for women? *Research in Sports Medicine*, 18(2):140–156, 2010.
- [85] A. Leardini, M. G. Benedetti, L. Berti, D. Bettinelli, R. Nativo, and S. Giannini. Rear-foot, mid-foot and fore-foot motion during the stance phase of gait. *Gait and Posture*, 25(3):453–462, mar 2007.
- [86] P. Lundgren, C. Nester, A. Liu, A. Arndt, R. Jones, A. Stacoff, P. Wolf, and A. Lundberg. Invasive in vivo measurement of rear-, mid- and forefoot motion during walking. *Gait and Posture*, 28(1):93–100, 2008.
- [87] Ameersing Luximon and Yan Luximon. Shoe-last design innovation for better shoe fitting. *Computers in Industry*, 60(8):621–628, 2009.
- [88] Y. Luximon and A. Luximon. Sizing and grading of shoe lasts. *Handbook of Footwear Design and Manufacture*, pages 197–215, 2013.
- [89] E. A. Mailer and B. B. Adams. The wear and tear of 26.2: Dermatological injuries reported on marathon day. *British Journal of Sports Medicine*, 38(4):498–501, aug 2004.
- [90] Roger A Mann and John L Hagy. The function of the toes in walking and running. *Clinical Orthopaedics & Related Research*, July(142):24–29, 1979.
- [91] Sarah Margerum, Mike Ferrer, Karen Young, and Sudhakar Rajulu. Relating Linear and Volumetric Variables through Body Scanning to Improve Human Interfaces in Space. In *International Conference on 3D Body Scanning Technologies*, pages 10–22, Lugano, Switzerland, oct 2010.
- [92] José M. Martínez-Martínez, José D. Martín-Guerrero, Emilio Soria-Olivas, José A. Bernabeu, Pablo Escandell-Montero, Rafael Hernández Stark, Antonio J. Serrano-López, and Enrique Montiel. Use of SOMs for footwear comfort evaluation. 28(7):1763–1773.
- [93] Ian M Meginnis, Richard A Rhodes, and Kristine N Davis. Performance of the Z-2 Space Suit in a Simulated Microgravity Environment. In *48th International Conference on Environmental Systems*, Albuquerque, NM, jul 2018.
- [94] Qichang Mei, Yaodong Gu, Liangliang Xiang, Peimin Yu, Zixiang Gao, Vickie Shim, and Justin Fernandez. Foot shape and plantar pressure relationships in shod and barefoot populations. 19(4):1211–1224.
- [95] Alberto E. Minetti, Gaspare Pavei, and Carlo M. Biancardi. The energetics and mechanics of level and gradient skipping: Preliminary results for a potential gait of choice in low gravity environments. *Planetary and Space Science*, 74(1):142–145, dec 2012.

- [96] Wade Motawi. Footwear Pattern Making and Last Design. Walid Motawi, June 2020. Google-Books-ID: eo0gEAAAQBAJ.
- [97] Casey A. Myers, Weldyn Allen, Peter J. Laz, Jake Lawler-Schwartz, and Bryan P. Conrad. Motorized self-lacing technology reduces foot-shoe motion in basketball shoes during dynamic cutting tasks. 11:S189–S191. Publisher: Taylor & Francis eprint: <https://doi.org/10.1080/19424280.2019.1606326>.
- [98] A. Mündermann, D. J. Stefanyshyn, and B. M. Nigg. Relationship between footwear comfort of shoe inserts and anthropometric and sensory factors. 33(11):1939–1945.
- [99] NASA. Anthropometry and Biomechanics. In NASA-STD-3000 Man-Systems Integration Standards Volume I, volume 1, chapter 3. NASA, Houston, TX, 1995.
- [100] NASA. Small Business Innovation Research (SBIR) & Small Business Technology Transfer (STTR) Fiscal Year 2019 General Solicitation, 2019.
- [101] Dava Newman and Michael Barratt. Life support and performance issues for extravehicular activity (EVA). In Susanne Churchill, editor, Fundamentals of Space Life Sciences, volume 11, chapter 22, pages 1–61. Krieger Publishing Co., Malabar, FL, 1997.
- [102] Dava J. Newman and Harold L. Alexander. Human locomotion and workload for simulated lunar and Martian environments. Acta Astronautica, 29(8):613–620, 1993.
- [103] JR Norcross, KG Clowers, Tim Clark, Lauren Harvill, Richard M. Morency, Leah C. Stroud, Jessica R. Vos, and Michael L. Gernhardt. Metabolic Costs and Biomechanics of Level Ambulation in a Planetary Suit. Technical Report February, NASA STI Program Office, Houston, TX, 2010.
- [104] J.R. Norcross, L.R. Lee, K.G. Clowers, R.M. Morency, L. Desantis, J.K. DeWitt, J.A. Jones, J.R. Voss, and M.L. Gernhardt. Feasibility of Performing a Suited 10-km Ambulation on the Moon - Final Report of the EVA Walkback Test (EWT). Technical report, NASA STI Program Office, Houston, TX, 2009.
- [105] G Oladipo, I Bob-Manuel, and G Ezenatein. Different Weight Bearing Conditions Amongst Nigerians. The Internet Journal of Biological Anthropology, 3(1):1–7, 2008.
- [106] Padhraig F. O'Loughlin, Christopher D. Murawski, Christopher Egan, and John G. Kennedy. Ankle instability in sports. The Physician and Sportsmedicine, 37(2):93–103, jun 2009.
- [107] Roedolph A. Opperman, James M.A. Waldie, Alan Natapoff, Dava J. Newman, and Jeffrey A. Jones. Probability of spacesuit-induced fingernail trauma is associated with hand circumference. Aviation Space and Environmental Medicine, 81(10):907–913, oct 2010.
- [108] Byoung Keon Park and Matthew P. Reed. Parametric body shape model of standing children aged 3–11 years. Ergonomics, 58(10):1714–1725, oct 2015.
- [109] Byoung Keon D. Park, Sheila Ebert, and Matthew P. Reed. A parametric model of child body shape in seated postures. Traffic Injury Prevention, 18(5):533–536, 2017.
- [110] D. G. Parry, L. R. Curry, D. B. Hanson, and G. B. Towle. A study of techniques and equipment for the evaluation of extravehicular protective garments. Technical report, Wright-Patterson Air Force Base, Dayton, OH, 1966.

- [111] Fabian Pedregosa, Ron Weiss, Matthieu Brucher, Gaël Varoquaux, Alexandre Gramfort, Vincent Michel, Bertrand Thirion, Olivier Grisel, Mathieu Blondel, Peter Prettenhofer, Ron Weiss, Vincent Dubourg, Jake Vanderplas, Alexandre Passos, David Cournapeau, Matthieu Brucher, Matthieu Perrot, Édouard Duchesnay, L. Buitinck, G. Louppe, Olivier Grisel, Fabian Pedregosa, and A. Mueller. Scikit-learn: Machine Learning in Python. *Journal of Machine Learning Research*, 12(85):2825–2830, 2011.
- [112] Bulkard Polster. Mathematics: What is the best way to lace your shoes? 420(6915):476.
- [113] David S Portree and Robert C Trevino. *Walking to Olympus: An EVA Chronology*. NASA History Office, Washington, DC, 1997.
- [114] Carina Price and Christopher Nester. Foot dimensions and morphology in healthy weight, overweight and obese males. *Clinical Biomechanics*, 37:125–130, 2016.
- [115] Moira K. Pryhoda, Rachel J. Wathen, Jay Dicharry, Kevin B. Shelburne, Daniel Feeney, Kathryn Harrison, and Bradley S. Davidson. Alternative upper configurations during agility-based movements: part 1, biomechanical performance. 13(1):91–103.
- [116] John R. Rebula, Lauro V. Ojeda, Peter G. Adamczyk, and Arthur D. Kuo. Measurement of foot placement and its variability with inertial sensors. *Gait and Posture*, 38(4):974–980, 2013.
- [117] Matthew P Reed, Sheila M Ebert, and Brian D Corner. Statistical Analysis to Develop a Three-Dimensional Surface Model of a Midsize-Male Foot. Technical Report October, US Army TARDEC, 2013.
- [118] Matthew P. Reed and Matthew B. Parkinson. Modeling variability in torso shape for chair and seat design. *Proceedings of the ASME Design Engineering Technical Conference*, 1(PARTS A AND B):561–569, 2008.
- [119] M.P. Reed, Ulrich Raschke, Rishi Tirumali, and M.B. Parkinson. Developing and Implementing Parametric Human Body Shape Models in Ergonomics Software. In *3rd Digital Human Modeling Symposium*, pages 1–8, 2014.
- [120] Deborah Riebe, Barry A. Franklin, Paul D. Thompson, Carol Ewing Garber, Geoffrey P. Whitfield, Meir Magal, and Linda S. Pescatello. Updating ACSM’s recommendations for exercise preparticipation health screening. *Medicine and Science in Sports and Exercise*, 47(11):2473–2479, nov 2015.
- [121] Amy J. Ross, Joseph J. Kosmo, Nikolay Moiseyev, Anatoly Stoklitsky, Daniel Barry, and Edward Hodgson. Comparative space suit boot test. In *SAE Technical Papers*, San Antonio, TX, 2002. SAE International.
- [122] Radu Bogdan Rusu and Steve Cousins. 3D is here: Point Cloud Library (PCL). In *Proceedings - IEEE International Conference on Robotics and Automation*, Shanghai, China, 2011.
- [123] John Salvatier, Thomas V. Wiecki, and Christopher Fonnesbeck. Probabilistic programming in Python using PyMC3. *PeerJ Computer Science*, 2:e55, April 2016. Publisher: PeerJ Inc.

- [124] Kumar Sambhav, Puneet Tandon, and S. G. Dhande. Computer aided design and development of customized shoe last. *8(6):819–826*.
- [125] Richard A. Scheuring, Jeffrey A. Jones, Joseph D. Novak, James D. Polk, David B. Gillis, Josef Schmid, James M. Duncan, and Jeffrey R. Davis. The Apollo Medical Operations Project: Recommendations to improve crew health and performance for future exploration missions and lunar surface operations. *Acta Astronautica*, *63*(7-10):980–987, oct 2008.
- [126] Richard A. Scheuring, Charles H. Mathers, Jeffrey A. Jones, and Mary L. Wear. Musculoskeletal injuries and minor trauma in space: Incidence and injury mechanisms in U.S. astronauts. *Aviation Space and Environmental Medicine*, *80*(2):117–124, feb 2009.
- [127] Richard a. Scheuring, P. McCulloch, Mary Van Baalen, C Minard, R Watson, S Bowen, and Terri Blatt. Shoulder injuries in US astronauts related to EVA suit design. In *Aerospace Medical Association 83rd Annual Scientific Meeting*, Atlanta, GA, may 2012.
- [128] Patricia Schmidt. *An Investigation of Space Suit Mobility With Applications to EVA Operations*. PhD thesis, Massachusetts Institute of Technology, Cambridge, MA, Sept 2001.
- [129] Robert Wolfgang Schuster, Andrew Cresswell, and Luke Kelly. Reliability and quality of statistical shape and deformation models constructed from optical foot scans. *115:110137*.
- [130] Young Young Shen and Allison P. Anderson. Extended Kalman Filter for Magnetometer-Free Estimation of Spacesuit Wearer Joint Kinematics Using Inertial Measurements. In *FUSION 2019 - 22nd International Conference on Information Fusion*, Ottawa, Canada, 2019.
- [131] Kristina Stanković, Toon Huysmans, Femke Danckaers, Jan Sijbers, and Brian G. Booth. Subject-specific identification of three dimensional foot shape deviations using statistical shape analysis. *Expert Systems with Applications*, *151*:113372, aug 2020.
- [132] Darren J. Stefanyshyn and Benno M. Nigg. Mechanical energy contribution of the metatarsophalangeal joint to running and sprinting. *Journal of Biomechanics*, *30*(11-12):1081–1085, nov 1997.
- [133] Leia Stirling, Damian Kelty-Stephen, Richard Fineman, Monica L.H. Jones, Byoung Keon Daniel Park, Matthew P. Reed, Joseph Parham, and Hyeg Joo Choi. Static, Dynamic, and Cognitive Fit of Exosystems for the Human Operator. *Human Factors*, *62*(3):424–440, 2020.
- [134] N. M. Stolwijk, K. L.M. Koenraadt, J. W.K. Louwerens, D. Grim, J. Duysens, and N. L.W. Keijsers. Foot lengthening and shortening during gait: A parameter to investigate foot function? *39*(2):773–777.
- [135] Samuel Strauss. Extravehicular Mobility Unit Training Suit Symptom Study Report. Technical Report March, NASA Johnson Space Center, Houston, TX, 2004.
- [136] Samuel Strauss, Ralph L. Krog, and Alan H. Feiveson. Extravehicular mobility unit training and astronaut injuries. *Aviation Space and Environmental Medicine*, *76*(5):469–474, may 2005.
- [137] Kenneth S. Thomas and Harold J. McMann. *U. S. Spacesuits: Second Edition*. Springer, Chichester, UK, 2nd edition, 2012.

- [138] W E Thornton, G Wyckliffe Hoffler, and J A Rummel. Anthropometric changes and fluid shifts. Biomedical results from Skylab, NASA SP-37:330–338, 1987.
- [139] Daniele Tomassoni, Enea Traini, and Francesco Amenta. Gender and age related differences in foot morphology. Maturitas, 79(4):421–427, 2014.
- [140] Inge Van den Herrewege, Kris Cuppens, Mario Broeckx, Bettina Barisch-Fritz, Jos Vander Sloten, Alberto Leardini, and Louis Peeraer. Dynamic 3D scanning as a markerless method to calculate multi-segment foot kinematics during stance phase: Methodology and first application. Journal of Biomechanics, 47(11):2531–2539, aug 2014.
- [141] Bart Van Gheluwe, Rudi Tielemans, and Philip Roosen. The influence of heel counter rigidity on rearfoot motion during running. Journal of applied biomechanics, 11(1):47–67, 1995.
- [142] Madhusudhan Venkadesan, Ali Yawar, Carolyn M. Eng, Marcelo A. Dias, Dhiraj K. Singh, Steven M. Tommasini, Andrew H. Haims, Mahesh M. Bandi, and Shreyas Mandre. Stiffness of the human foot and evolution of the transverse arch. 579(7797):97–100.
- [143] Steven F. Viegas, David Williams, Jeffrey Jones, Samuel Strauss, and Jonathan Clark. Physical demands and injuries to the upper extremity associated with the space program. Journal of Hand Surgery, 29(3):359–366, 2004.
- [144] Alexandra S. Voloshina, Arthur D. Kuo, Monica A. Daley, and Daniel P. Ferris. Biomechanics and energetics of walking on uneven terrain. Journal of Experimental Biology, 216(21):3963–3970, nov 2013.
- [145] Linh Q. Vu, Han Kim, Lawrence J. H. Schulze, and Sudhakar L. Rajulu. Evaluating lumbar shape deformation with fabric strain sensors. page 0018720820965302. Publisher: SAGE Publications Inc.
- [146] John W. Wannop, Darren J. Stefanyshyn, Robert B. Anderson, Michael J. Coughlin, and Richard Kent. Development of a Footwear Sizing System in the National Football League. Sports Health, 11(1):40–46, 2019.
- [147] John W. Wannop, Jay T. Worobets, Rodrigo Ruiz, and Darren J. Stefanyshyn. Footwear traction and three-dimensional kinematics of level, downhill, uphill and cross-slope walking. Gait and Posture, 40(1):118–122, 2014.
- [148] Lauren Welte, Luke A. Kelly, Sarah E. Kessler, Daniel E. Lieberman, Susan E. D’Andrea, Glen A. Lichtwark, and Michael J. Rainbow. The extensibility of the plantar fascia influences the windlass mechanism during human running. 288(1943):20202095. Publisher: Royal Society.
- [149] Lauren Welte, Luke A. Kelly, Glen A. Lichtwark, and Michael J. Rainbow. Influence of the windlass mechanism on arch-spring mechanics during dynamic foot arch deformation. 15(145):20180270. Publisher: Royal Society.
- [150] David R Williams and Brian J Johnson. EMU Shoulder Injury Tiger Team Report. Technical Report September, NASA STI Program Office, Houston, TX, 2003.

- [151] Markus Windolf, Nils Götzen, and Michael Morlock. Systematic accuracy and precision analysis of video motion capturing systems-exemplified on the Vicon-460 system. *Journal of Biomechanics*, 41(12):2776–2780, 2008.
- [152] Jacob O. Wobbrock, Leah Findlater, Darren Gergle, and James J. Higgins. The aligned rank transform for nonparametric factorial analyses using only anova procedures. In *Proceedings of the 2011 annual conference on Human factors in computing systems - CHI '11*, page 143. ACM Press.
- [153] P. Wolf, A. Stacoff, A. Liu, C. Nester, A. Arndt, A. Lundberg, and E. Stuessi. Functional units of the human foot. *Gait and Posture*, 28(3):434–441, 2008.
- [154] R. E. Wunderlich and P. R. Cavanagh. Gender differences in adult foot shape: Implications for shoe design. *Medicine and Science in Sports and Exercise*, 33(4):605–611, apr 2001.
- [155] Shuping Xiong, Ravindra S. Goonetilleke, Jianhui Zhao, Wenyan Li, and Channa P. Witana. Foot deformations under different load-bearing conditions and their relationships to stature and body weight. *Anthropological Science*, 117(2):77–88, 2009.
- [156] In-Kwon Yeo and Richard A Johnson. A new family of power transformations to improve normality or symmetry. *Biometrika*, 87(4):954–959, dec 2000.
- [157] Karl E. Zelik and Eric C. Honert. Ankle and foot power in gait analysis: Implications for science, technology and clinical assessment. *Journal of Biomechanics*, 75:1–12, 2018.
- [158] Ju Zhang, Jacqui Hislop-Jambrich, and Thor F. Besier. Predictive statistical models of baseline variations in 3-D femoral cortex morphology. *Medical Engineering and Physics*, 38(5):450–457, 2016.
- [159] Qian-Yi Zhou, Jaesik Park, and Vladlen Koltun. Open3D: A Modern Library for 3D Data Processing. *arXiv:1801.09847*, 2018.
- [160] Hui Zou and Trevor Hastie. Regularization and variable selection via the elastic net. *Journal of the Royal Statistical Society. Series B: Statistical Methodology*, 67(2):301–320, 2005.